FINITE ELEMENT MODELING OF CYCLICALLY LOADED FRP-RETROFITTED RC SQUAT SHEAR WALLS

ALI REZAIEFAR

A Thesis

in

The Department

of

Building, Civil, and Environmental Engineering

Presented in Partial Fulfillment of the Requirements

For the Degree of Master of Applied Science (Civil Engineering) at

Concordia University

Montréal, Québec, Canada

April 2013

CONCORDIA UNIVERSITY
School of Graduate Studies

This is to certify that the thesis prepared

By: Ali Rezaiefar

Entitled: Finite Element Modeling of Cyclically Loaded FRP-Retrofitted RC Squat Shear Walls

and submitted in partial fulfillment of the requirements for the degree of

Master of Applied Science (Civil Engineering)

complies with the regulations of the University and meets the accepted standards with respect to originality and quality.

Signed by the final examining committee:

Lucia Tirca	Chair, Examiner
Lan Lin	Examiner
Ramin Sedaghati	Examiner
Khaled Galal	Supervisor

Approved by _____
Chair of Department or Graduate Program Director

April 2013

_____
Dean of Faculty

ABSTRACT

FINITE ELEMENT MODELING OF CYCLICALLY LOADED FRP-RETROFITTED RC SQUAT SHEAR WALLS

ALI REZAIEFAR

Establishing effective retrofit methods for upgrading the seismic performance of existing reinforced concrete (RC) shear walls requires reliable means for estimating the behaviour of RC shear walls with various geometry and reinforcement configurations. Generally, experimental testing of retrofitted RC shear walls is considered as the most reliable method of performance evaluation, yet this requires great efforts in terms of the testing equipment and time in addition to the high cost. On the other hand, a numerical model that would consider the main parameters that influence the complex performance of original and retrofitted RC shear walls is seen to be an effective tool for parametric studies and development of code provisions for the design or evaluation purposes. A number of experimental tests are available in the literature which could be used for the primary verification of possible numerical analyses. Similarly, a number of numerical and analytical approaches are available with a great potential for improvements in order to converge into a precise and usable analytical approach.

In this thesis, numerical modeling of RC shear walls using general purpose finite element analysis package ANSYS is explored. A total of seven wall specimens from four experimental programs were modeled and analysed under monotonic and reversed cyclic loading and the numerical predictions were in good correlation with the experimental data. One of the experimentally tested models was then selected for further detailed

investigation on the influence of the concrete compressive strength and the addition of externally-bonded carbon fibre-reinforced polymer (CFRP) composite sheet on the behaviour of the squat RC shear walls and their modes of failure.

To Mahsa

AKNOWLEGMENT

It is with sincere gratitude that I thank my advisor Dr. Khaled Galal for positively believing in my work. It would not be possible for me to accomplish any of my research goals without his financial and academic support.

I would like to thank Mr. Krzysztof Rosiak and CADes Structures Inc. for helping me realize the relations between the academic research and the real world industry and the financial support during my research.

There were always great people in my life to learn from namely; Dr. Morteza Aboutalebi, Dr. Hossam El-Sokkary, Dr. Hossein Azimi, and Mr. Hamid Arabzadeh that I can't thank them with the words I know. I also would like to extend my gratitude to my friends and colleagues at Concordia University namely; Ihab, Javad, Nima, Farzad, Arash, Babak, Hani, Ahmad and others who provided a friendly environment for me where I could follow my research. I would like to thank the special people of my life, my parents, my family and friends.

Finally, I dedicate this thesis to my wife for her patience, love and passion during my studies. Without her support, my life would have had a different definition.

TABLE OF CONTENTS

LIST OF FIGURES

LIST OF TABLES

CHAPTER 1

INTRODUCTION

1.1 GENERAL

Reinforced concrete (RC) shear walls are the main lateral force resisting system in many RC structures. Several factors affect the seismic behaviour and ductility of a RC shear wall, particularly its shear span-to-depth ratio and its shear capacity in relation to the flexural capacity. Squat shear walls are found in many existing low-rise RC buildings such as nuclear power plant facilities, airport buildings and office/residential buildings that use a flat plate system for gravity loads. RC squat shear walls are characterised by their low height-to-length ratio or low shear span-to-depth ratio. As such, the response of RC squat shear walls to lateral loads will be dominated by shear behaviour, with reduced contribution from the classic beam theory and the plane-sections hypothesis. Shear behaviour of RC squat elements is a complex phenomenon, especially when considering the cyclic nature of acting lateral loads.

Last decades witnessed the development of several retrofitting methods for shear deficient RC shear walls towards improving their seismic performance in terms of the overall strength, ductility, and energy dissipation capacities. Among these, fiber-reinforced polymer (FRP) composite materials have received increasing attention in the past few years as a potential material for retrofitting of existing RC structures. Despite the various research efforts reported in the literature in proposing different FRP-retrofitting methods for existing RC squat walls, there is still a need to thoroughly

investigate the effect of major design parameters, such as the material properties, geometry, arrangement of reinforcement bars and additional external reinforcement on the overall seismic performance of the system.

Typically, the seismic performance of a retrofitted RC shear walls is evaluated experimentally through assessing its hysteretic lateral force displacement relationships. Although experimental testing is seen to be the most evident approach to assess the performance of a shear wall, numerical simulations would provide valuable tools for parametric studies and assessments of the seismic response of RC squat shear walls.

This thesis investigates the details of numerical modeling of RC squat shear walls using Finite Element (FE) method. Amongst many general purpose FE analysis packages available in the market, ANSYS is adopted for the simulations of this research considering its extensive materials and elements library and the global reputation for the accuracy of the results of analyses performed previously.

The study adopts three-dimensional geometry modeling approach while addressing the most effective parts of the geometry along with major failure criteria of the constituent materials namely concrete, steel reinforcement bars, FRP sheets and the bond interface to improve the accuracy of the results. On the other hand, the use of symmetry and a special meshing technique helped reducing the analysis time consumption.

1.2 OBJECTIVES AND SCOPE OF WORK

The main objective of this research is to investigate, numerically, the effect of shear capacity on the ductility of RC squat shear walls, both existing and FRP-retrofitted, when subjected to cyclic load excitations simulating seismic effects.

In order to achieve the objective of this research, the scope of work is to:

- Outline an appropriate numerical modeling approach for the analysis of RC shear walls under monotonic and cyclic loading that best describes the geometry and failure criteria using a widely accepted general purpose FE package.
- Apply the numerical modeling to study the failure modes of RC squat shear walls in more details.
- Evaluate the effect of externally bonded FRP reinforcement content on the failure mode and seismic performance of unretrofitted and FRP-retrofitted RC squat shear walls using the numerical modeling.
- Evaluate the effects of concrete strength on the shear capacity and seismic performance of unretrofitted and FRP-retrofitted RC squat shear walls.

1.3 ORGANIZATION OF THE THESIS

This thesis is composed of six chapters. Chapter 2 reviews the available literature in order to generate the basis of the modeling i.e. geometry, loading, supports, etc. and to identify relevant experimental works in the area of FRP-retrofit of RC squat shear walls. In Chapter 3, the modeling procedure in terms of the geometry, elements, boundary conditions and failure criteria is described. Pilot modeling and sensitivity analyses are conducted whenever needed in order to identify the validity of the material properties and failure criteria. As for Chapter 4, it is mainly concerned with comparing and correlating the FE results with the relevant experimental data and quantifying the difference. A final calibration of the analysis considerations is performed by comparing the results of FE analysis with those of related experimental tests in order to measure the scope and amount of error at various stages of the analysis. In Chapter 5, the behaviour of a squat shear wall model from the cases studied in Chapter 4 is explained in details under

monotonic and cyclic loading in terms of stress distribution and internal forces of the various parts and constitutes of the wall model. Appropriate shear degradation models available in the literature are used to evaluate the mode of failure of the wall. A series of models are developed in order to study the effects of concrete compressive strength on the seismic performance of existing RC squat shear walls. The effects of an additional layer of FRP external wrap on the type of behaviour, overall performance and the mode of failure of the walls with various concrete compressive strengths are discussed and conclusions are made. Finally, Chapter 6 provides the conclusions drawn from the findings of Chapters 3, 4 and 5 and proposes areas for future research.

CHAPTER 2

LITERATURE REVIEW

2.1 INTRODUCTION

From the various studies available in the field of seismic retrofitting of reinforced concrete (RC) structures and structural members, a review of the references related to the field of numerical nonlinear modeling of the seismic retrofitting of RC shear walls is presented in this chapter.

2.2 SEISMIC RETROFITTING OF SHEAR WALLS

2.2.1 Overview

Reinforced concrete shear walls are commonly used in concrete buildings to resist the lateral forces acting on them due to their high in-plane stiffness. These lateral forces are caused by earthquake or wind excitations. The term “structural wall” is used instead of “shear wall” by Paulay and Priestley (1992) to emphasize on the significance of the in-plane bending moments and axial forces on the behaviour of this structural element, in addition to the shear forces. Brittle behaviour of shear walls caused by undesirable modes of failure is prevented in the modern seismic codes of design by providing special design/detailing practices. A well-designed/detailed wall provides high energy dissipation, ductility, and strength to the building structure. Walls designed based on the older versions of the seismic codes −prior to the enforcement of ductile energy dissipation seismic performance− fail to undergo a ductile behaviour due to the poor design and detailing.

In general, the seismic performance of a building structure that is damaged by a minor earthquake or that is not damaged but vulnerable to future earthquakes, could be upgraded using two different schemes: global and local retrofitting. Additional structural members provide the strength and ductility in a globally upgraded structure while local upgrading aims to improve the capacity of structural members separately in a way that the upgraded structure passes the requirements of the up-to-date codes (Moehle, 2000).Various methods of retrofitting have been proposed and tested by researchers based on the modes of failure of the shear walls. Most of these tests normally consider the plastic hinge region as the vulnerable or damaged part of the entire wall. For brittle failure modes with minimum or no ductility, the retrofit intervention aims at eliminating the non-ductile behaviour and modifying it to ductile modes. For original walls that have limited ductility with low energy dissipation capacity, the retrofit aims to modify the performance to be more ductile with higher energy dissipation capacity. Pauley and Priestley (1992) state that the principal source of energy dissipation in a laterally loaded cantilever wall should be yielding of the flexural reinforcement in the plastic hinge regions, normally located at the base of the wall.

A flexural mode of failure of RC shear walls occurs when there is a sufficient shear capacity that develops yielding of the wall's flexural reinforcement. Flexural failure mode is necessary to ensure a *ductile performance* for RC shear walls subjected to in-plane bending moments, shear and axial forces. Lack of sufficient shear capacity causes a shear failure, which is brittle in nature. Modern seismic design codes adopt a *capacity design philosophy* by ensuring that the shear capacity of the wall exceeds its flexural capacity along the wall height. Besides the two main failure modes of shear and flexural,

there are three other possible modes of failure based on the instability of thin-walled sections (local buckling of web), in-plane splitting failure, and rocking failure (Galal and El-Sokkary, 2008). The three latter cases will not be considered in this study as they are not as common as the main two failure modes of the RC shear walls. Seismic upgrade is defined as "an improvement in the seismic performance of the shear walls based on the prevention of brittle failure modes or improving their ductile performance by enhancing their stiffness, strength, ductility, or a combination of them". A *repair* is defined as restoring the original state of a damaged structure without aiming for increasing its capacity. If the repair of damaged walls improves the performance of the structure comparing to its original state, the repair process is called *rehabilitation*. *Strengthening* describes increasing the capacity and/or ductility of an undamaged structural element. *Retrofit* is commonly used to describe an intervention that could be either one of the three above described techniques, or a combination of them (Galal and El-Sokkary, 2008).

2.2.2 Traditional retrofit methods

Fiorato et al. (1983) used the replacement of concrete as a repair method for shear wall specimens with barbell sections with a height-to-width ratio of 2.4. The walls were subjected to reverse monotonic cyclic loading and axial loads simultaneously up to failure. The concrete replacement method resulted in a lower stiffness for the repaired specimens comparing to the original ones but the lateral strength and ductility were reported to be fully restored by the repair technique (Fiorato et al., 1983).

Replacement of concrete in the damaged parts of shear walls was studied by Lefas et al. (1990) where four slender rectangular walls were tested to damage and three of them repaired by replacing the concrete and strengthening the buckled reinforcement bars in a

150x100mm region of the compressive toes of the walls. The flexural cracks on the body of the walls were also filled with epoxy injection. The repaired specimens were subjected again to a monotonic reverse cyclic loading and exhibited lower stiffness and less ductility but a full restoration of wall strength was stated. Completely filling the cracks by epoxy injection had a marginal effect on the improvement of the structural characteristics of the repaired walls. A comparison between the crack patterns and failure modes of the original and repaired walls implied a marginal effect of the repair method on these structural characteristics.

Vecchio et al. (2002) repaired two damaged wide-flanged squat shear walls by replacing the crushed concrete and re-tested the walls by subjecting them to the lateral loading that caused the original damage. The barbell-sectioned shear wall specimens had a 2020mm height and 2885mm width with a web thickness of 75mm, also the flange parts of the specimens were consisted of 3045x100mm shells. The concrete used as the fulfillment material had approximately double the strength of the original walls concrete. The first repair scenario was to replace the damaged parts of the web only while in the second repair scenario the crushed concrete replacement technique was done to the flanges. The effectiveness of this repair method was assessed through the test results that showed that the seismic efficiency indicators of the wall such as strength, stiffness, and energy dissipation capacity were almost restored in the repaired walls.

In addition to the above studies, there has been several other research works done in the field of traditional repair of shear walls using similar techniques. They are not included in this chapter as they are out of the scope of this study.

2.2.3 Recent retrofit methods

In addition to the traditional methods applicable to the repair cases, improving the performance of damaged or non-damaged wall structures by applying external layers of bar or plate elements was studied by a number of authors considering the material for the bonding elements to be steel or FRP where the latter case will be discussed in the next part of this chapter.

The use of steel plates and bars as external bonding materials to shear wall was studied by Elnashai and Pinho (1998). Experimental tests followed by analytical and numerical analyses on 1:2.5 scale shear wall specimen were conducted to study the effects of various methods of application of steel plates and bars on stiffness, strength, and ductility as the three main parameters of wall seismic performance. In the stiffness-only phase, steel plates were glued to the surface of the wall to cover the area of expected plastic hinge region for the non-damaged walls and the heavily cracked regions for the damaged specimen on the two boundary regions of the walls as shown in Figure 2.1(a). The experimental results indicated an increase in the level of stiffness to be controlled totally by the position of the bonded plates, and their dimensions. In the strength-only phase, two main strengthening methods of adding external unbounded steel reinforcement bars and external unbounded steel plates were conducted in order to increase the strength of the wall without influencing the stiffness as shown in Figure 2.1(b). The level of strength was stated to be controllable by the area and position of the steel plates or the re-bars. In the ductility-only interventions, U-shaped external confinement steel plates were added to the area where additional ductility was required as shown in Figure 2.1(c). The proposed ductility-only intervention technique was stated to be externally efficient to be used as

tool for upgrading structures in which improper detailing leads to insufficient ductility capacity. The controlling parameters in the ductility-only intervention were stated to be the thickness, height, and spacing of the external U-shaped plates. A series of finite element modeling was provided also by Elnashai and Pinho (1998) in order to study the effects of various parameters on the characteristics of the wall.

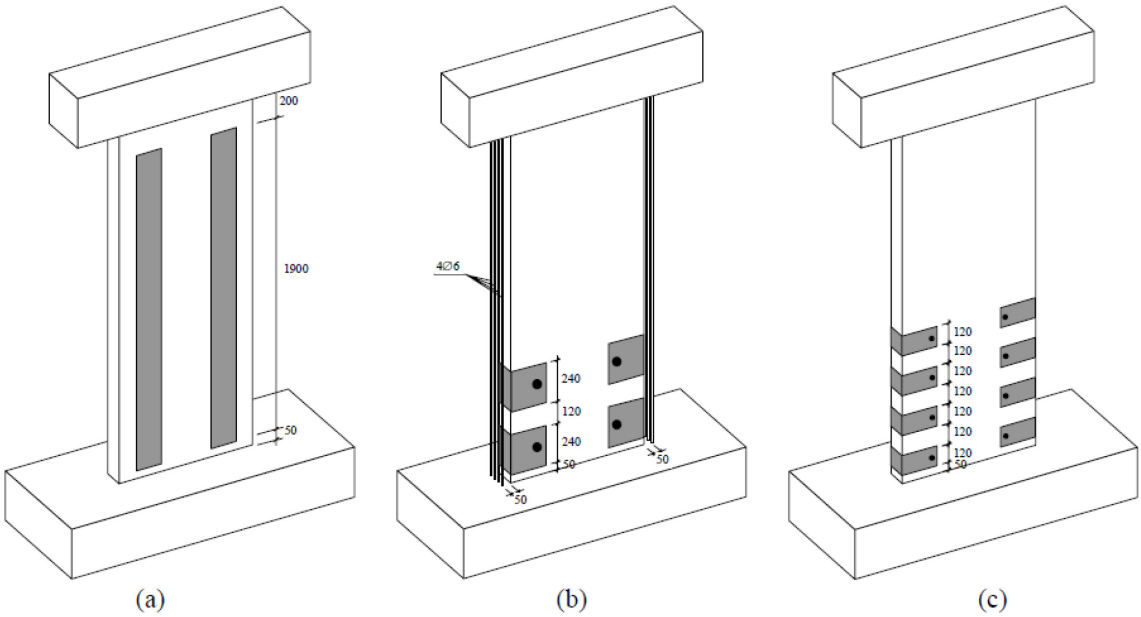

Figure 2.1 Strengthening techniques adopted by Elnashai and Pinho (1998)

2.3 RETROFITTING SHEAR WALLS USING FRP: EXPERIMENTAL STUDIES

The use of FRP composites for the purpose of retrofitting RC shear walls was investigated through an early experimental and analytical program by Lombard et al. (2000). The experimental program consisted of four 2.0x1.5x0.1m RC shear wall specimens loaded to failure under a quasi-static cyclic horizontal excitation applied to the top of the wall. A control wall without any retrofitting was tested initially and then repaired using one layer of vertical Carbon Fibre Reinforced Polymer (CFRP) two sheets

on both faces of the wall after replacing the heavily cracked and crushed concrete at the toes of the wall and injection of mortar in the light cracks. The repaired wall was tested again under the same loading history as the control wall. The test results showed 29% increase in the yield load and almost 90% recovery of the initial elastic stiffness as well as 80% increase in the ultimate load-carrying capacity of the wall after applying the repair method. The third specimen tested by Lombard et al. (2000) had the same geometry and strengthening scheme as the repaired wall without being initially tested while three layers of CFRP tow sheets in a vertical-horizontal-vertical arrangement were used on the surface of the wall for the strengthening of the fourth specimen. The application of one vertical layer of CFRP on the surface of the wall resulted in 82% increase in the cracking load compared to the control wall but the test results showed that the application of additional two layers of CFRP does not affect the cracking force significantly. The yield load was increase by 25% and 39% for the third and fourth specimens. According to Lombard et al. (2000), the main advantage of multiple layers of CFRP in the fourth specimen was indicated to be a significant increase in the ultimate failure load (132%) compared to that of the third specimen (46%).

The rehabilitation of squat shear walls with a height-to-width ratio of 1.0 using FRP reinforcement after initially being loaded to failure was studied by Antoniades et al. (2003). The retrofit procedure consisted of replacement of the heavily damaged concrete by high-strength mortar, lap welding of fractured reinforcement and wrapping the walls with FRP jackets in various schemes. A total of five wall specimens were designed and constructed based on the provisions of the Eurocode 8 (1996) being the code of practice at the time of that research.

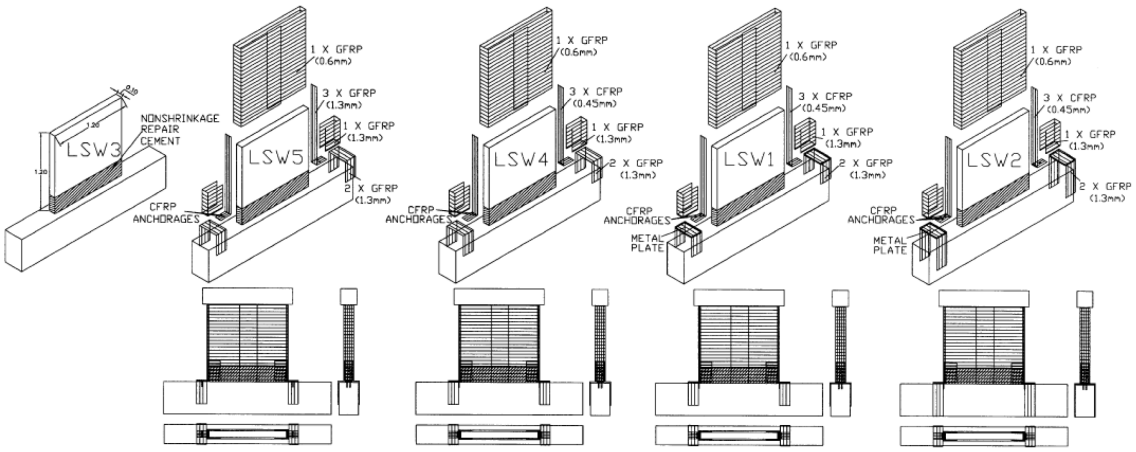

Figure 2.2 Details of the specimens tested by Antoniades et al. (2003)

All specimens were initially loaded to failure and a flexural mode of failure was reported. The heavily cracked concrete was removed from the 250 mm bottom regions of the walls, the crushed reinforcement bars were replaced, and a non-shrinking high-strength mortar was used for the fulfillment of the repair region as the primary stage of repair. The second stage of repair was consisted of strengthening the walls with CFRP and GFRP (Glass Fibre Reinforced Polymer) sheets "FRP-strengthened walls" except for "LSW3" specimen which was kept as the "repair-only" wall for comparison of the effectiveness of the second stage of repair. The results of tests showed a strength increase in the FRP-strengthened walls ranging between 2% and 32% with respect to the repair-only case (Antoniades et al., 2003).

An experimental program was carried by Peterson and Mitchell (2003) in order to determine the effectiveness of the combined use of headed reinforcement, carbon fiber wrap, and reinforced concrete collars retrofitting method for the retrofitting of a shear wall core system designed in the 1960's using old code provisions with design and detailing deficiencies, poor confinement of the boundary elements, lap splicing in the plastic hinge regions, poor anchorage of the transverse reinforcement, and insufficient

shear strength to develop the plastic hinge. A total of four specimens were constructed and tested under reversed cyclic loading in two pairs of as-built and retrofitted walls. The location of lap splice of the vertical reinforcement in the first pair (W1 and WR1) of walls was at the bottom of the wall while for the second pair (W2 and WR2), the lap splicing was at a height of 600mm from the bottom of the wall.

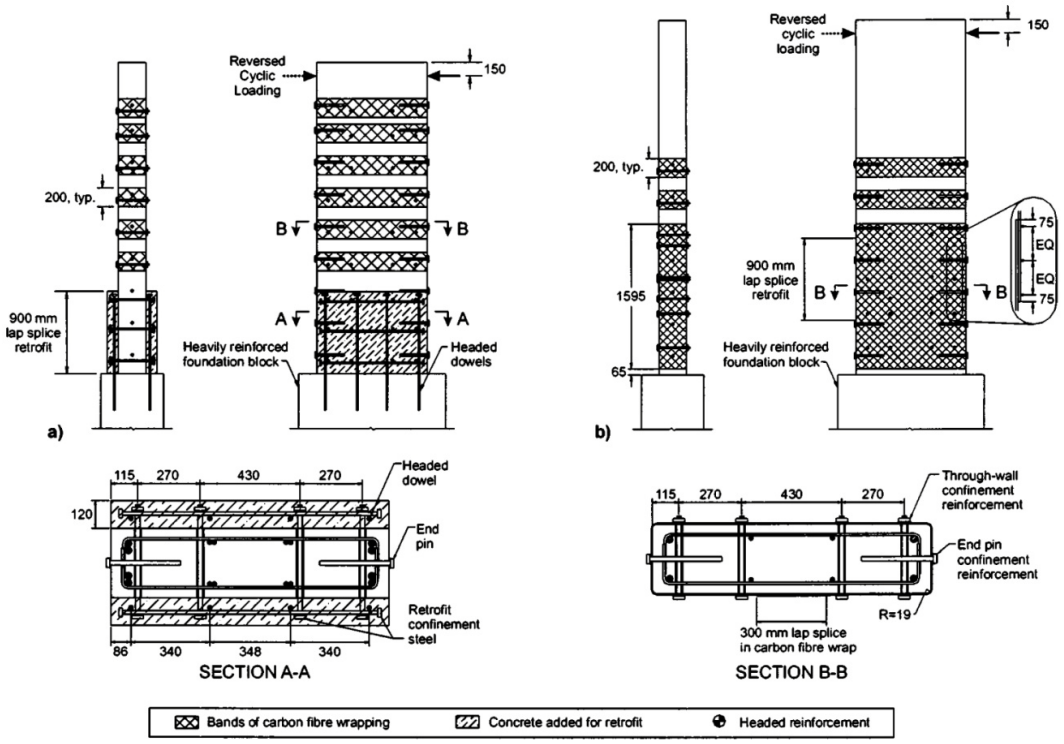

Figure 2.3 Details of the specimens tested by Peterson and Mitchell (2003): (a) WR1 and (b) WR2

Retofit strategies for WR1, and WR2 are shown in Figure 2.3 where the use of headed reinforcement, and carbon fibers to improve the seismic performance of the walls was adopted. The displacement ductility of the wall was improved from 1.5 for W1 to 3.8 for WR1, and from 4.0 for W2 to 6.3 for WR2; also, WR1 and WR2 specimens absorbed over seven and three times respectively as much energy as W1 and W2 during the tests. The combination of headed reinforcement and carbon fiber wrap was shown to be

effective in increasing the confinement of the wall boundary element regions and the anchorage of the transverse reinforcement (Peterson and Mitchell, 2003).

The experimental tests by Ghobara and Khalil (2004) were the first in which the walls were tested under horizontal and vertical actuations in order to model the shear force and overturning moment on the top of the wall simultanusely. The wall specimens were considered to be the plastic hinge region of the shear wall system of an imaginary eight-story building. A total of three speciments consisted of one control wall (CW), and two retrofitted walls (RW1 and RW2) were tested under a constant axial force, an in-plane moment, and a shear force on the top of each specimen. The walls were considered to be designed to comply with the 1963 version of ACI and CSA codes of practice in order to model an older code design that requires rehabilitation. After testing the CW specimen, deficiencies in shear capacity and ductility were observed. A rehabilitation scheme to improve the strength by using two wrapping layers of CFRP material with fibres woven at ±45°, and the ductility by using U-shaped partial hoopes of CFRP uni-directional sheets wrapped around the edge elements with FRP anchors was applied to the RW1 specimen. The RW2 specimen was identical to RW1 but an improved anchoring system using 16mm steel bolts with circular 60mm diameter stell washers was applied to the top and bottom of the ±45° wrapps and to the edges of the U-shaped hoops as shown in Figure 2.4.

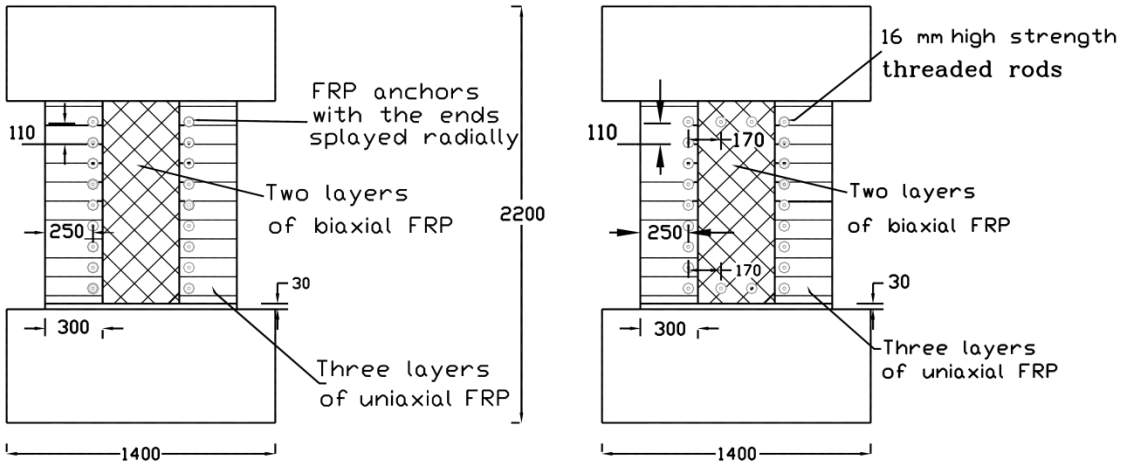

Figure 2.4 Details of the specimens tested by Ghobara and Khalil (2004)

Ghobara and Khalil (2004) reported that the rehabilitated walls sustained an average of 50% more load and 60% more lateral drift than the control wall. Displacement ductility levels of 4 and 6 were reported for RW1 and RW2, respectively, while the energy dissipated by RW2 was reported to be significantly more than that of RW1.

Hiotakis et al. (2004) conducted an experimental program on five wall specimens with the same geometry and loading schedule as Lombard et al. (2000) with some improvements on the base anchorage system for CFRP sheets as well as providing lateral supports for the prevention of premature failure due to lateral buckling and adjustments on the arrangement of the strain gauges. In addition to the four specimens identical to those tested by Lombard et al. (2000), one specimen with one horizontal and three vertical layers of CFRP sheets on each side of the wall was tested. The repair system recovered 88% of the original elastic stiffness and improved the yield load by 22%; also a 44% increase in the load-carrying capacity was reported for the repaired wall. The secant stiffness of the wall was improved significantly (213%) for the first strengthened wall, the strengthened wall also exhibited 19% increase in the yield strength as well as 45%

increase in the cracking strength of the control wall. the results obtained from the second strengthened wall corresponded to a 64% increase in the yield strength and 57% in the stiffness compared to the control wall. the strengthening method used in the third strengthened wall resulted in 55% increase in the yield strength, 148% in the secant stiffness, and 160% in the maximum lateral load resistance of the control wall.

Experimental tests on RC frames with partition walls were conducted by Hwang et al. (2004) in which five large-sclae isolated specimens, one frame and four walls were tested. Three of the four wall specimens were identical with different retrofit schemes while the fourth wall specimen was designed with higher amount of reinforcement and wall thickness. Specimen PF was a pure frame, which intended to draw a comparison between frame and wall, the details of frame in all four wall specimens were identical to PF. The test wall of specimen WF-12 was consisted of a 120mm thickness, with 300x500mm boundary elements (columns of the frame); an overal length of 3500mm, and height of 1500mm without retrofitting in order to use as the control specimen. Only thermal reinforcements were used in the wall specimen WF-12 and similar specimens. SpecimenWF-12-FV was strengthened with four layers of CFRP laminates of 0.1375mm thickness, two layers at each side of the wall in vertical direction. Total of eight layers of CFRP laminates with same properties as of those used for WF-12-FV were attached to the surface of WF-12-FHV, two horizontally and two vertically on each side. The retrofitting scheme and end anchorages of the specimens are shown in Figure 2.5.

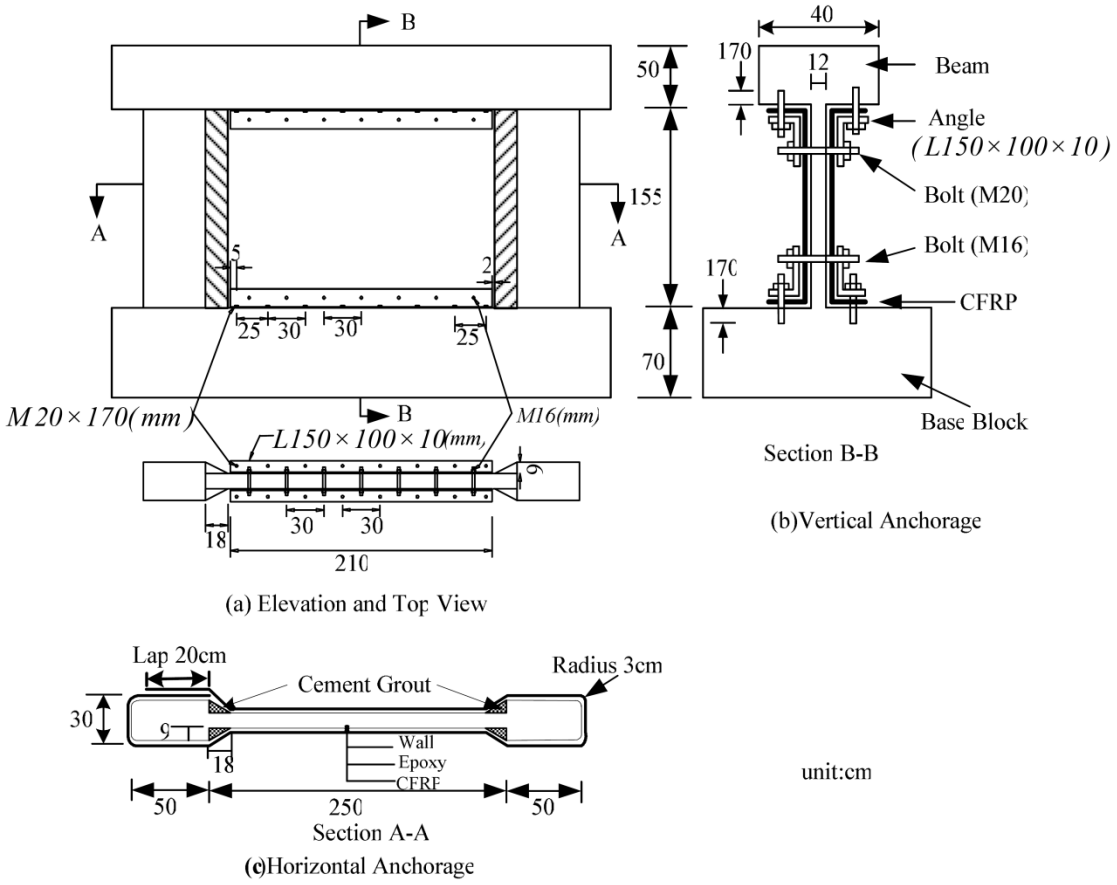

Figure 2.5 Details of the specimens tested by Hwang et al. (2004)

Specimen WF-15 of Hwang et al. (2004) had a structural wall with thickness of 150mm. The vertical and horizontal reinforcements of WF-15 was approximately 0.5% of the wall sross section, which provided a threshold of the qualified wall behaviour. No retrofint system was considered for WF-15. The test results indicated that the CFRP with sufficient end anchorage is an effective retrofitting measure.

A total of 10 shear wall specimens were tested by Elnady (2008) consisted of three control walls CW1 to CW3, and seven rehabilitated walls RW3 to RW9 as a continuation to the works performed by Ghobara and Khalil (2004). The purpose of rehabilitation was stated to be prevention from brittle failure in shear or bond slip and to improve the ductility of the RC structural walls. RW3 to RW5 specimens were repaired after being

tested as control walls CW1 to CW3. The rehabilitation schemes for the specimens tested by Elnady (2008) are listed in table 2-1 and selected specimens are shown in Figure 2.6. The seismic retrofit was involved the use of steel anchor bolts, CFRP wraps, and fillet weld of the lap spliced reinforcement at the base of the wall.

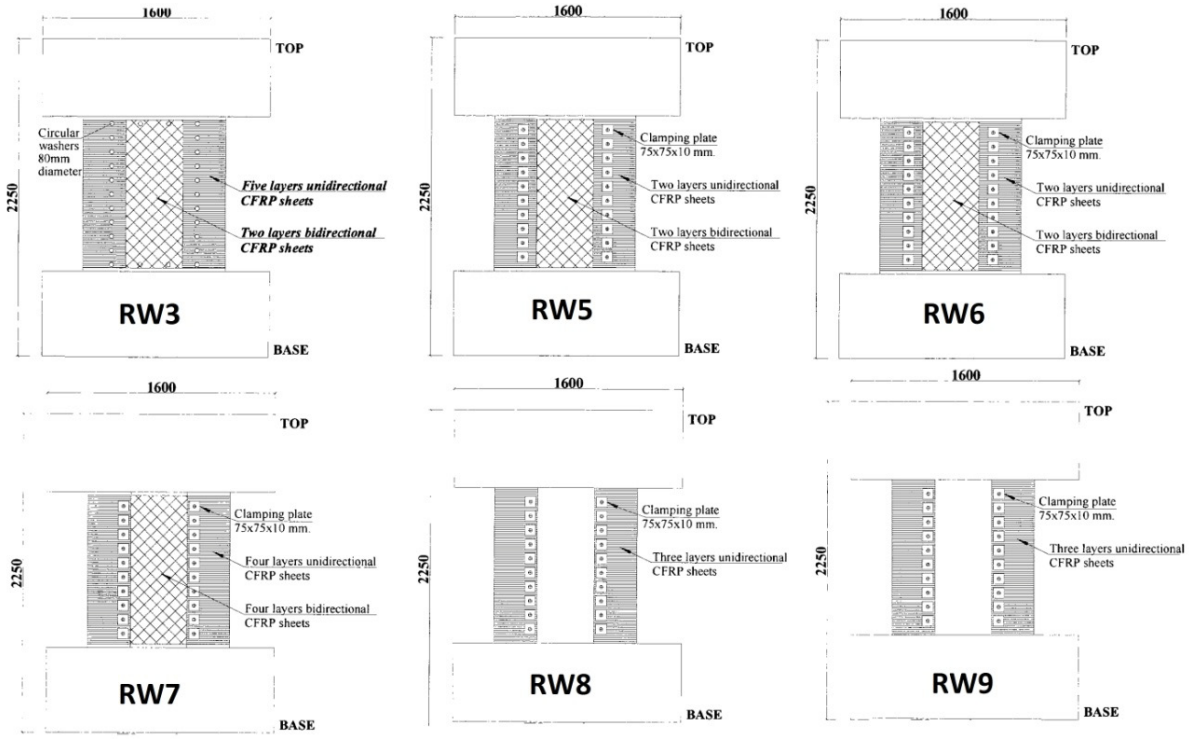

Figure 2.6 Details of selective specimens tested by Elnady (2008)

Elnady (2008) stated that the experimental program was successful in duplicating failure modes observed in earthquakes. Based on the experimental results of Elnady (2008), the moment to shear ratio is a significant factor that affects the behaviour of the structural walls and influences their failure mode, retrofitting the walls using CFRP sheets eliminated the brittle shear failure mode, the CFRP confined end column elements showed a significant contribution to to the tested walls ductile response, and confinement of concrete using steel anchor bolts successfully improved the ductile behaviour.

Table 2.1 Details of the wall specimens tested by Elnady (2008)

Specimen	Steel Reinforcement		Confinement		Shear CFRP layers	Steel anchors
	Flexural	Shear	steel	CFRP layers		
CW2	6-15M	6mm@180mm	-	-	-	-
CW3	6-15M	6mm@180mm	-	-	-	-
RW3	6-15M	6mm@50 mm	6mm@50mm	5	2	12.5@100mm
RW4	6-15M	6mm@100mm	6mm@50mm	2	2	12.5@100mm
RW5	6-15M	6mm@50 mm	6mm@50mm	2	2	12.5@100mm
RW6	8-20M	6mm@100mm	6mm@50mm	4	4	12.5@100mm
RW7	8-20M	6mm@100mm	6mm@50mm	4	4	12.5@100mm
RW8	6-20M	10M@100mm	6mm@50mm	3	-	10.0@100mm
RW9	6-20M	10M@100mm	6mm@50mm	3	-	10.0@100mm

An innovative method of application of FRP to the wall as a retrofit method was announced by Kobayashi (2005) in which bundles of Aramid strands were passed through drilled holes on the walls as sewing paths in cross-diagonal directions. The diagonal cracks were tied with the FRP bands installed in every diagonal two-holes as shown in Figure 2.7.

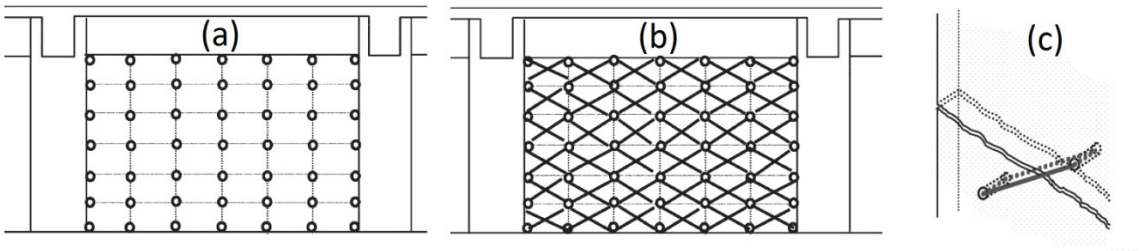

Figure 2.7 Details of retrofit method by Kobayashi (2005) 2 (a) drilled holes (b) FRP bands passed through the holes (c) a sample crack tied with a FRP band

Several advantages were indicated for the proposed method as: no need to wall surface preparation by means of smoothening, and applying epoxy primer; a good anchorage will be provided during this method for the FRP bands to act under tension; and cost reduction considering the amount of materials required for retrofit comared to the wrapping with FRP laminates (Kobayashi, 2005). A total of three specimens were tested

by Kobayashi (2005) in terms of a control wall "W03N" without strengthening, a strengthened wall "W02R" using the proposed method; and a repaired wall "W03N-R" which was previousely tested as the control wall and repaired by removing the crushed parts of concrete and replacing them with new mortar, and strengthened by FRP bands. The results of experimental tests were proofs of effectiveness of the proposed method of strengthening using FRP bands by improving the shear capacity and deformability of the wall panel.

Experimental tests on seismically damaged RC structural walls by Li and Lim (2010) were consisted of a total of four specimens in two main categories of low-rise (LW) and medium-rise (MW) walls with height to width ratio of 1.125 and 1.75 respectively, were tested to failure under a constant axial force applied by two vertical actuators and a quasi-static lateral load history applied by a horizontal actuator. The two low rised specimens "LW2" and "LW3" were of a rectangular 120x1700mm cross section while the two medium rised specimens "MW1" and "MW2" had 300mm thickness with the same width as the "LW" type. For all specimens, the web reinforcement was comprised a double orthogonal grid of 10-mm diameter bars spaced at 250 mm. The boundary elements of the walls were rectangular with 300x150mm sections for all the specimens. After testing the four specimens to failure, heavily cracked and spalled concrete was removed from the base of the walls and replaced by a polymer modified cementicious repair mortar, other significant cracks at the base of the walls were injected with epoxy, and a sealing of epoxy was applied to the remaining cracks. Subsequent to repair, specimens were strengthened with FRP sheets on the surface and U-shaped wrapping of the boundary elements as described in Figure 2.8.

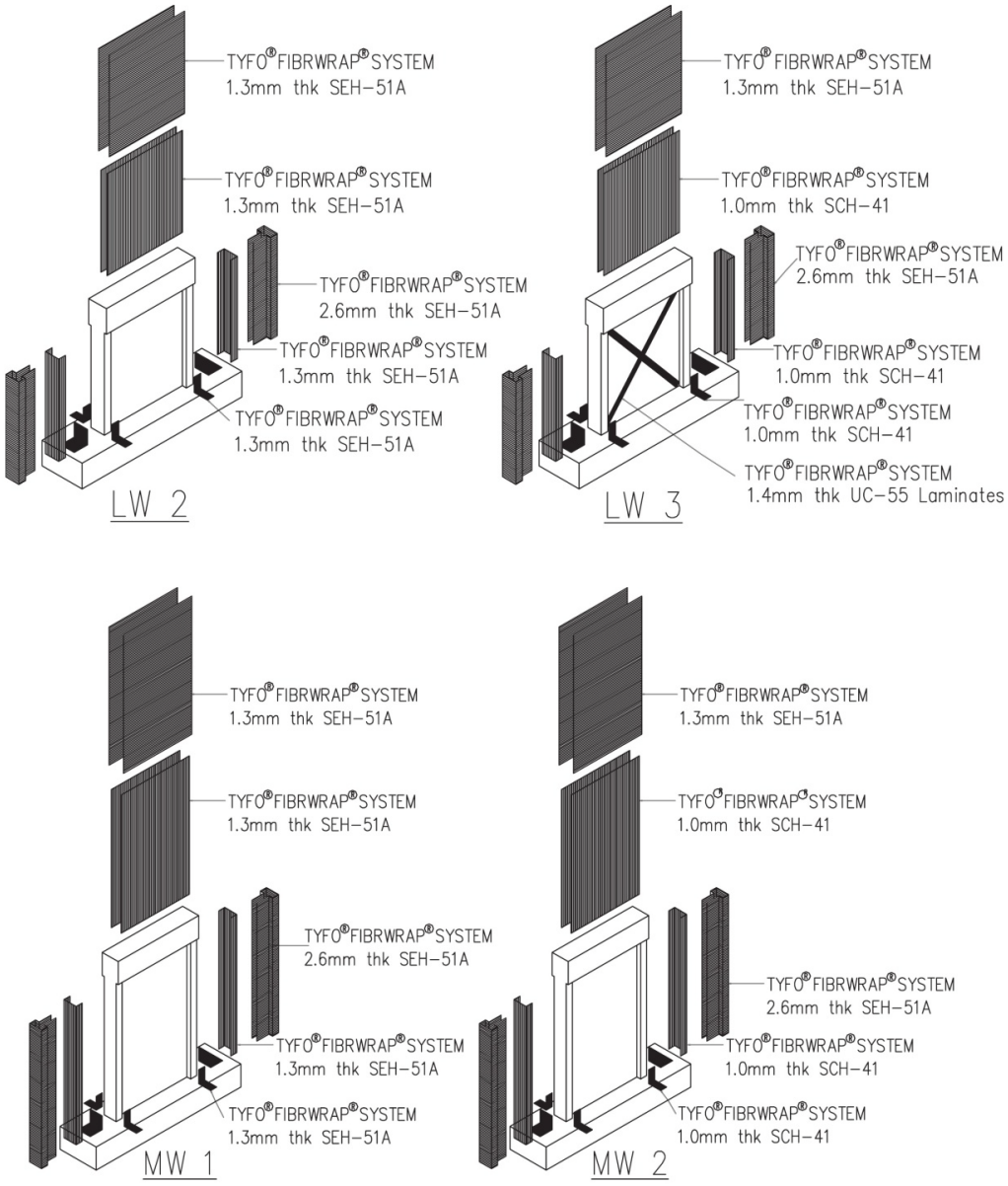

Figure 2.8 Details of specimens and repair schemes tested by Li and Lim (2010)

Li and Lim (2010) indicated that the repair method was not capable of restoring the full stiffness capacity but the specimen strengthened by CFRP exhibitted a better performance regarding the stiffness compared to the GFRP strengthened walls, Also the dissipated energy of the repaired specimens was stated to be significantly larger than those of the original counterparts for both the “LW” and “MW” specimens.

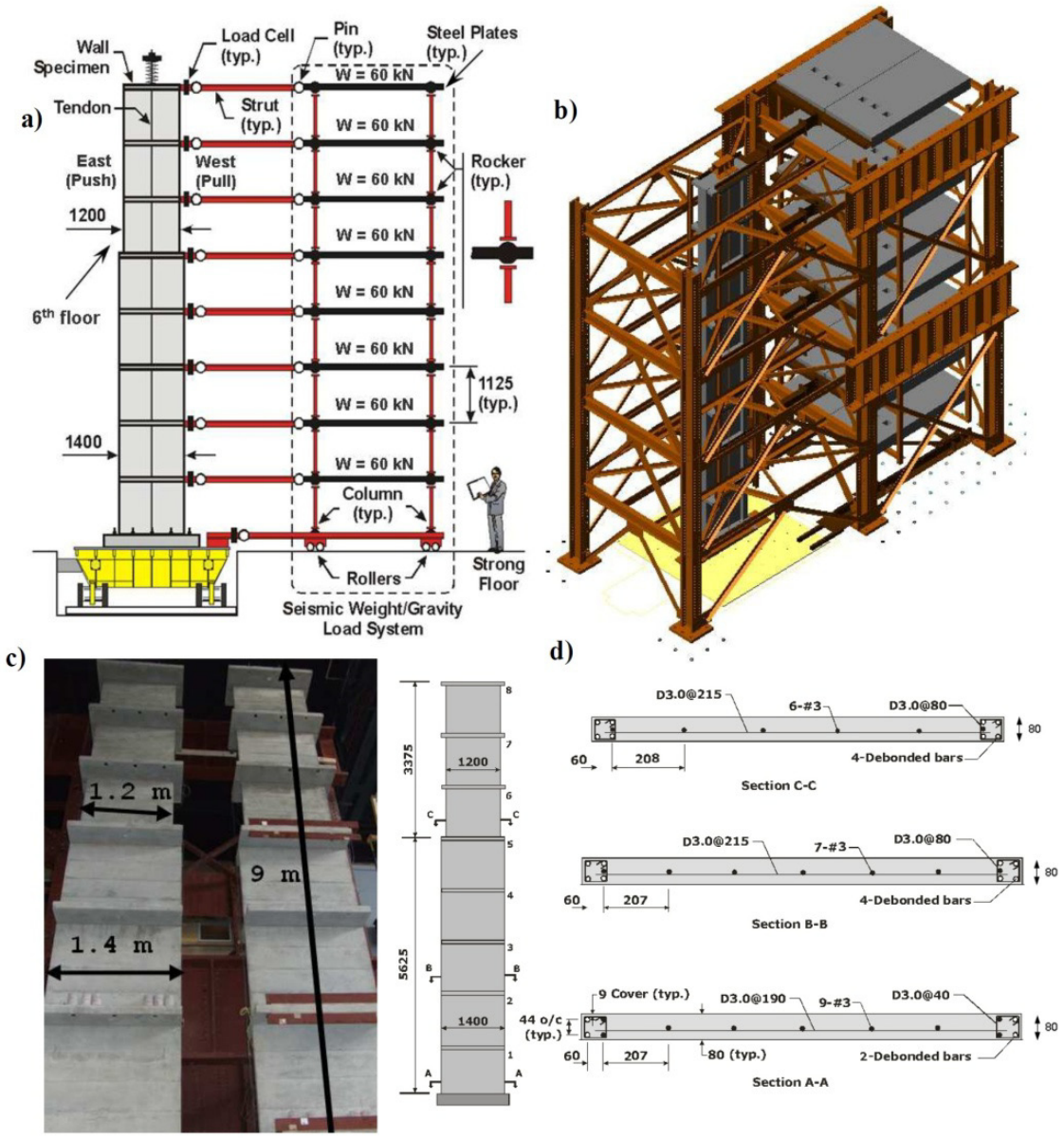

Figure 2.9 Details of the test assembly on the shake table of École Polytechnique de Montreal and the rehabilitated 8-story walls tested in El-Sokkary et al. (2012)

El-Sokkary et al. (2012) studied the effects of rehabilitation of shear walls by CFRP laminates through a shake table test program on two 8-storey cantilevered shear walls of 1:0.429 scale. The program was consisted of testing the walls under several levels of ground motion excitations and then retrofitting the walls using CFRP laminates and

subject them again to the same excitation histories in order to study the effectiveness of the rehabilitation techniques.

The test assembly and specimens details are shown in Figure 2.9. The results of tests on the original walls showed severe inelastic deformations at the 6th storey level due to the effects of higher modes of vibration; also, the base plastic hinge of the walls experienced significant inelastic deformations. A rehabilitation scheme was proposed by El-Sokkary et al. (2012) in order to enhance the overal seismic behaviour of the original walls by strengthening the two locations with nonlinear response.

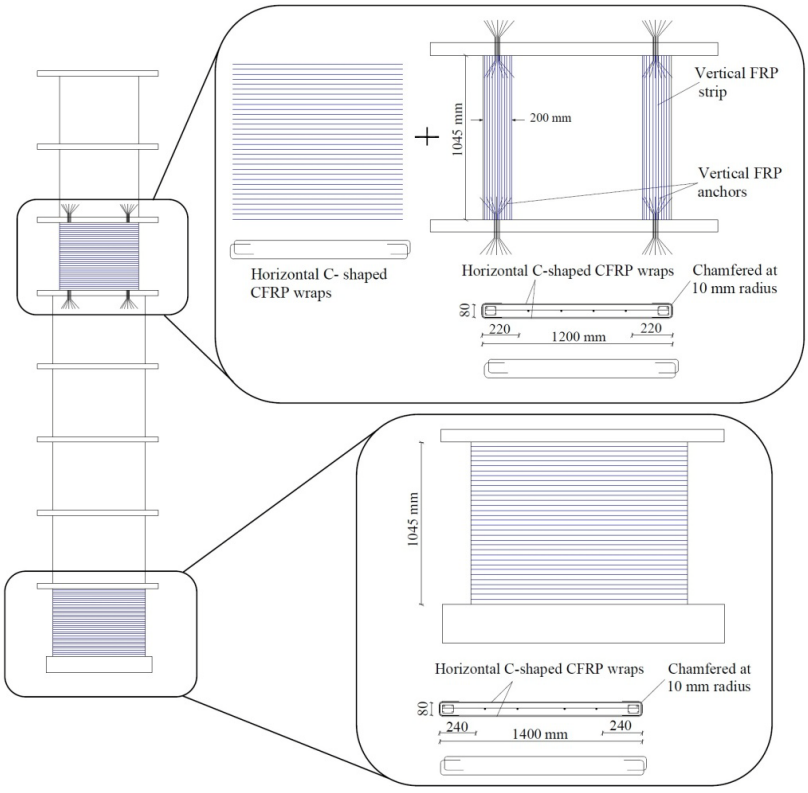

Figure 2.10 Retrofitting schemes for base and 6th storey panels (El-Sokkary et al., 2012)

Since the cause of nonlinear behaviour in the 6th storey was different from the base of the wall, different rehabilitation details were used for these two regions. The base of the wall was rehabilitated using horizontal wraps, only to provide additional confinement to the

boundary zones in order to improve the ductility without increasing the flexural capacity of the wall. The target of rehabilitation at the sixth storey level was to increase the flexural strength of the wall in order to prevent the plastic deformations. The boundary zones of the panel at sixth storey elevation were wrapped by vertical CFRP sheets providing additional flexural strength; also, the shear capacity of the panel was improved by providing horizontal wraps in order to prevent shear failure prior to reach the flexural capacity. Following rehabilitation, the overal performance of the walls was proven to be satisfactorily improved.

El-Sokkary and Galal (2013) continued the research by experimentaly testing a wall panel representing the 6th story of their previous shake table tests under reversed cyclic loading as shown in Figure 2.11.

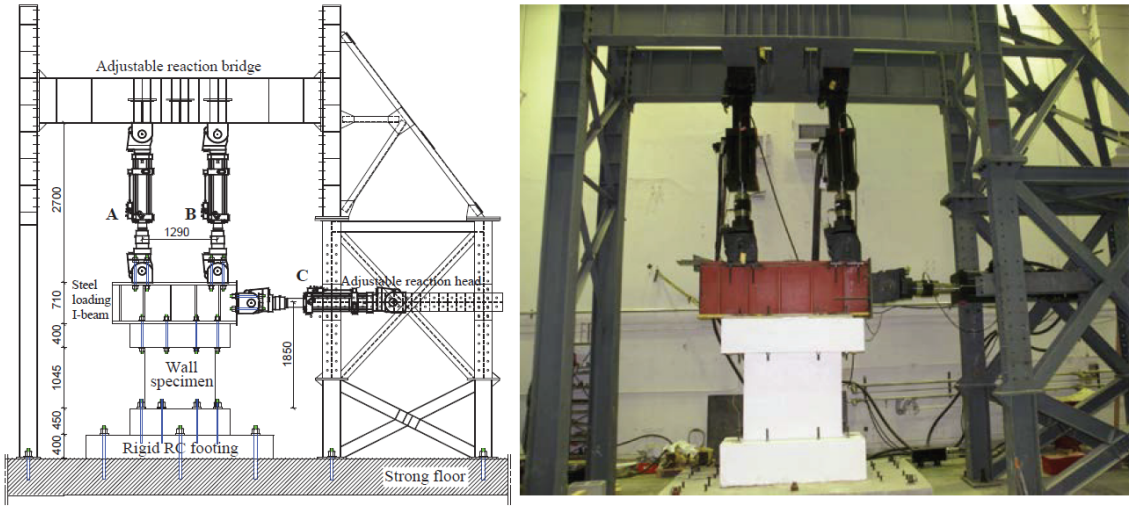

Figure 2.11 Details of the test assembly of the reversed-cyclic tests of El-Sokkary and Galal (2013)

The main intention of the experimental program performed by El-Sokkary and Galal (2013) was to study the effectiveness of CFRP external wraps on increasing the wall's capacity in order to resist the high forces induced due to the higher modes effects. The wall specimens were tested under constant axial load and increasing cycles of

synchronized top moment and lateral load with a top moment-to-shear ratio of 2.75 up to failure. Figure 2.12 shows the two retrofitting methods tested by El-Sokkary and Galal (2013). The first retrofitting scheme was consisted of two layers of uni-directional CFRP sheets applied vertically and anchored to the top and bottom blocks by FRP fan anchors (El-Sokkary et al. 2012) on the edges, above which uni-directional horizontal C-shaped CFRP sheets were applied. The second wall was strengthened by applying X-FRP bracing on the two sides of the wall as shown in Figure 2.12.

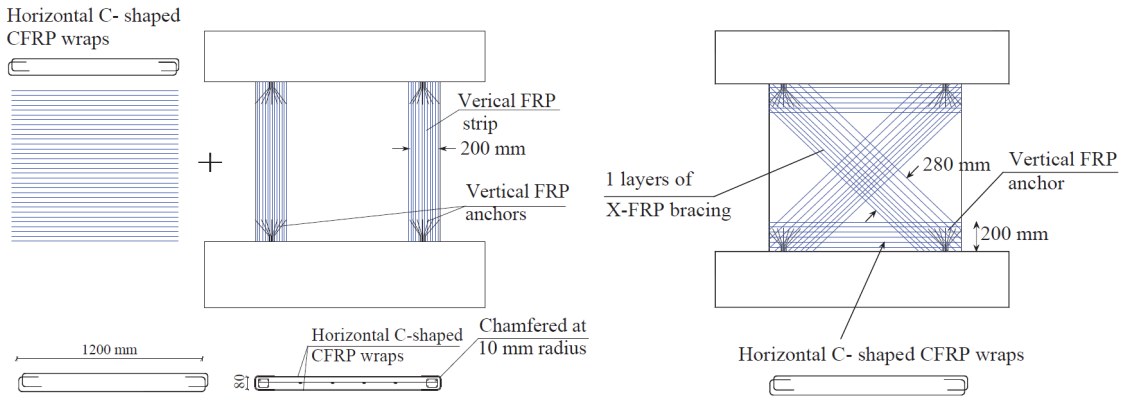

Figure 2.12 Retrofitting schemes for the wall panels tested by El-Sokkary and Galal (2013)

The strengthened wall showed satisfactory performance with improved flexural and shear strengths compared to the control wall but the load and deformability capacities of the two strengthened wall were different due to the nature of cracks propagation based on the orientation of the applied CFRP sheets (El-Sokkary and Galal, 2013).

2.4 RETROFITTING SHEAR WALLS USING FRP: NUMERICAL AND ANALYTHICAL WORKS

Compared to the extensive analytical and numerical research work done on modeling FRP-rehabilitated RC beams and columns, there are only a few numerical investigations on RC shear walls that are available in the literature. Appropriate modeling of a typical

RC shear wall retrofitted with FRP sheets envolves capturing the major characteristics of reinforced concrete, FRP laminates, and bond interface between FRP and shear wall surface. One of the first significant studies on the behaviour of RC shear walls using numerical methods was performed by Sittipunt and Wood (1993) in which a FE modeling approach was developed and verified using available experimental data. They studied the effects of various parameters such as material models and reinforcement arrangement on the cyclic behaviour of RC shear walls. The main effort of the study was on the comparison of various available material models for concrete and steel and initial tests were done in order to use the most useful material models respecting important factors namely; *simplicity*, *stability* and *reliability*. The material model used for concrete was based on the *smeared crack model* with fixed orthogonal cracks using the strength criterion for crack initiation and propagation. Reliability of the material model has been proved through cyclic analysis of slender shear walls and the results were compared to appropriate experimental data.

Li et al. (2005) proposed a nonlinear 3D FE model in order to perform cyclic analysis on an I-shaped wall representing the lower portion of the shear wall system of a 25-story building in Singapore. The geometry of the model was consisted of two flange walls with lenghts of 657mm and one center wall with a length of 955mm and 45mm thickness overall as shown in Figure 2.13. The height of the walls were 1314mm which was equal to 2.6 times the story height of the building in a 1/5 scale.

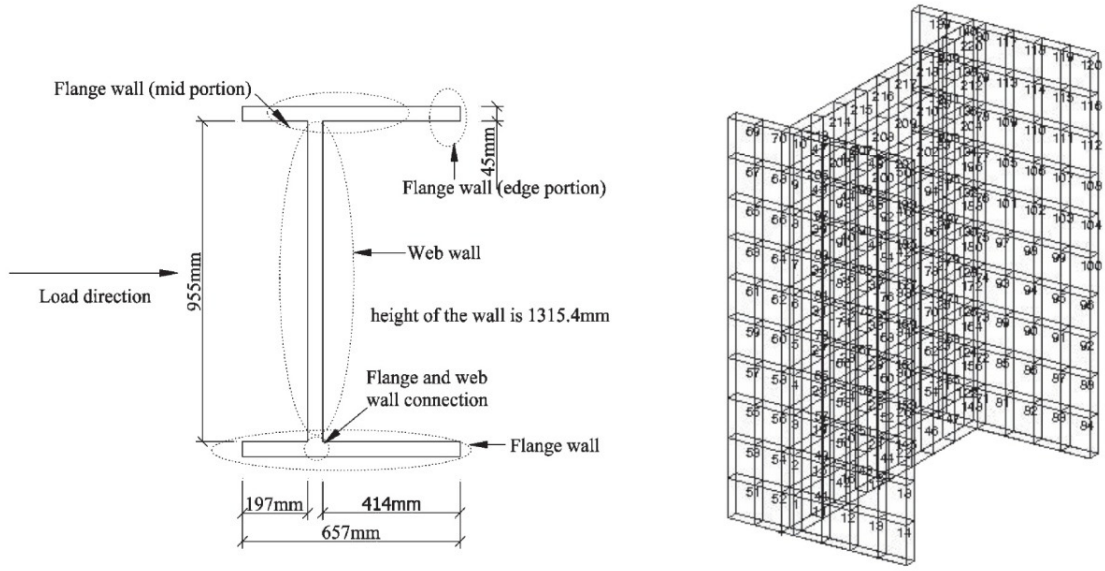

Figure 2.13 Plan view and 3D mesh of the wall model presented by Li et al. (2005)

The wall model mesh was consisted of 220 elements as sketched in Figure 2.13 using 8-node solid brick elements. The reinforcing steel bars were superposed onto the wall by using the smeared rebar option of the concrete element in ABAQUS FE package. The longitudinal reinforcement bars used in the center and flange walls were 8mm and 10mm diameter bars respectively and 6mm bars were used as the horizontal reinforcement in all regions of the model. In order to simulate the effects of GFRP wrapping, a total of 525 constrains were defined using spring elements at the appropriate nodes. The material properties of steel reinforcement bars used in the model were based on elastic perfectly plastic behaviour in both compression and tension with yield stresses 525MPa and 480MPa for the longitudinal bars used in the center wall and flanges respectively and 350MPa for the horizontal bars. The stiffness of the spring elements representing GFRP material was 69.65GPa based on previous experimental tests. The concrete material model used was based on the damaged plasticity model of ABAQUS in which two main

failure modes of cracking under uniaxial tension and crushing under uniaxial compression are defined.

Modelling of RC shear walls using planar elements under reversed cyclic loading was conducted by Palermo and Vecchio (2007) using the modified compression field theory (MCFT) (Vecchio and Collins, 1986) and the distributed stress field model (DSFM) by VecTor2 (Vecchio, 1989) software package. One of the major concerns of the study was covering the stress-strain curve for concrete under compression as well as the hystresis loops in a material model along with the cracking capability of the material. The concrete strength in the models analyzed in the study varied from 21.7 to 53.6 MPa and the authors reported crushing to be the ultimate failure for majority of the wall models. Smeared type of reinforcement were considered assuming the perfectly bonded reinforcement smeared through the concrete ignoring the effects of possible buckling of steel rebar following the concrete crushing. The authors stated that the assumption of full bond between reinforcment and concrete provides satisfactory results. The material properties used for concrete and steel in the study were based on the basic models provided by VecTor2 software package namely a trilinear stress-strain curve for steel which covers the linear elastic region, the yield region, and the strain-hardening zone; an initial stress-stress curve requiring solely the cylinder compressive strength. The information required for the material models to be defined in particular cases were obtained from the experimental data in the literature. A total of five experimentally tested specimens from the literature were modeled under two main categories regarding the wall geometry namely *slender shear walls* with a height-to-width ratio greater than 2.0 and *squat shear walls* with height-to-width ratios smaller than 2.0 by Palermo and Vecchio

(2007). Examples of the FE meshes used in the study are presented in Figure 2.14. Palermo and Vecchio (2007) stated that the models satisfactorily simulated the observed behaviour including peak strength, postpeak response, ductility, energy dissipation, and failure mechanism. The only discrepency which was considered as "noticable" reported to be the displacement corresponding to the peak lateral load.

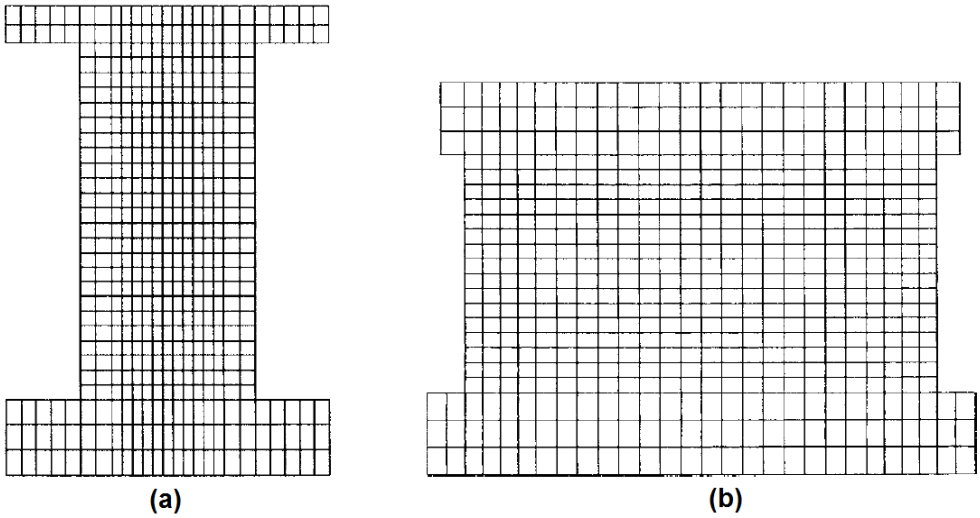

Figure 2.14 FE mesh used by Palermo and Vecchio (2007) (a) slender shear wall (b) squat shear wall

Khomwan et al. (2010) developed a nonlinear FE model for the analysis of RC plane stress members strengthened by FRP external sheets under monotonic and cyclic loading. The bonding interface between FRP and concrete surface was taken into consideration using a two-dimensional membrane contact element in order to capture the debonding failure mechanism at the interface between concrete surface and FRP sheets. The work was consisted of FE modeling of experimentally tested RC beams and shear walls under cyclic loading. Smeared cracking model was used to simulate the mechanical behaviour of concrete material with discrete steel reinforcement bars in order to simulate the experimental works of Lombard et al. (1999) on RC shear walls rehabilitated using

external layers of FRP. The FE mesh used in the study is shown in Figure 2.15. The analysis stated to be capable of approaching the force-displacement of shear walls as well as the failure modes comparing to the respective experimental data within an acceptable margin of error.

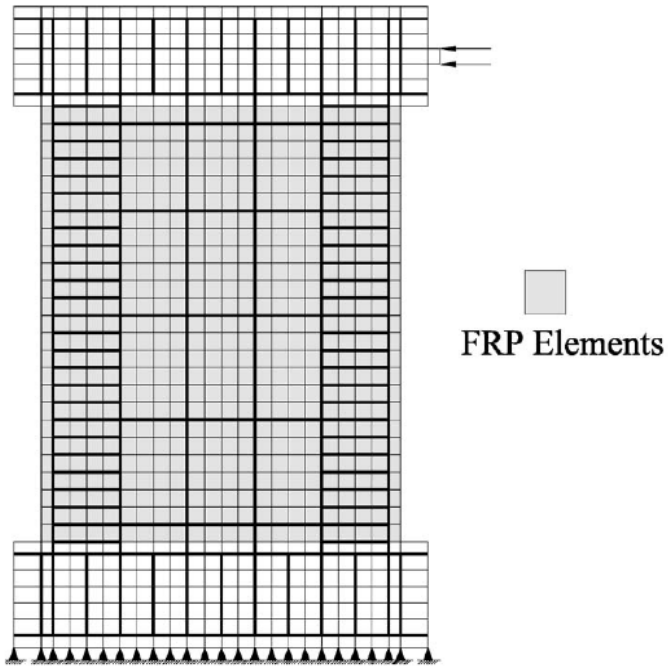

Figure 2.15 FE mesh of RC shear walls modeled by Khomwan et al. (2010)

One of the most recent works on the FE modeling of shear walls retrofitted with externally bonded sheets under cyclic loading has been performed by Cortes-Puentes and Palermo (2012) in which a total four specimens from the experimental literature were analysed using VecTor2 FE package (Wong and Vecchio, 2002) in a 2D planar geometry. Three of the four modeled specimens were consisted of RC shear walls retrofitted using steel plates in various arrangements as well as one to simulate one of the test specimens of Lombard et al. (1999) using a single vertical layer of CFRP bonded to the surface of concrete shear wall on both sides. A minimum of 13 rectangular plane

stress elements in each direction was used in the FE mesh as shown in Figure 2.16 considering the same mesh for the top and bottom blocks as for the main wall region.

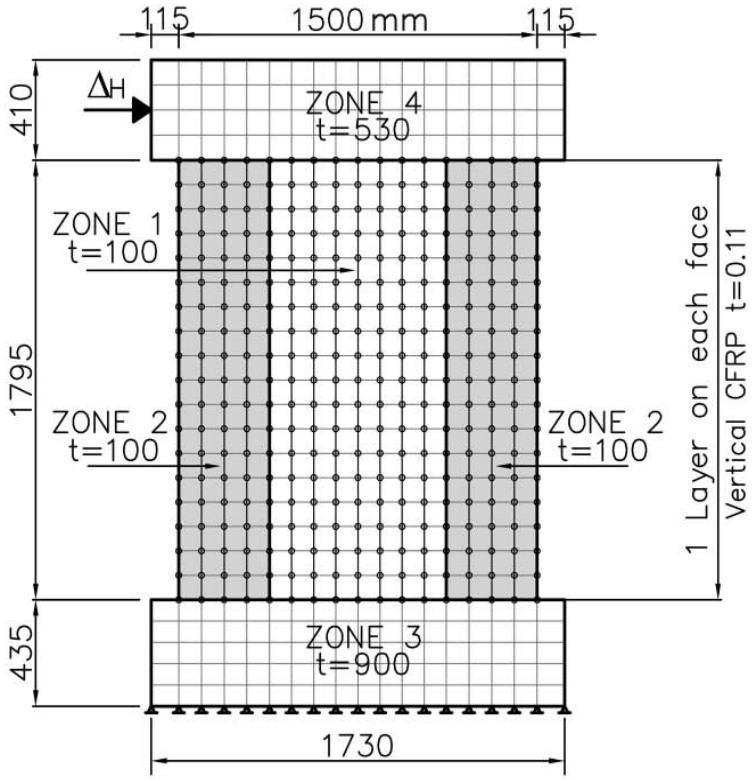

Figure 2.16 FE mesh of the shear wall model by Cortes-Puentes and Palermo (2012)

The smeared cracking model was adopted for the concrete material with uniformly smeared steel reinforcement in different regions of the wall model as well as discrete reinforcement bars and plates in some cases using truss bars with uniform cross-sectional areas. One of the major aspects of the study was stated to be the modelling of bond interface between external reinforcement and concrete using two-node non-dimensional link elements available in the elements library of the software package used. The bond-slip mechanism was modeled based on the fracture energy method as discussed later on in chapter 3. The results of FE modeling stated to be in good agreement with the experimental data.

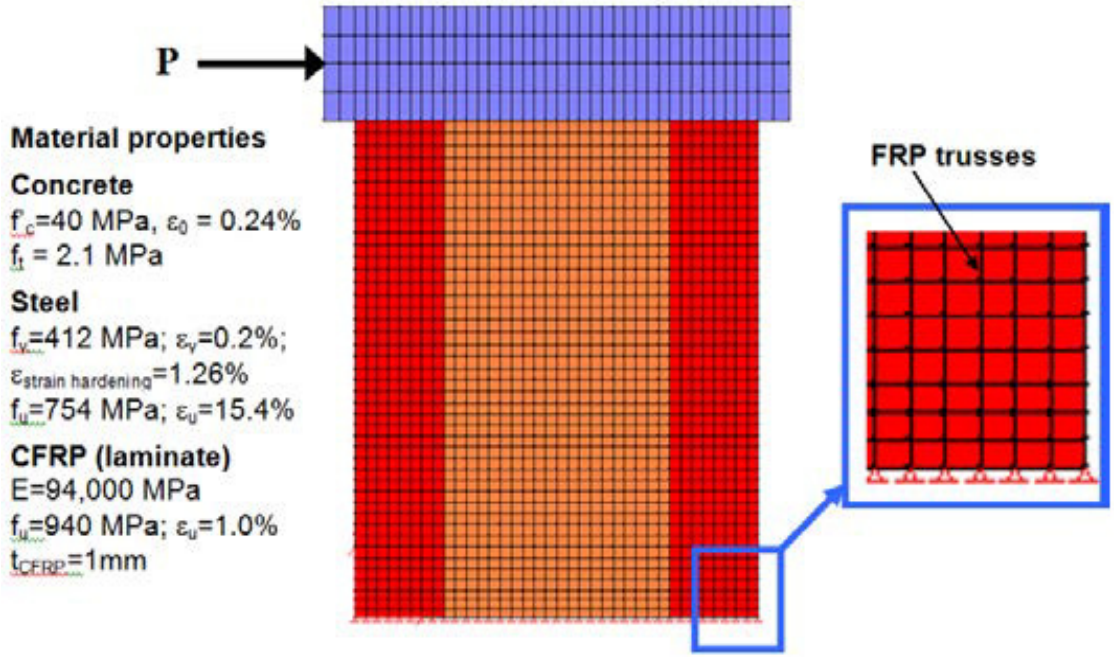

Figure 2.17 FE mesh and material properties used by Cruz-Noguez et al. (2012)

Cruz-Noguez et al. (2012) presented an analytical model for the nonlinear analysis of RC shear walls repaired and strengthened in flexure with externally-bonded FRP sheets. the effects of Intermediate Crack (IC) debonding was taken into account by an interactive analysis approach in which the material properties of concrete and the bonding interface updates as the analysis advances based on the cracks propagation through the thickness of the wall. The IC debonding phenomenon which was previously studied through extensive experimental and analytical works on RC beams is discussed later in chapter 3. Four-node quadrilateral elements were used to model the concrete based on the smeared cracking theory with uniformly smeared reinforcement steel through the wall regions. The bottom block was neglected in the analysis and the base of the wall was considered to be fixed in all directions.

The material model used for steel reinforcement was elastic-plastic with strain hardening and for FRP sheets were presented by a series of discrete truss elements made of a brittle

material with zero compressive strength. The bond-slip relationship between concrete and FRP was modeled by a tri-linear approximation of the IC debonding model proposed by Lu et al. (2005-a). The IC debonding was stated to be of major importance in the behaviour of RC shear walls retrofitted with FRP external layers under cyclic loads. The debonding criterion used was stated to be a simple approach and easy to implement into FE packages where user-defined elements to define the bond-slip model is not available.

CHAPTER 3

ANALYSIS METHODOLOGY

3.1 GENERAL

This chapter describes the FE modeling approach used for the simulation of reinforced concrete (RC) shear walls retrofitted by external layers of fibre-reinforced polymer (FRP) composites and the analysis methodology. The FE models are developed using general purpose finite elements program package ANSYS13.0 (2010). The chapter describes the geometry, meshing, element attributes, materials behaviour, and interface considerations. In order to verify the material models used and failure criteria, pilot analysis on prism models are conducted where necessary.

3.2 MODELING CONSIDERATIONS

3.2.1 Geometry

The geometry of the FE models used in this study consists of typical main parts that form the tested wall specimens in the reported literature. The geometry of specimens in almost all of the reported experimental programs described in the previous chapter consists of three main parts, namely, the loading block, support block, and the main wall region. The loading and support blocks are made of reinforced concrete with additional width and length compare to the main wall region in order to transfer the loads from the loading devices to the wall region without stress concentrations and from the wall region to the supporting floor. Typical wall specimen geometry is shown in Figure 3.1 where B-B, H-

B, T-B, B-T, H-T, T-T, B-W, H-W, and T-W represent the width, height, and thickness of the bottom block, top block, and the wall, respectively.

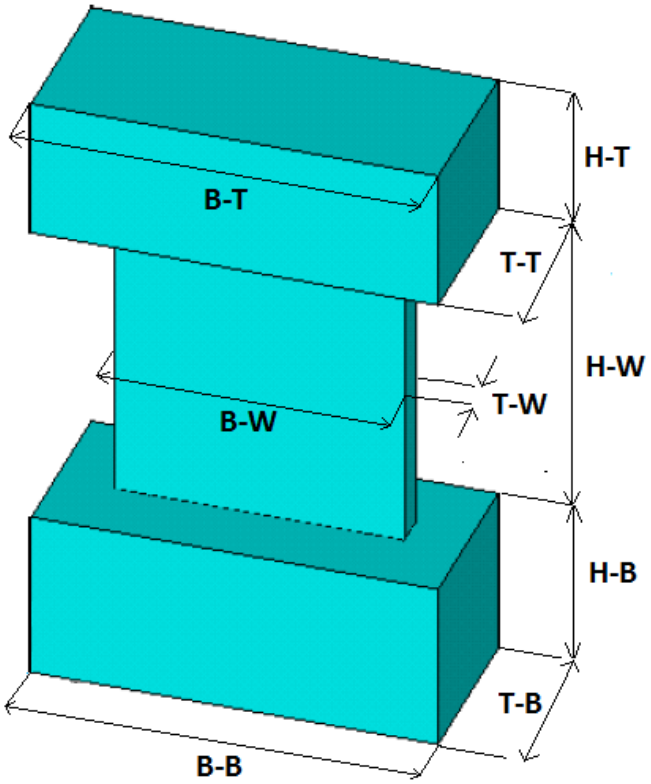

Figure 3.1 Typical geometry of a wall specimen

In case of simulating a test setup, the model must contain the effects of all parts of the model shown in Figure 3.1 in order to achieve an accurate estimation of the actual behaviour of a specimen while the use of geometric symmetry decreases the number of elements and analysis time without significantly affecting the results of the analysis.

3.2.2 Material models

The material properties considered in the modeling have the most significant effect on the results of simulation. In case of modeling a FRP-retrofitted RC shear wall specimen, there are four main material models to be considered namely, concrete, steel, FRP composite, and the bond interface between FRP and concrete surface where the latter two

models do not exist in the modeling of existing shear walls. ANSYS offers an extensive materials library to simulate the behaviour of various materials based on the mechanical stress-strain relationship and other phenomena (ANSYS, 2010-a).

3.2.2.1 Steel reinforcement

A variety of different material models is available in case of modeling steel rebar based on the stress-strain relationship of steel under monotonic and cyclic loading. A typical stress-strain relationship of steel reinforcement consists of an elastic range, a yield plateau, a strain-hardening region, and a load reversal part as shown in Figure 3.2.

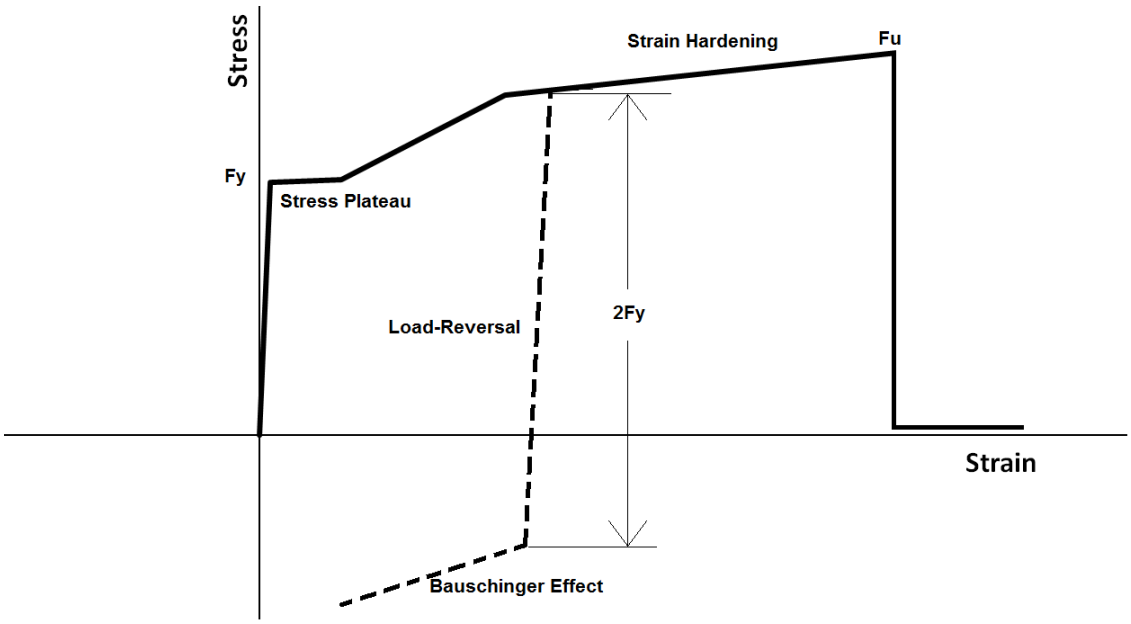

Figure 3.2 Reinforcing steel stress-strain relationship

In cases of very simple analysis e.g. linear static, only the initial modulus of elasticity, Poisson's ratio, and a yield stress are required as the properties of the material model while for more sophisticated problems, more parameters must be defined in terms of a material model (Sittipunt and Wood, 1993). The reinforcing steel material has a significant effect on the overall response of the RC shear wall to cyclic loading; hence,

the proposed material for steel reinforcement must be precise enough with considerations of all the important aspects of the actual stress-strain relationship without increasing the analysis time by adding unnecessary parameters into the model. Although several material models are available in the materials library of ANSYS, a bilinear isotropic type of behaviour with an initial modulus of elasticity, a yield stress limit, and a strain hardening was commonly used in most of the previous numerical studies (Kachlakev, 2001), (Jia, 2003), (Wolanski, 2004) and (Britton, 2010). The Material model used in the simulations of this study follows a Multilinear-kinematic behaviour which is suggested by ANSYS (2010-b) as the appropriate model for cyclic analysis. A pilot model of a steel bar was simulated here in order to check the cyclic behaviour of this material model under a simple cyclic load history as shown in Figure 3.3 and the force-displacement curve is plotted in Figure 3.4. The ultimate failure of steel is defined as a rupture point in which the strain will continue to increase and the stress approaches to a value close to zero.

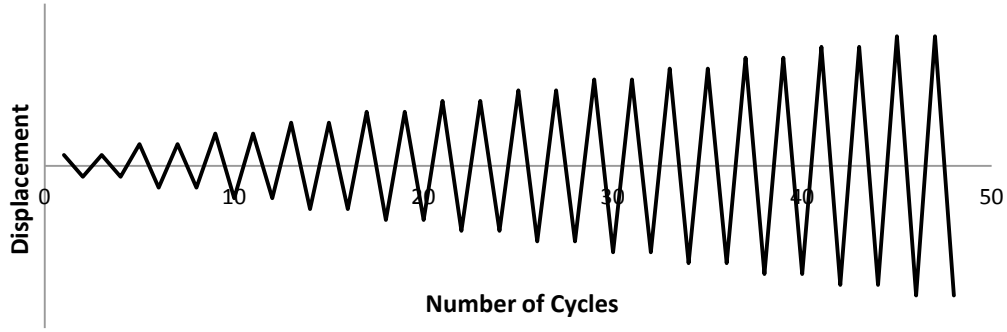

Figure 3.3 Cyclic loading history applied to the prism model for steel material

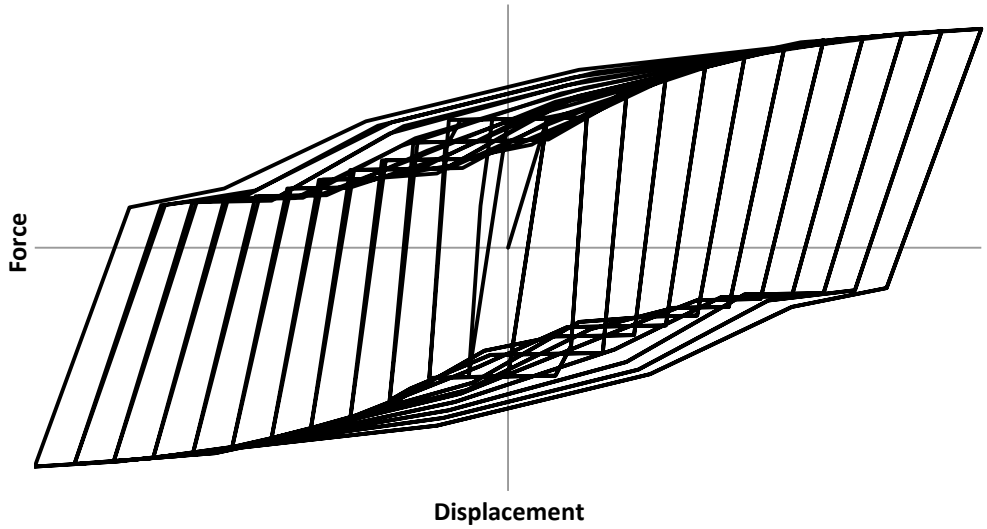

Figure 3.4 Load-Displacement of a steel prism under cyclic loading

3.2.2.2 Concrete

Due to the nature of concrete material which is a mixture of aggregates with different sizes and mechanical properties and a cement paste with certain strength, the compressive stress-strain curve follows a nonlinear pattern in which the modulus of elasticity and yield stress are not as clear as in steel material. As a theoretical definition, the initial slope of the stress-strain curve defines the modulus of elasticity; however, this *initial tangent modulus of elasticity* is not often calculated for the analysis and design purposes since it only covers a very short range of stresses and strains in the beginning of loading. On the other hand, a *secant modulus of elasticity* at any point on the stress-strain curve is defined as the slope of a line from the origin to that point. In order to get to a practical definition for the modulus of elasticity of concrete, it is common to calculate the secant modulus at the point corresponding to $0.4f'_c$ for the design purposes where f'_c is the 28-day characteristic compressive strength driven from specific strength tests (FIB, 2010). Several equations are offered by various references in order to calculate the modulus of elasticity of concrete based on the latter definition namely,

$$E_c = \left(3300\sqrt{f_c'} + 6900\right) \cdot \left(\frac{\gamma_c}{2300}\right)^{1.5} \quad \textit{(Paulay and Priestley, 1992)} \qquad \textit{(Eq. 3.1)}$$

Where E_c and f'_c are in MPa and γ_c is the density of concrete in kg/m^3. A simplified equation (Eq. 3.2) is used by the Canadian Standards Association (CSA) which is based on Eq. 3.1 and could be used for *normal strength concrete* with a compressive strength ranging between 20 and 40 MPa (CSA-A23.3, 2008)

$$E_c = 4500 \cdot \sqrt{f_c'} \qquad \textit{(CSA-A23.3, 2008)} \qquad \textit{(Eq. 3.2)}$$

The value of E_c resulted from Eq. 3.1 or Eq. 3.2 estimates the modulus of elasticity of concrete regardless of the types of aggregates and tends to be overestimating; however, the initial tangent modulus could be estimated by a 10% increase in the value of E_c from Eq. 3.1 (Wight and MacGregor, 2011). FIB (2010) takes into account the effects of aggregates strength by using the following equation in which α_E represents the effect of aggregate type on the modulus of elasticity

$$E_{ci} = E_{co} \cdot \alpha_E \left(\frac{f_c' + \Delta_f}{10}\right)^{\frac{1}{3}} \qquad \textit{(FIB, 2010)} \qquad \textit{(Eq. 3.3)}$$

Where E_{ci} and f'_c are in MPa, Δ_f is 8MPa, E_{co} is 21500MPa and the value of α_E must be driven from the appropriate tests on the aggregates which could be found for a number of commonly used aggregates in Table 3.1.

As could be seen in Table 3.1, the value of modulus of elasticity is very sensitive to the aggregates type and could be changed by up to 50% only by changing the type of aggregates.

Table 3.1 Effect of aggregates type on the modulus of elasticity of concrete (FIB, 2010)

Types of aggregate	α_E	$E_{co}.\alpha_E$ [MPa]
Basalt, dense limestone aggregates	1.2	25800

Quartzite aggregates	1.0	21500
Limestone aggregates	0.9	19400
Sandstone aggregates	0.7	15100

The value achieved from Eq. 3.3 for the modulus of elasticity of concrete represents the initial tangent modulus which is higher than those driven from Eq. 3.1 and Eq. 3.2 for most of the aggregate types. A reduced modulus of elasticity is suggested by FIB (2010) for the purpose of design where a concrete structure is analysed only using an elastic analysis method. The possible irreversible deformations caused by initial plastic strains are taken care of by using the following equation for the calculation of modulus of elasticity.

$$E_c = \alpha_i \cdot E_{ci} \quad \textit{(FIB, 2010)} \qquad \textit{(Eq. 3.4)}$$

Where:

$$\alpha_i = 0.8 + 0.2\frac{f_c' + \Delta_f}{88} \leq 1.0 \quad \textit{(FIB, 2010)} \qquad \textit{(Eq. 3.5)}$$

The secant modulus of elasticity resulted from three latter equations is calculated for various values of f'$_c$ and listed in Table 3.2.

Since the values in Table 3.2 are reduced in order to take into account the effects of plastic strains in linear analysis, the initial tangent modulus for various values of f'$_c$ is also calculated in order to use in the nonlinear analyses of the present study and listed in Table 3.3. Values of modulus of elasticity from Eq. 3.1 are in compliance with those resulted from Eq. 3.3 if limestone is considered to be the main type of aggregate for the concrete material based on tables 3.2 and 3.3.

The Poisson's ratio of concrete varies between 0.14 and 0.26 for a range of tensile and compressive stresses between $0.6f'_c$ and $0.8f_t$ (FIB, 2010), the estimation of ν_c=0.2 is suggested by most of the references.

Table 3.2. Secant modulus of elasticity (E_c) of concrete for various strengths [MPa]

	α_i	f'_c [MPa]					
		20	25	30	35	40	45
Eq. 3.1	N/A	23086	24943	26621	28165	29602	30951
Eq. 3.2	N/A	20125	22500	24648	26622	28460	N/A
Eq. 3.3	1.2	31405	33610	35686	37663	39565	41404
	1	26171	28008	29738	31386	32971	34504
	0.9	23554	25207	26764	28248	29673	31053
	0.7	18320	19606	20817	21970	23079	24153

Table 3.3. Tangent modulus of elasticity (E_{ci}) of concrete for various strengths [MPa]

	α_i	f'_c [MPa]					
		20	25	30	35	40	45
Eq. 3.1	N/A	25394	27437	29283	30981	32562	34046
Eq. 3.2	N/A	22137	24750	27112	29285	31307	N/A
Eq. 3.3	1.2	36364	38411	40261	41954	43521	44983
	1	30303	32009	33551	34962	36268	37486
	0.9	27273	28808	30195	31466	32641	33737
	0.7	21212	22407	23485	24473	25387	26240

The uniaxial compressive stress-strain curve for the models of the present study is based on the *Modified Hognestad* model in which an initial strain ε_0 is defined in Eq. 3.6 based on the values of f'_c and E_{ci} and the stress at each point of the curve is calculated using the initial and previous points on curve using Eq. 3.7 (Hognestad, 1951).

$$\varepsilon_0 = \frac{2f'_c}{E_{ci}} \qquad \textit{(Eq. 3.6)}$$

$$f = \frac{E_{ci}\varepsilon}{1+\left(\varepsilon/\varepsilon_0\right)^2} \qquad \textit{(Eq. 3.7)}$$

The stress-strain curves are generated for a variety of compressive strengths using Eq. 3.7 and plotted in Figure 3.5.

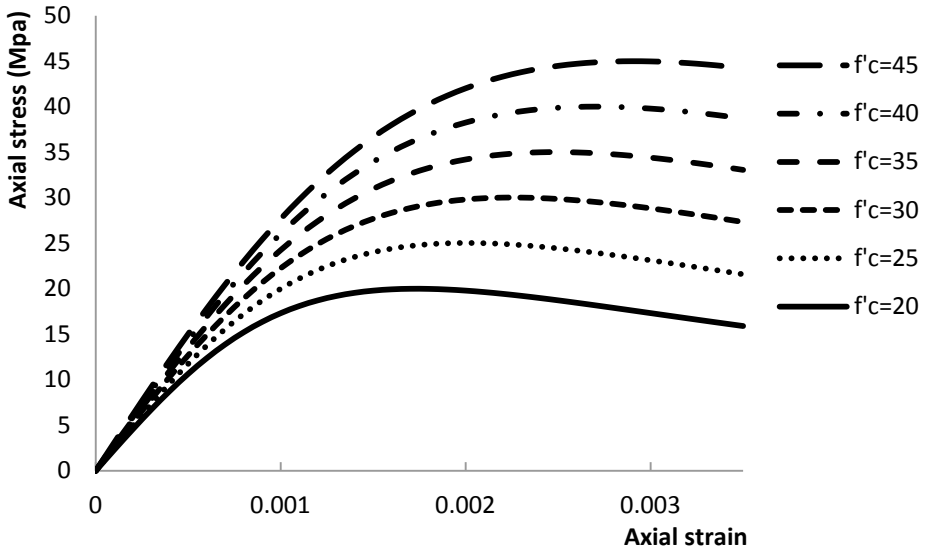

Figure 3.5. Compressive stress-strain curves for concrete with various strengths

Although concrete material is mainly characterized as "compressive", the tensile strength has to be taken into account in the analysis of RC members. The term "tensile strength" is mainly referred to the uniaxial tensile strength in MPa in this study. The most accurate way of achieving tensile strength, f_t, is experimental testing; however, FIB (2010) provides a range for the tensile strength based on the compressive strength namely,

$$f_{tm} = 0.3 \cdot (f_c')^{\frac{2}{3}} \qquad [f'_c \leq 50\ MPa] \qquad (Eq.\ 3.8)$$

$$f_{tm} = 2.12 \cdot ln\left(1 + 0.1 \cdot \left(f_c' + \Delta_f\right)\right) \qquad [f'_c > 50\ MPa] \qquad (Eq.\ 3.9)$$

The value of f_{tm} obtained from Eq. 3.8 or Eq. 3.9 is the mean value for the range of tensile strength. The lower and upper bound values for the tensile strength are estimated to be 70% and 130% of the mean value respectively as suggested by FIB (2010). A plot of the tensile strength range for a variety of compressive strengths is shown in Figure 3.6 based on Eq. 3.8 and Eq. 3.9.

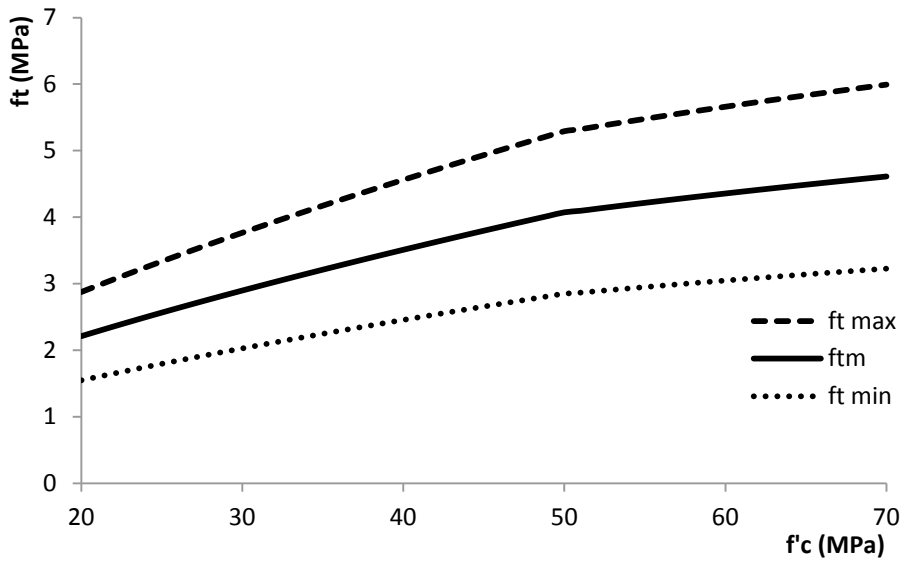

Figure 3.6. Range of tensile strength based on compressive strength for concrete

When concrete is subjected to tensile stresses, cracking occurs in the material. The energy required for a tensile crack of unit area to be propagated is the *fracture energy*. FIB (2010) formulates the fracture energy based on the compressive strength of concrete namely,

$$G_F = 73 \cdot f_{cm}^{0.18} \qquad \textit{(FIB, 2010)} \qquad \textit{(Eq. 3.10)}$$

In which f_{cm} is the mean compressive strength of concrete in MPa calculated from Eq. 3.11 and G_F is the fracture energy of concrete in N/m.

$$f_{cm} = f_c' + \Delta_f \qquad \textit{(FIB, 2010)} \qquad \textit{(Eq. 3.11)}$$

The state of stress in concrete elements is not uniaxial for most of the structures. When an element is subjected to stress in two mutually perpendicular directions, the state of stress will become *biaxial*. Although a pure biaxial state in which the stress in a third direction is zero tends to be rare, many elements exhibit a stress state very close to biaxial in which the amount of stress in a third direction is negligible compared to any other two

directions e.g. web of deep beams, shear walls, etc. as shown in Figure 3.7 for three cases of the stress state in the third direction namely, $\sigma_{zp}>0$, $\sigma_{zp}<0$ and $\sigma_{zp}=0$ where the latter case represents a pure biaxial state.

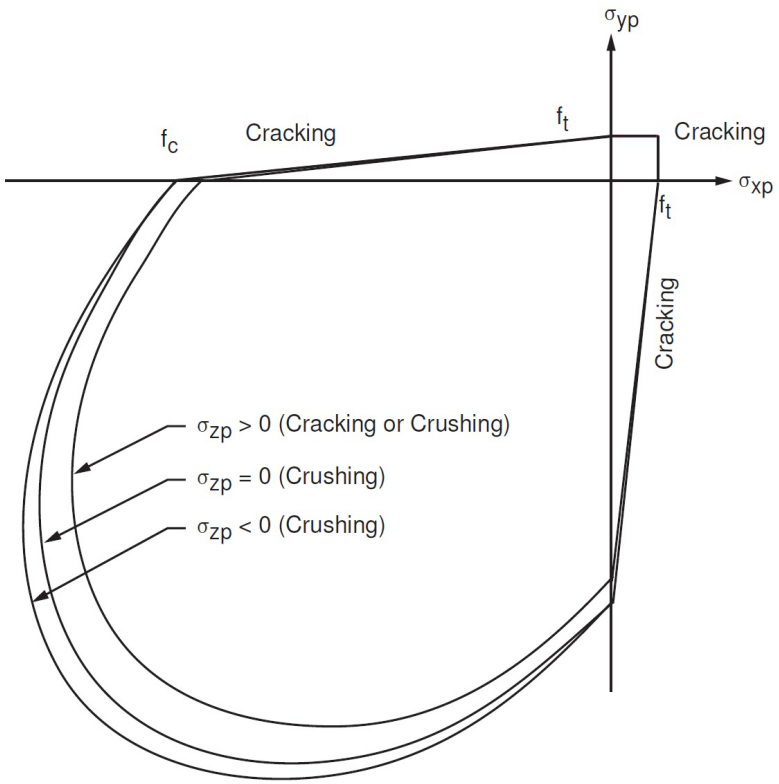

Figure 3.7. Concrete failure mode under nearly biaxial stress state (ANSYS, 2010-b)

The cracking and crushing of concrete occurs based on the state of stress in the three directions. If the stresses in two directions are zero, a uniaxial behaviour is expected based on the previously discussed equations. If tensile stresses apply to concrete in both X and Y directions, cracking will occur in both XZ and YZ surfaces regardless of the stress in Z direction and the failure stress is slightly higher than the uniaxial state of stress; if compressive stress applies in one direction (X or Y) and tensile in the other direction, cracking will occur in the surface perpendicular to the tensile stress regardless of the stress in third direction. The other case would be a state in which compressive stresses are applied in X and Y directions which leads to higher failure stresses but the

type of failure depends on the stress in Z direction; if tensile stress is applied in Z direction, the failure mode would be cracking in XY surface or crushing depending on the significance of stress in Z direction, if no tensile stress is applied in Z direction, the mode of failure is crushing.

Based on the above statements, a nonlinear material model is defined for concrete in the present study which is a combination of three material models namely:

- Linear Elastic model; to represent the initial slope of the stress-strain curve as a start point for the analysis with a modulus of elasticity and a Poisson's ratio.
- Multi-linear inelastic model; to represent the compressive stress-strain relationship as a curve with a certain number of points based on experimental data or verified equations as discussed earlier.
- Smeared cracking and crushing model; to add a certain cracking and crushing limit under tensile and compressive stresses respectively onto the Multi-linear inelastic model. The cracking, crushing and other parameters used in order to define the concrete behaviour are discussed later on.

If the cracking and crushing are ignored in the analysis, the material follows a multi-linear isotropic behaviour and any element reaches the ultimate stress induced in Eq. 3.7 is considered as "failed" and the procedure continues until the structure becomes statically unstable. A pilot model is used in order to check the material models used to define the failure criteria of concrete in this study. The model consists of a concrete block with unit dimensions under a uniaxial loading protocol shown in Figure 3.8.

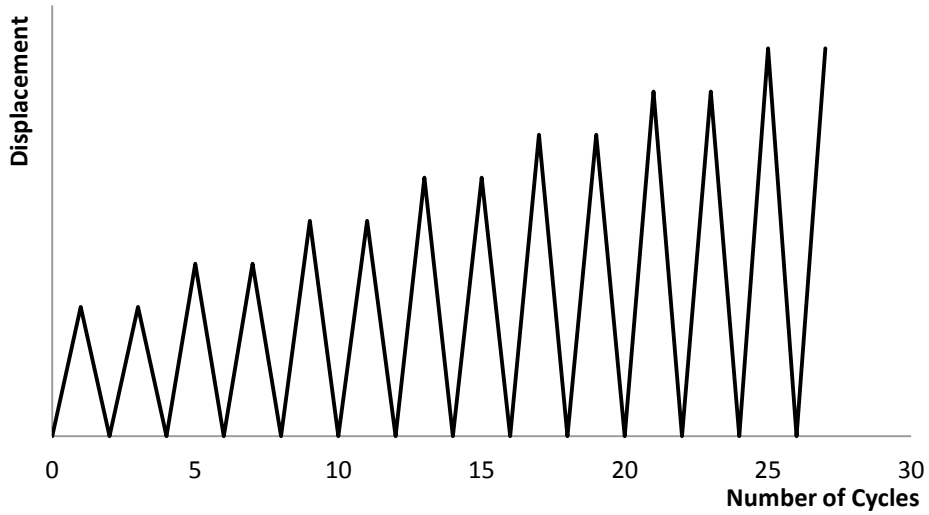

Figure 3.8. Cyclic load history applied to the test prism model for concrete material

If the concrete model which contains the cracking, crushing and other failure criteria parameters related to concrete is excluded from the model, the output for stress-strain curve of the model would be as per Figure 3.9.

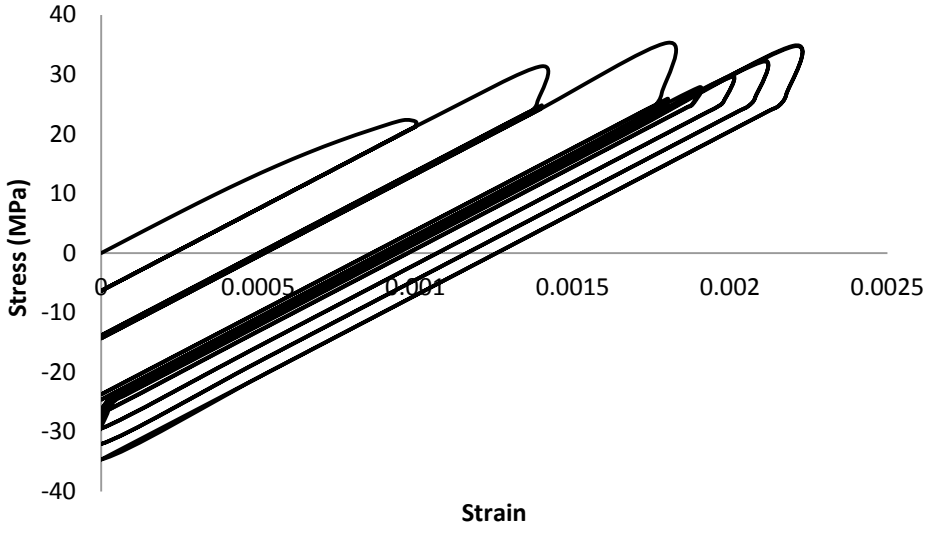

Figure 3.9. Stress-strain output for concrete prism model excluding smeared cracking material model

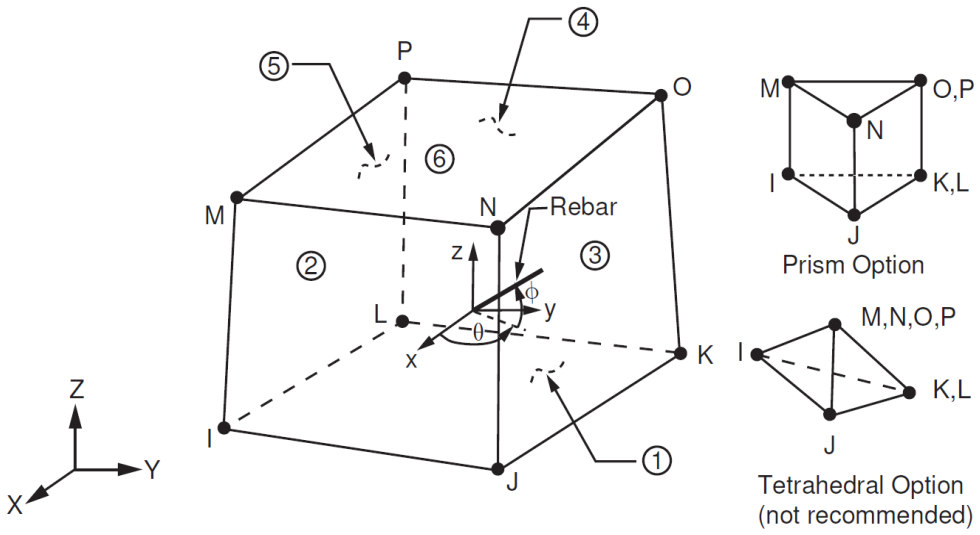

Figure 3.10. Geometry of a SOLID65 element (ANSYS, 2010-a)

There are 9 constants to be defined for a concrete smeared cracking material model namely;

- Open shear transfer coefficient (β_t)
- Closed shear transfer coefficient (β_c)
- Uniaxial cracking strength (f_t)
- Uniaxial crushing stress (f'_c)
- Biaxial crushing stress (f_{cb})
- Ambient hydrostatic stress state (σ_h^a)
- Biaxial crushing stress under the ambient hydrostatic stress state (f_1)
- Uniaxial crushing stress under the ambient hydrostatic stress state (f_2)
- Tensile cracking stiffness factor (T_c)

The presence of a crack at an integration point of SOLID65 element shown in Figure 3.10 is represented through modification of the stress-strain relations by introducing a plane of

weakness in a direction normal to the crack face which effectively considers the crack to be smeared through the element rather than being discrete at a certain location. Also, a shear transfer coefficient β_t is introduced which represents a shear strength reduction factor for those subsequent loads which induce sliding (shear) across the crack face. When an element reaches the uniaxial tensile strength f_{ct} in any of the three main directions at an integration point, the crack opens and the stress in that direction reduces by the tensile stress relaxation factor T_c (proposed default value=0.6) and stress diminishes to zero at a strain six times the cracking strain ε^{ck} (by default), while the stiffness of the element is defined by a secant modulus R^t at any stress between $T_c f_t$ and zero during the diminishing phase as shown in Figure 3.11. When a crack closes, the compressive strength of the element is restored to the pre-cracked situation and all compressive stresses normal to the crack plane are transmitted across the crack, but a shear transfer coefficient β_c is used for the shear strength of the cracked-closed element. There are 16 possible scenarios for the combination of opened and closed cracks at every integration point taking into account the possibility of crack closure since cracking might occur in three planes at any of the eight integration points of a SOLID65 (I, J, K, L, M, N, O, P) shown in Figure 3.10 (Hognestad, 1951). For more information on the possibility and type of output in any of the 16 combinations refer to (ANSYS, 2010-a) and (ANSYS, 2010-b).

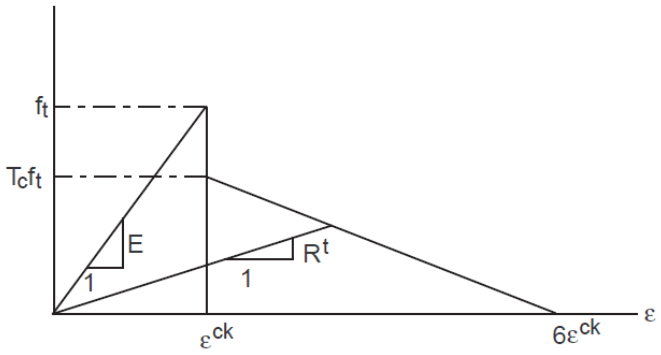

Figure 3.11. Strength of a cracked section (ANSYS, 2010-b)

However, the latter four constants of the smeared cracking model for concrete should be obtained from specific experimental tests (ANSYS, 2010-a); default values could be used from the following equations in situations with a low hydrostatic stress component (Willam and Warnke, 1975):

$f_{cb}=1.2f_{ck}$ *(Eq. 3.12)*

$f_1=1.45f_{ck}$ *(Eq. 3.13)*

$f_2=1.725f_{ck}$ *(Eq. 3.14)*

A low hydrostatic stress state is a case where:

$$|\sigma_h| \leq \sqrt{3} f_c' \qquad \textit{(Eq. 3.15)}$$

If the material at an integration point fails in uniaxial, biaxial, or triaxial compression, the material is assumed to crush at that point. In ANSYS, crushing is defined as the complete deterioration of the structural integrity of the material (e.g. material spalling) and material strength is assumed to have degraded to an extent such that the contribution to the stiffness of an element at the integration point can be ignored. In order to avoid divergence of analysis, a negligible value (e.g. $f'_c \times 10^{-6}$) is defined as the strength of the material at any crushed integration point (ANSYS, 2010-a). The value of β_t is suggested

to be between 0.1 and 0.3 by Kachlakev and Miller (2001) based on pilot modelings on the effectiveness of each parameter of smeared cracking material model of ANSYS. The value of β_c is also suggested by the same authors to be close to 1.0.

The same prism model which was analyzed earlier without taking into account the concrete smeared cracking model is analysed again including the latter model and the output data as stress-strain curve is presented in Figure 3.12.

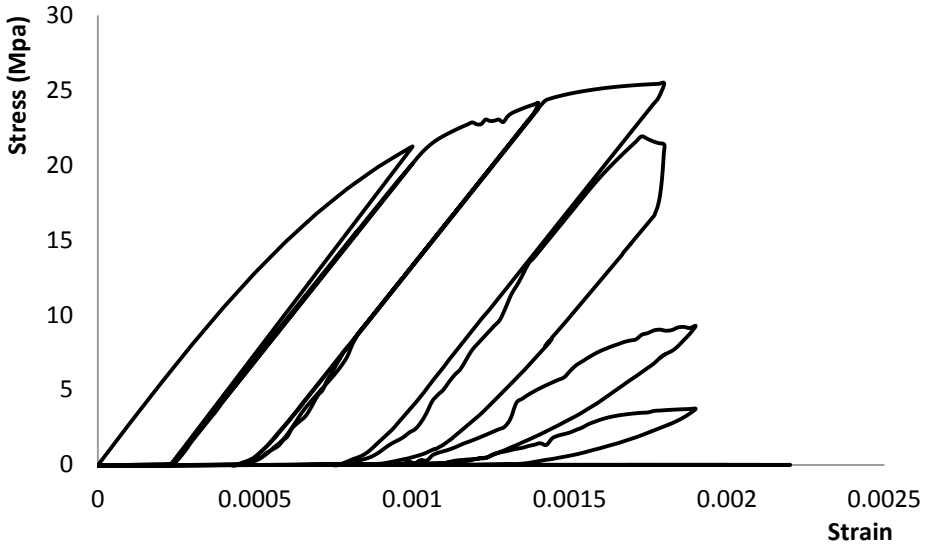

Figure 3.12. Stress-strain output for the test concrete prism model including smeared cracking material model

3.2.2.3 FRP

FRP composites are used in various forms and shapes depending on the type and method of application. Considering the planar geometry of a shear wall structure, the most used method of application of FRP is the bonding of FRP sheets in forms of laminates of wraps to the surface of the wall (Peterson and Mitchell, 2003). A typical FRP ply consists of two main elements; matrix and fibre as shown in Figure 3-13. Strength of the ply is mainly provided by the fibers while the main role of matrix material is to keep the fibers together. Various arrangements of a FRP laminate are possible from the combination of

two or more plies in different directions; also, the fibers might be arranged in more than one direction in a ply (Vasiliev and Morozov, 2007).

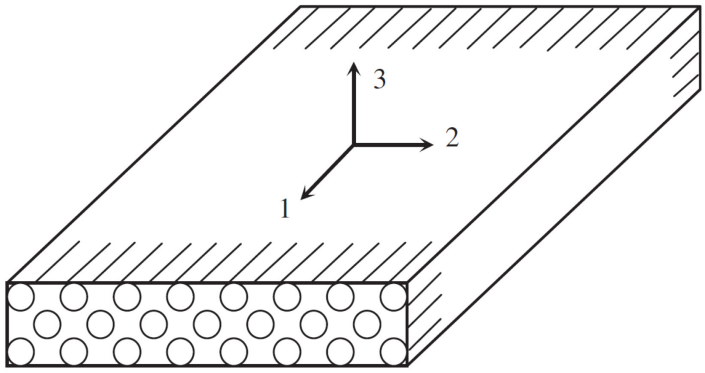

Figure 3.13 A typical unidirectional composite ply (Vasiliev and Morozov, 2007)

The mechanical properties of FRP sheets are available based on the coupon tests conducted by the manufacturers in terms of the elastic modulus, ultimate stress, and strain at failure assuming a linear elastic type of behaviour for the fibers and composites respectively. The material model used in this study for FRP sheets is a linear elastic-up-to-failure material with ultimate stress and strain based on the coupon tests available in the literature.

3.2.2.4 Bond interface

The interface between concrete and FRP sheet has a significant effect on the seismic performance of the retrofitted shear wall. The bond between FRP and concrete is generated by allying a layer of epoxy resin as adhesive material; in some experimental works, mechanical anchorage devices also used to ensure the prevention of de-bonding (Hiotakis et al., 2004), (Ghobarah and Khalil, 2004), (Elnady, 2008). In cases where the adhesive layer is the only bonding material, calculation of debonding failure mechanism is to be considered relative to the mechanical properties of FRP layer(s) and concrete. A simple approach is to consider the bond-slip relationship equal to that of the adhesive

layer but since the adhesive layer has a specific strength in terms of modulus of elasticity (E_{epx}) and rapture stress (f_{epx}) significantly greater than that of concrete, the failure of concrete at the bonding surface by means of fracture energy must be considered as the strength of the bonding layer.

In addition to the fracture energy method which is resulted from direct pullout tests, another failure criterion based on the intermediate cracking (IC) in concrete at the bonding surface is stated to be of significant importance (Teng et al., 2003), (Yao et al., 2005), (Dai et al., 2005), (Lu et al., 2007) , (Rosenboom and Rizkalla, 2008), (Ombres, 2010). Various models are proposed in order to properly address the debonding failure criterion in flexural RC members strengthened with FRP layers, in some models the debonding mechanism is stated to be a function of FRP material properties while some others used the concrete fracture energy as the failure criterion to address the debonding mechanism, some more sophisticated models considered the IC debonding as the mode of failure and more behaviour parameters have involved. The following is a brief review of the most significant models available for the prediction of bond-slip relationship.

a) ACI model

A simple relationship was proposed by ACI (2002) in order to evaluate the design debonding strain of the FRP material (ε_{deb}).

$$\varepsilon_{deb} = K_m \varepsilon_{fu} \qquad \textit{(ACI, 2002)} \qquad \textit{(Eq. 3.16)}$$

Where ε_{fu} is the ultimate rupture strain of the FRP and K_m is a reduction factor as

$$K_m = \begin{cases} \frac{1}{60\varepsilon_{fu}}\left(1 - \frac{nE_f t_f}{360{,}000}\right) \leq 0.9 \; for \; nE_f t_f \leq 180000 \\ \frac{1}{60\varepsilon_{fu}}\left(\frac{90000}{nE_f t_f}\right) \leq 0.9 \; for \; nE_f t_f > 180000 \end{cases} \qquad \textit{(Eq. 3.17)}$$

In which n is the number of FRP layers, E_f is the elastic modulus and t_f is the thickness of each FRP layer respectively.

The ACI model accounts for the calculation of debonding strain based on the material properties of the FRP through a linear approach without taking into consideration the concrete material behaviour effects on the debonding mechanism.

b) Fracture Energy model

In the fracture energy model (Sato and Vecchio, 2003) the bond-slip relationship is obtained from the following equations where U_{max} (MPa) is the maximum bond stress, S_{max} (mm) is the corresponding slip at U_{max}, S_{ult} (mm) is the ultimate bond slip correspond to zero stress at failure, and G_f (MPa.mm) is the fracture energy of concrete.

Umax=(54f'c)0.19 *(Sato and Vecchio, 2003)* *(Eq. 3.18)*

Gf=(Umax/6.6)2 *(Eq. 3.19)*

Smax=0.057Gf0.5 *(Eq. 3.20)*

Sult=2Gf/Umax *(Eq. 3.21)*

All parameters in above equations are calculated based on the compressive strength of concrete f'_c (Sato and Vecchio, 2003), and will result in a linear bond-slip mechanism as shown in Figure 3.14 for various f'_c values. The approach was used in the 2D-FE models of RC shear walls strengthened with steel and FRP sheets under cyclic loading by Cortes-Puntes and Palermo (2012) and stated to give acceptable estimates compared to the experimental data.

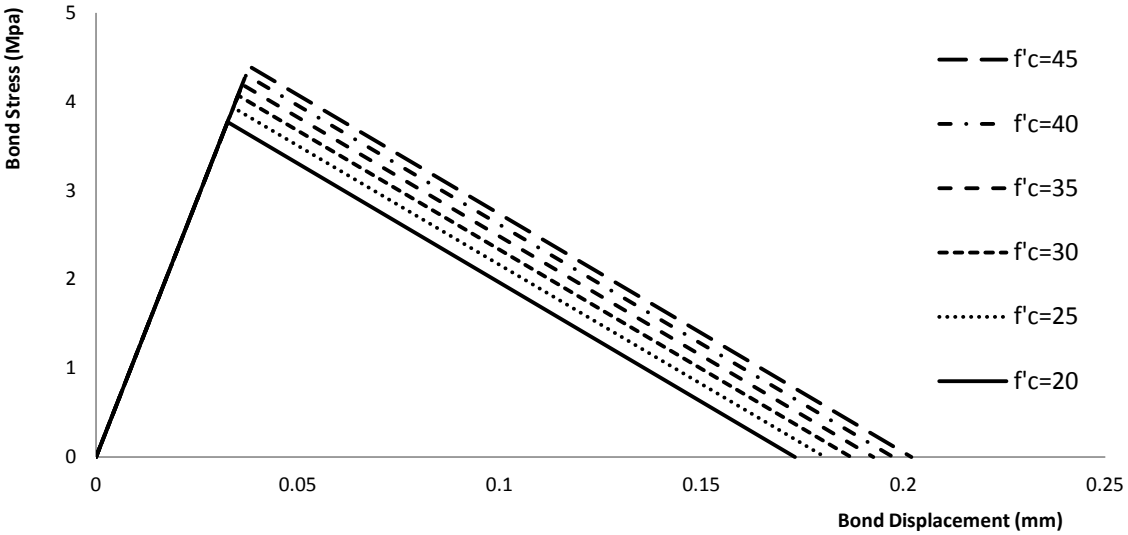

Figure 3.14 Bond slip relation based on concrete fracture energy model (Sato and Vecchio, 2003)

c) Italian Code model (CNR DT/200, 2004)

A simplified method was proposed by the Italian Code (CNR DT/200, 2004) to evaluate the maximum design IC debonding strain (ε_{fdd}) for FRP reinforcement based on fracture mechanics approach as

$$\varepsilon_{fdd} = \frac{k_{cr}}{\gamma_{fd}\sqrt{\gamma_c}}\sqrt{\frac{2\Gamma_{Fk}}{E_f t_f}} \qquad \textit{(CNR DT/200, 2004)} \qquad \textit{(Eq. 3.22)}$$

Where E_f and t_f are the elastic modulus and the thickness of FRP respectively, γ_{fd} and γ_c are partial factors for FRP and concrete respectively and Γ_{FK} is the fracture energy resulted from the following equation

$$\Gamma_{FK} = k_G k_b \sqrt{f_{ck} f_{ctm}} \qquad \textit{(Eq. 3.23)}$$

In which f_{ck} and f_{ctm} (MPa) are concrete compressive and average tensile strength respectively; k_G=*0.03* is a coefficient determined experimentally and k_b is a geometrical factor based on the widths of beam (b) and FRP (b_f) expressed as following for $b_f/b \geq 0.33$:

$$k_b = \sqrt{\frac{2b_f/b}{1+b_f/400}} \qquad \textit{(Eq. 3.24)}$$

In cases where $b_f/b<0.33$, the value of k_b corresponding to $b_f/b=0.33$ shall be used. A typical bond-slip relation based on Eq. 3.22 is shown in Figure 3.15 for f_{ck}=20MPa (CNR DT/200, 2004).

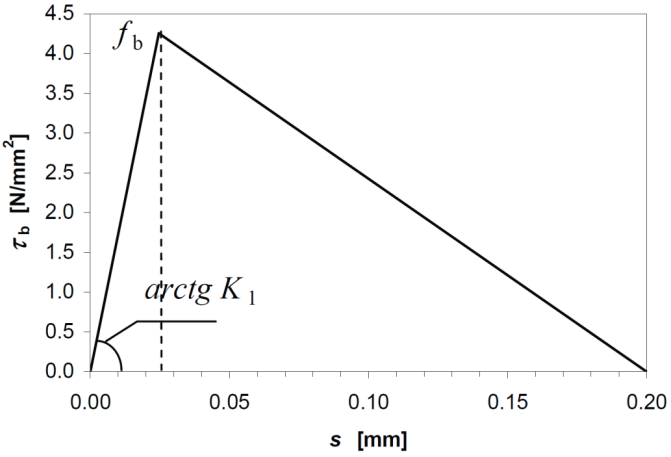

Figure 3.15 Typical bond-slip relation based on the Italian Code (CNR DT/200, 2004) model

d) Lu et al. (2005) model

The bond-slip relationship model proposed by Lu et al. (2005-a) based on specialized pullout tests and verified through meso-scale FE analysis is given based on τ-S relationship where τ is the shear stress (MPa) and S is the relative displacement (mm).

$$\tau = \begin{cases} \tau_{max}\sqrt{S/S_0} \; ; if \; S \leq S_0 \\ \tau_{max}e^{-\alpha(S/S_0-1)} \; ; if \; S > S_0 \end{cases} \qquad \textit{(Lu et al. 2005-a)} \qquad \textit{(Eq. 3.25)}$$

Where

$$\tau_{max} = 1.5\beta_w f_t \qquad \textit{(Eq. 3.26)}$$

$$S_0 = 0.0195\beta_w f_t \qquad \textit{(Eq. 3.27)}$$

$$\beta_w = \sqrt{\frac{2.25 - b_f/b_c}{1.25 + b_f/b_c}} \qquad \textit{(Eq. 3.28)}$$

$$\alpha = \frac{1}{\frac{G_f}{\tau_{max} s_0} - \frac{2}{3}} \qquad \textit{(Eq. 3.29)}$$

$$G_f = 0.308 \beta_w^2 \sqrt{f_t} \qquad \textit{(Eq. 3.30)}$$

Where b_f and b_c are the widths of FRP and concrete member respectively, f_t is the tensile strength of concrete (MPa), and G_f is the interfacial fracture energy of concrete member (MPa.mm) (Lu et al., 2005-a).

The model proposed by Lu et al. (2005-a) is mainly based on the tensile strength of concrete and found to be the most accurate estimation of the actual bond-slip behaviour of RC beams strengthened with FRP sheets (Ombres, 2010). Figure 3.16 shows schematic bond-slip relationships for a number of values for concrete tensile strength based on Eq. 3.25.

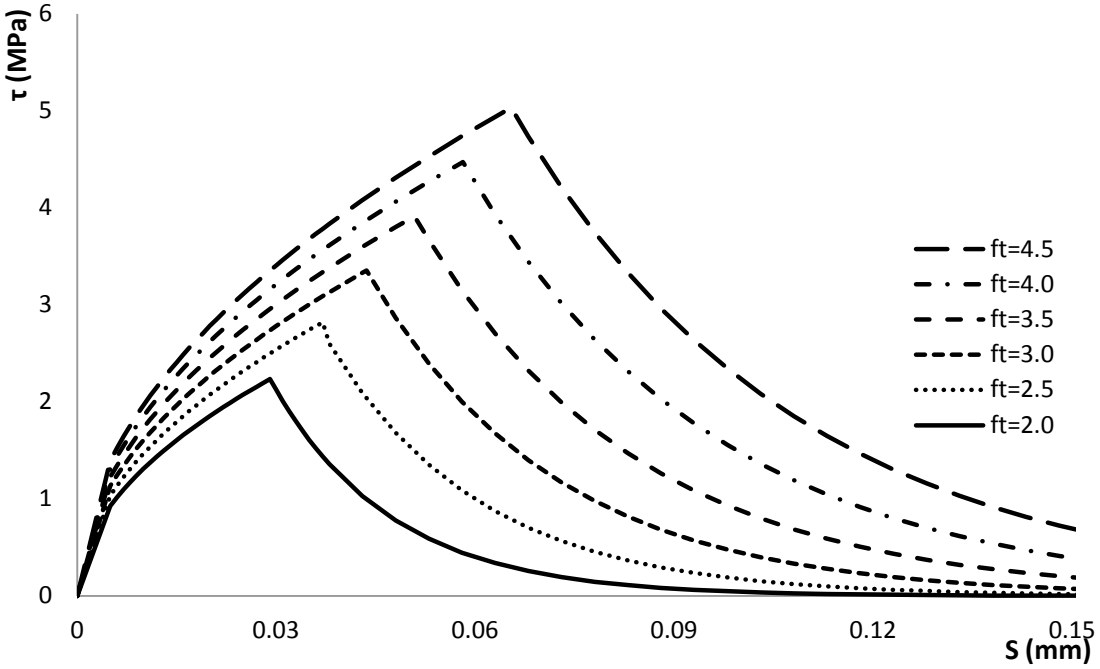

Figure 3.16 Bond-slip relationship considering IC debonding failure mechanism (Lu et al., 2005-a)

3.2.3 ANSYS Elements

The elements used for the modeling of every part of the shear wall specimens of this study are selected from the elements library of ANSYS. Types of elements and the DOFs must meet the required boundary conditions for the failure criteria to be met. The elements are listed based on their relevance in the models.

3.2.3.1 Reinforced Concrete Element (SOLID65)

SOLID65 is a general solid element defined by eight nodes with three translational degrees of freedom at each node. The element is capable of modeling the cracking in tension and crushing in compression and it is well suited for the 3D modeling of solids with or without reinforcement materials. The main purpose of the element is to model the concrete behaviour based on the criteria described previously. Other cases in which the element is used for, are the modeling of the reinforced composites and geological materials (ANSYS, 2010-a). The element is also capable of modeling plastic deformation and creep. The geometry of SOLID65 is shown earlier in Figure 3.10 where the three possible shapes of cube, prism and tetrahedral are described with details on the rebar directions and the coordinate system of the element. Each of the eight nodes (I-O) has three translational DOFs in X, Y, and Z direction respectively. Cracking is supported at any surface in any direction by means of the angle between the normal of the crack surface to the global directions.

SOLID65 allows the presence of four different materials in each element; one matrix element which could be considered as a brittle material such as concrete and a maximum of three different reinforcing materials each with its own direction and volume as a ratio of the matrix material. The concrete material (if assigned to the matrix for SOLID65) is

capable of directional integration point cracking and crushing besides incorporating plastic behaviour as discussed previously. The reinforcement supports uniaxial stiffness only and is assumed to be smeared throughout the element (ANSYS, 2010-a). Although the reinforcement capability of SOLID65 is proved to be useful, the rebar could be modeled separately using link elements bonded to the concrete elements. In this case, the nodes of the "discrete" rebar elements are to be coincident with the nodes of concrete elements in all degrees of freedom; in this study, the steel reinforcement bars are modeled as combination of smeared and discrete elements.

3.2.3.2 Steel reinforcement element (LINK180)

There are two different elements used in this study to simulate the embedded reinforcement bars in concrete, a smeared reinforcement in the boundary regions of the wall in the direction of wall thickness "Global Z" by means of the embedded smeared reinforcement capability of SOLID65, and a discrete type of reinforcement bars in all other directions. The element used for the discrete reinforcement bars is LINK180 (ANSYS, 2010-a) which is a 3D spar type element with two nodes and three translational DOFs at each node. Since no rotational DOF is considered at the nodes of LINK180, no bending or shear strength is provided. The element supports the material behaviour and failure criteria specified for steel material described previously in case of nonlinear analysis. Geometry of LINK180 element is shown in Figure 3.17. There are three real constants to be defined for every LINK180 element, the cross-sectional area, possibility of change in the cross-sectional area due to poison's ratio and strain hardening, and the type of behaviour as per compression/tension only or both (ANSYS, 2010-a). Another capability of LINK180 is the initial stress state in which a pre-stressed bar could be

defined and used in the analysis. However a variety of output is available for any LINK180 element, the axial stresses with strains in the elastic and plastic ranges are the most useful outputs in structural analysis. Since the stress-strain data is readable from every node of LINK180 elements, tracking of the behaviour of the model is possible through the analysis.

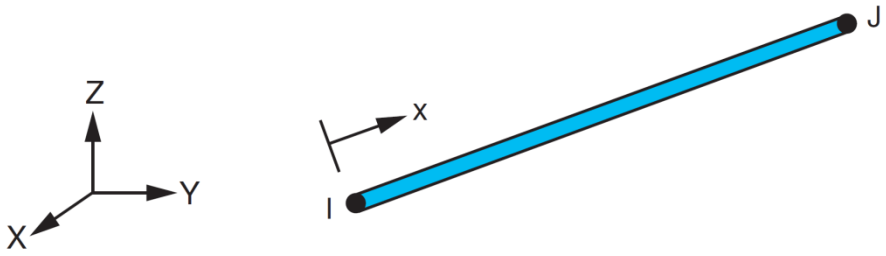

Figure 3.17 Geometry of LINK180 element (ANSYS, 2010-a)

3.2.3.3 FRP sheet element (LINK180)

The element used for the modeling of FRP sheets in this study is LINK180 which was previously described. The tension-only capability of LINK180 is used in the analysis for FRP elements since the main mechanical characteristics of FRP sheets are in the direction of fibers under tension. In order to simulate the planar sheets of FRP by link elements, the tributary area of each element is to be calculated considering the geometry of the model.

3.2.3.4 Bond interface element (COMBIN39)

Various available bond-slip models for the adhesive layer between FRP and concrete surface were discussed previously. A typical shear stress-relative displacement accounting for fracture energy and IC debonding is shown earlier in Figure 3.16 which is the basis of the simulation of bond-slip mechanism in this study. The element used for the simulation of bond-slip mechanism based on (Lu et al., 2005-a) model is COMBIN39.

COMBIN39 is a unidirectional element with nonlinear generalized force-deflection capability that can be used in any analysis. The element simulates a spring with a virtual length that has longitudinal or torsion behaviour in up to three directions at each node. The longitudinal option is a uniaxial tension-compression element with translational DOFs in X, Y, and Z global directions. The DOFs could be reduced in cases of 1D or 2D springs while a compression-only or tension-only type of behaviour is also available for the element. The element is defined by two node points and a generalized force-deflection curve as shown in Figure 3.18.

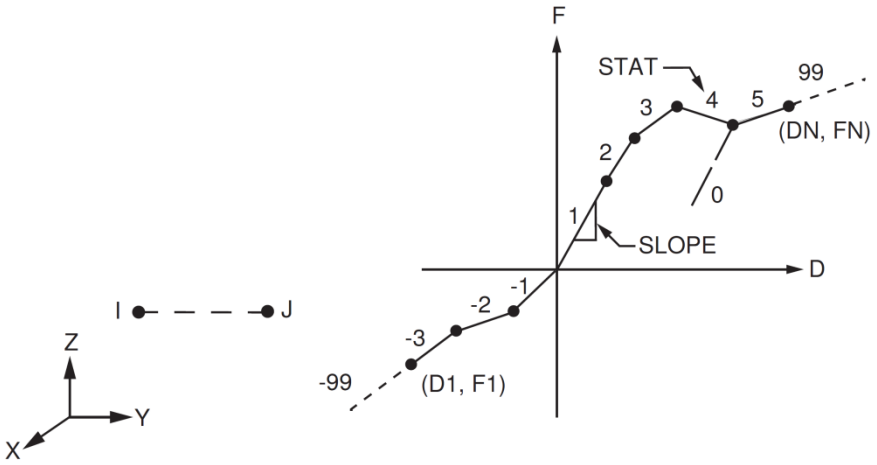

Figure 3.18 COMBIN39 element geometry and input function (ANSYS, 2010-a)

Slopes of the segments shown in Figure 3.18 could be positive or negative based on the actual material behaviour and could be defined differently for compression and tension. The unloading path could be defined to follow a reverse path on the loading curve or along a line parallel to the slope of the first loading path as shown as “0” path in Figure 3.18 (ANSYS, 2010-a). The output data available for COMBIN39 allows the user to get the nodal DOF results included in the overall nodal solution as well as the relative displacements between nodes I and J throughout the analysis history. The output data also

gives the status of each element at any instant of the loading history as well as the status of the force-deflection curve and current slope on the curve (ANSYS, 2010-a).

3.2.3.5 FRP layers interface element (COMBIN40)

Although the case of FRP layers interface failure is unlikely to occur as a failure criterion, in cased where multiple layers of FRP sheets are used by applying epoxy resin between adjacent layers a bond-slip relation is desirable for the persistence of the model. COMBIN40 element is used in such cases where a linear-up-to-failure with a sliding force and a spring constant define the bond interface between adjacent layers of FRP sheets based on the material properties of epoxy resin.

3.3 FAILURE CRITERIA

The failure criteria are dictated by the mechanical characteristics of the constituent materials (including the FRP-Concrete bond interface element) and the interactions between them. As previously stated, a typical FE assembly in this study is consisted of four different sub-assemblies namely, concrete, steel reinforcement, FRP composite, and the bonding interface. Each of these sub-assemblies is modeled by a material model assigned to appropriate meshes of elements in various regions of the geometry. The material model represents the failure criterion of the material in terms of mechanical properties and certain limitations. The nonlinear analysis continues while elements in various regions of the assembly are reaching their limits defined by material models, when an element fails, it is considered to be fully unloaded and the analysis continues until the unloading of failed elements causes geometric instability (ANSYS, 2010-b).

CHAPTER 4

MODELING RC SHEAR WALLS

In this Chapter, the analysis methodology and failure criteria discussed in Chapter 3 will be used to model a number of available reported experimental tests for un-retrofitted and FRP-retrofitted RC shear walls in order to verify the modeling and analysis. A total of seven specimens from four experimental programs are modeled and analyzed and the results are compared with the experimental data. The models are different in geometry, boundary conditions, material properties and loading scheme and they represent both slender and squat shear walls. A summary of the properties of the selected experimental specimens is shown in Table 4.1.

Table 4.1. Summary of loading and geometry of the modeled specimens

specimen ID[§]	Experimental work	Type of loading	H/L	f'_c	FRP
LSW14	Lefas et al. (1990)	Monotonic	1	48.3[†]	--
LSW26	Lefas et al. (1990)	Monotonic	2	30.1[†]	--
ZSW7	Zhang & Wang (2000)	Cyclic	2.14	36.8	--
LCW	Lombard et al. (2000)	Cyclic	1.19	40.2	--
LSW1	Lombard et al. (2000)	Cyclic	1.19	42	1V
HCW	Hiotakis et al. (2004)	Cyclic	1.19	36.2	--
HSW1	Hiotakis et al. (2004)	Cyclic	1.19	36.4	1V

[§]*The first letter is taken from the name of principal author and added to the original ID indicated in the reference*
[†]*Cube strength*

4.1 LEFAS ET AL. (1990)

The experimental work of Lefas et al. (1990) consisted of testing 13 structural wall specimens with constant thickness and a height-to-length ratio (H/L) of 1 and 2. The purpose of experimental work was to investigate on the effects of various parameters

such as axial load, concrete strength and wall dimensions on the mode of failure of RC shear walls. Lateral force was applied at the top of the wall through a rigid top block in a displacement-controlled monotonic incremental loading. Details of the two selected wall specimens are shown in Figure 4.1. Since the loading scheme of the tested walls was mainly through applying lateral displacement on the top of the wall, the top block was not included in the geometry of the models. Figure 4.2(a) shows the geometry and FE mesh and Figure 4-2(b) shows the arrangement of reinforcement bar elements.

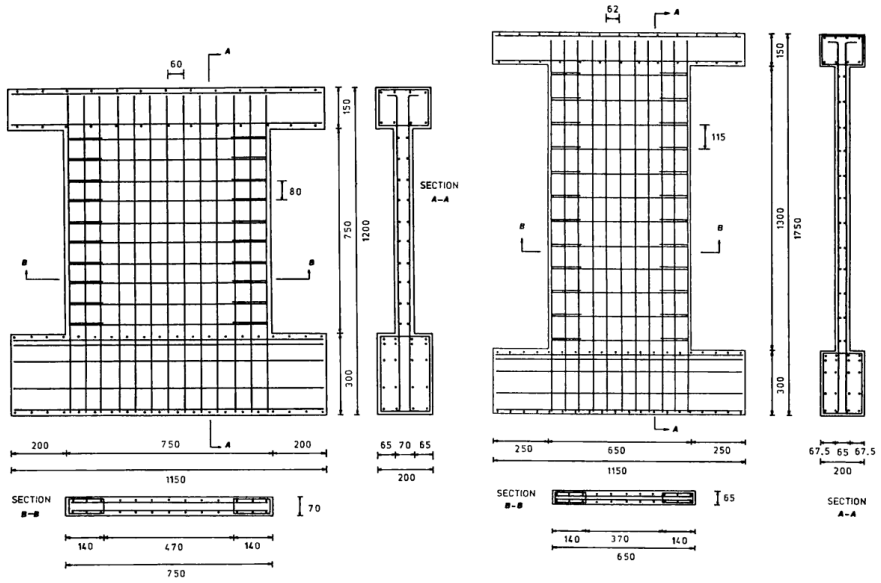

Figure 4.1. Details of the wall specimens tested by Lefas et al. (1990)

In the FE model, it was necessary to make some minor adjustments in the locations of reinforcement bars in order to comply with the element sizes of solid elements representing concrete. Nonlinear analysis under a monotonic displacement history was performed and the reaction forces from the horizontally restrained nodes were stored to compare the results of the FE analysis with the experimental tests.

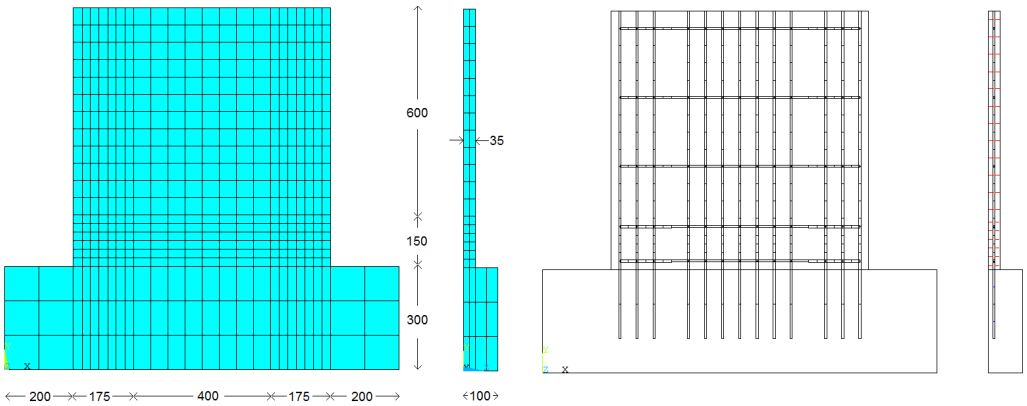

Figure 4.2 Details of the FE model FE-LSW14 (a) elements mesh (b) elements arrangement

For specimen SW14, Lefas et al. (1990) reported the initiation of first flexural cracks at 35kN lateral force with a corresponding displacement of 0.34mm. In the FE analysis, the first cracks appeared at the edge bottom of the wall as shown in Figure 4.3(a) at lateral load of 35.6kN at the top displacement of 0.32mm. The first inclined cracks of the tested walls were reported at 100kN lateral load and a corresponding displacement of 1.82mm. The generation of inclined cracks was in the early stages of FE analysis but the amount of these cracks started to grow significantly at 102.3kN lateral load with a 1.58mm top displacement. First experimentally measured yield of longitudinal steel reinforcement was at 170kN load and 3.9mm displacement, while the corresponding values from the FE model were 173.5kN and 2.94mm, respectively as shown in Figure 4.3(c). The ultimate failure load and displacement of the tested wall were reported to be 247kN and 10.75mm, whereas the numerically predicted values from the FE model were 267.1kN and 11.9mm, respectively. Based on the FE analysis, the wall followed the strut-and-tie model until failure at which five layers of the horizontal reinforcement bars yielded in the mid-height of the wall and the wall failed in the diagonal tension mode. Some crushed concrete

elements are seen in the compressive toe of the wall as well as the compressive diagonal, also a few crushed concrete elements are seen at the bottom of the web region of the wall due to the sliding shear stresses. Eight layers of the vertical reinforcement bars are yielded in tension as well as two layers in compression at the failure load as shown in Figure 4.3(c).

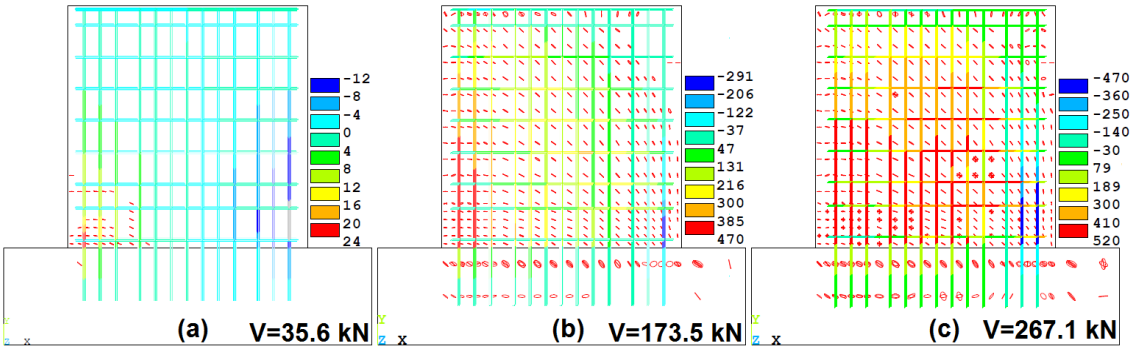

Figure 4.3. Crack pattern and rebars axial stresses in different stages of the analysis; (a): cracking, (b) yielding, (c) failure resulted from FE-LSW14

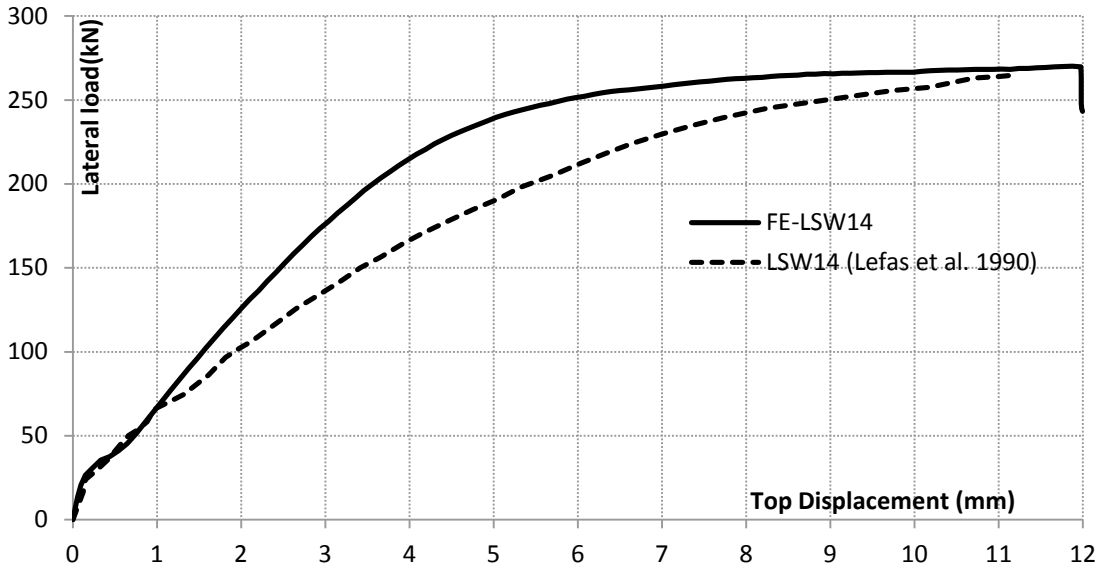

Figure 4.4. Lateral load-deformation resulted from FE-LSW14

Figure 4.4 shows a comparison between the lateral load-displacement relationships of the tested wall (Lefas et al., 1990) and the analytically predicted response from the FE

model. More detailed comparisons between the results of the FE analysis and the experimental test are presented in Table 4.4.

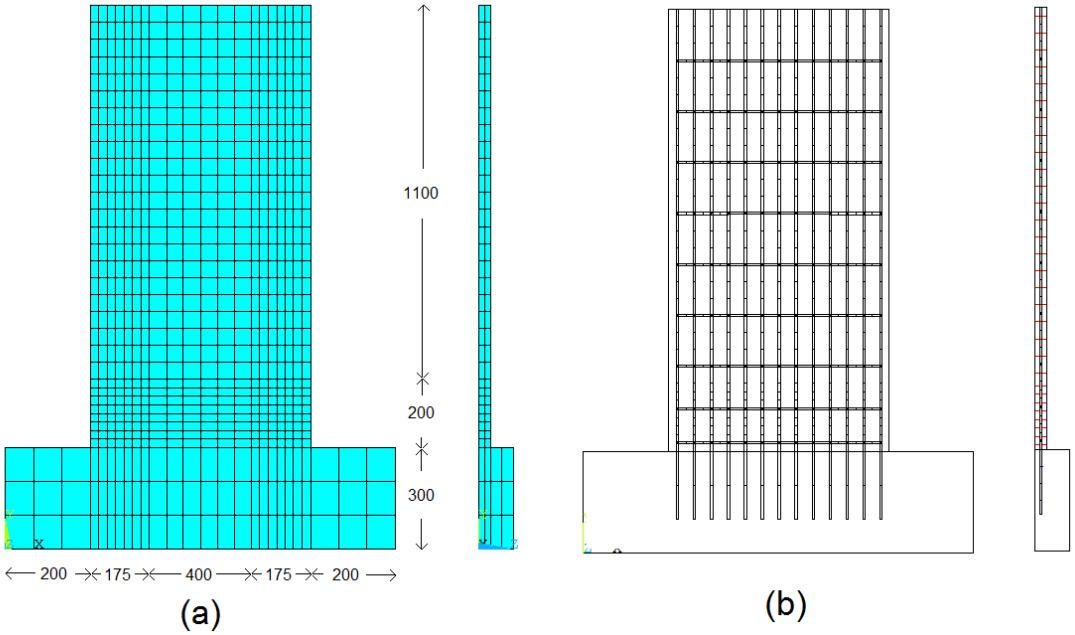

Figure 4.5 Details of the FE model FE-LSW26 (a) elements mesh (b) elements arrangement

Figure 4.5 shows the geometry and elements mesh as well as the elements arrangement and reinforcements for FE model of FE-LSW26. For the tested specimen LSW26, the initiation of first flexural cracks was reported at 10kN lateral force with a corresponding displacement of 0.39mm. As a result of FE analysis, first flexural cracks appeared at lateral load of 9.4kN with a corresponding displacement of 0.22mm as shown in figure 4-6(a). At lateral load of 68kN, the first inclined cracks were reported in the experimental tests with a corresponding displacement of 5.51mm. The generation of inclined cracks was in the early stages of FE analysis but the amount of these cracks started to grow significantly at 70.4kN lateral load with a displacement of 5.08mm respectively. First yielding of tensile longitudinal steel reinforcement was at 68kN load and 5.51mm displacement from the experimental tests, while 73.8kN and 5.32mm were the yielding

load and displacement from the FE analysis, respectively. The yielded tensile reinforcement bar and the cracks pattern at yielding load are shown in Figure 4.6(b). The ultimate failure load and displacement reported to be 123kN and 20.94mm in the experimental results. The load at failure is 152.21kN resulted from the FE analysis; also, ultimate lateral displacement is 23.8mm. The wall behaviour is following the strut-and-tie model with failure due to the yielding of four layers of the horizontal reinforcement in the mid-height and crushing of concrete in the compressive toe as well as the bottom of the web region as shown in Figure 4.6(c). Eight layers of the vertical reinforcement bars are yielded in tension and one layer in compression as shown in Figure 4.6(c).

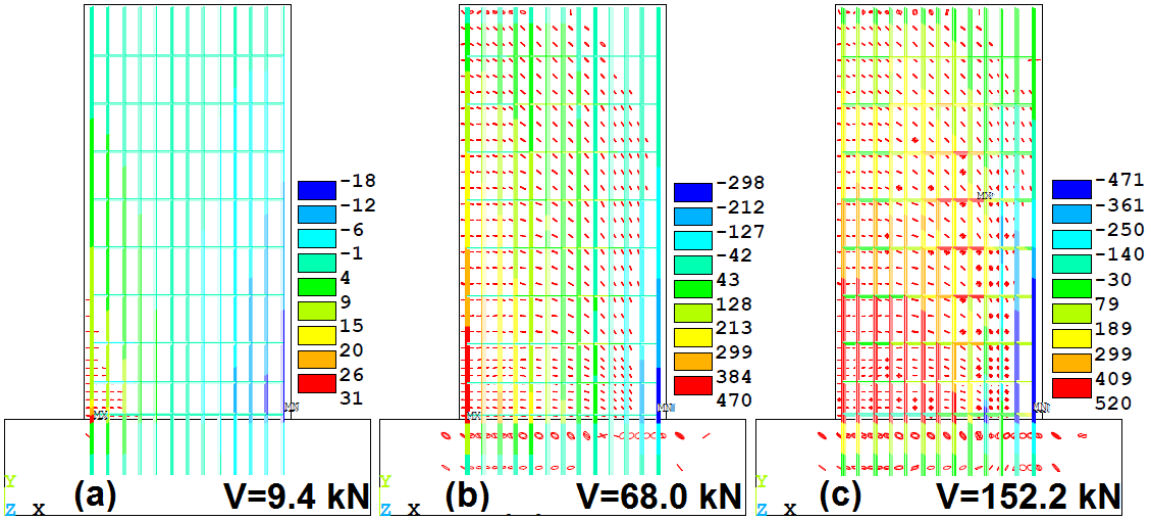

Figure 4.6. Crack pattern and rebars axial stresses in different stages of the analysis; (a): cracking, (b) yielding, (c) failure resulted from FE-LSW26

Figure 4.7 shows the lateral load-displacement curves of LSW26 specimen and the FE model.

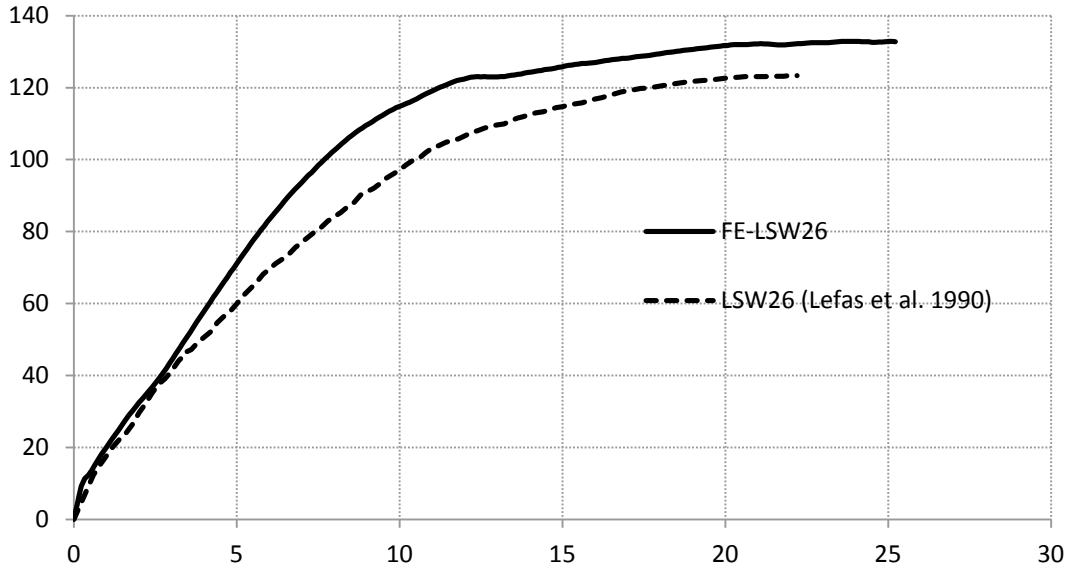

Figure 4.7. Lateral load-deformation for LSW26

4.2 ZHANG AND WANG (2000)

The experimental program by Zhang and Wang (2000) was conducted to study the effects of axial load on the seismic behaviour of shear walls. A total of four isolated cantilever walls were built and tested under comparable load histories of a target axial and a cyclic incremental lateral load. All four specimens (SW7, SW8, SW9, and SRCW12) were of identical dimensions with differences in the reinforcement data for the first three specimens, and in SRCW12, a combination of steel channel profiles and reinforcement bars were used in the boundary regions. SW7 specimen is modeled in this study with a schematic shown in Figure 4-8. The geometry and elements mesh for FE-ZSW7 are shown in Figure 4-9(a) based on the same considerations as for previous models. The elements arrangement and reinforcement bars are shown in Figure 4-9(b) where minor adjustments in the spacing between confinement bars in the boundary elements of the wall model were done in order to comply with the meshing and elements formation.

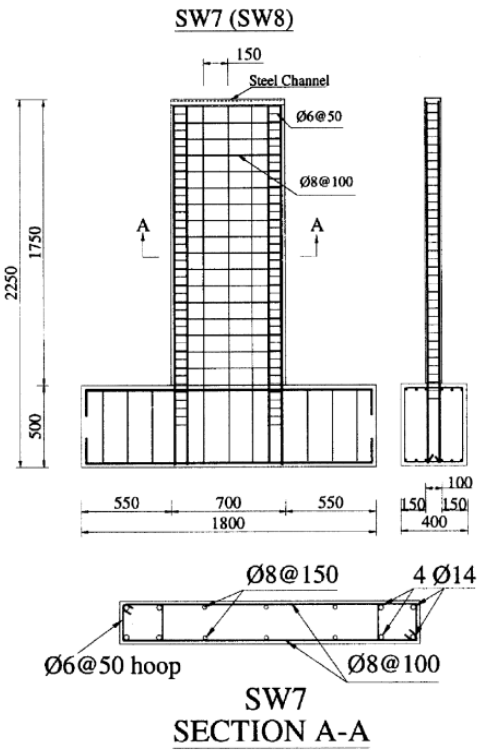

Figure 4.8 Details of Specimen ZSW7 (Zhang and Wang, 2000)

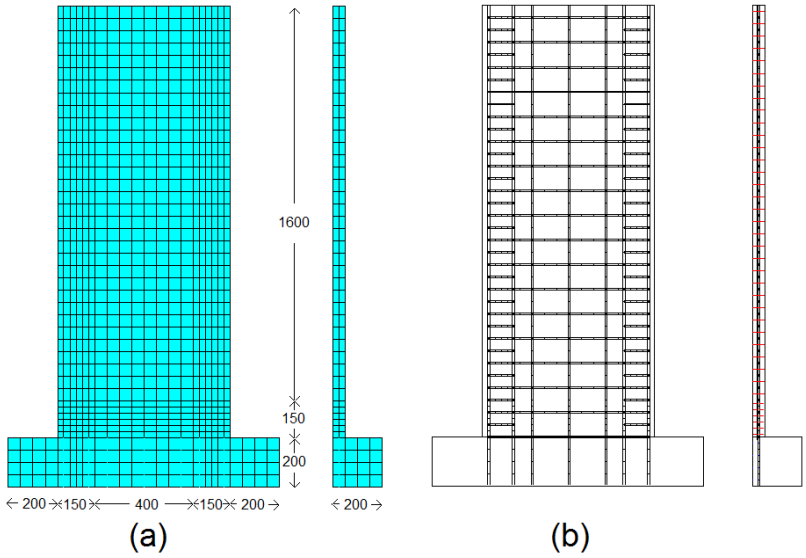

Figure 4.9 Details of the FE model FE-ZSW7 (a) elements mesh (b) elements arrangement

Since the oversized bottom block adds a considerable number of elements and nodes to the analysis without contributing to the targeted results, only a part of it is considered in the modeling. Several output data types are available after the analysis; however, only

the results matching those discussed in the experimental program are stated herein. Zhang and Wang (2000) stated the first cracks appeared in the boundary elements of the wall at the 95.6kN lateral load with a 1.92mm top displacement but the cracking load from the theoretical analysis done by Zhang and Wang (2000) was stated to be only 59.6kN. The authors then explained this observation as: "the discrepancy may be partly explained by the way that the theoretical first-cracking load is computed. In the experiment, cracks would not be observed if the width of the cracks is too small, but the theoretical first cracking load is computed as the load when the extreme fibre concrete reaches its tensile strength. Therefore, the observed value of the first-cracking load is usually much greater than the theoretical value computed in this way (Zhang and Wang, 2000)".

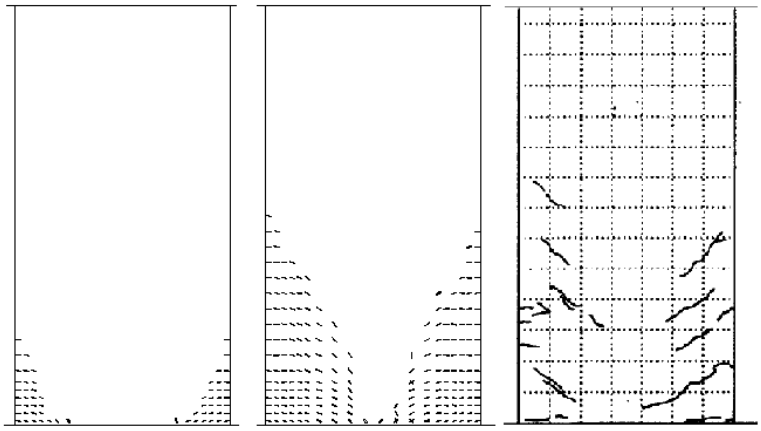

Figure 4.10 Crack pattern for SW7 (a) first cracks initiated in FE model (b) cracks in FE model at cracking load of experimental tests (c) cracks at cracking load in experimental tests (Zhang and Wang, 2000)

As for the results of FE analysis performed in this study, the first cracks at the bottom of boundary elements of the wall appeared in +67.9 kN in the push direction and -63.1 kN in pull direction as shown in figure 4-10(a). These values are close to the theoretical values stated by Zhang and Wang (2000). In addition, the cracking pattern at 95.23kN base

shear and corresponding lateral displacement of 2.16mm is plotted in figure 4-10(b), which is comparable to the experimental results of the wall tested by Zhang and Wang (2000) shown in figure 4-10(c). Yielding of steel was reported to occur at 171.6kN based on the theoretical analysis and 172.3kN based on the output data of the experimental test in a lateral displacement of 5.91mm (Zhang and Wang, 2000). The load at which the extreme layer of vertical rebars yielded in the FE analysis is 180.9 kN in push direction and -156.4 kN in pull direction with 6.78 mm and -5.68 mm top displacements respectively. The average yielding load and displacement from the FE analysis are 168.6 kN and 6.23 mm. The rebars axial stresses and cracks pattern are shown in Figure 4.11 in the yielding load and the failure stage of the FE analysis.

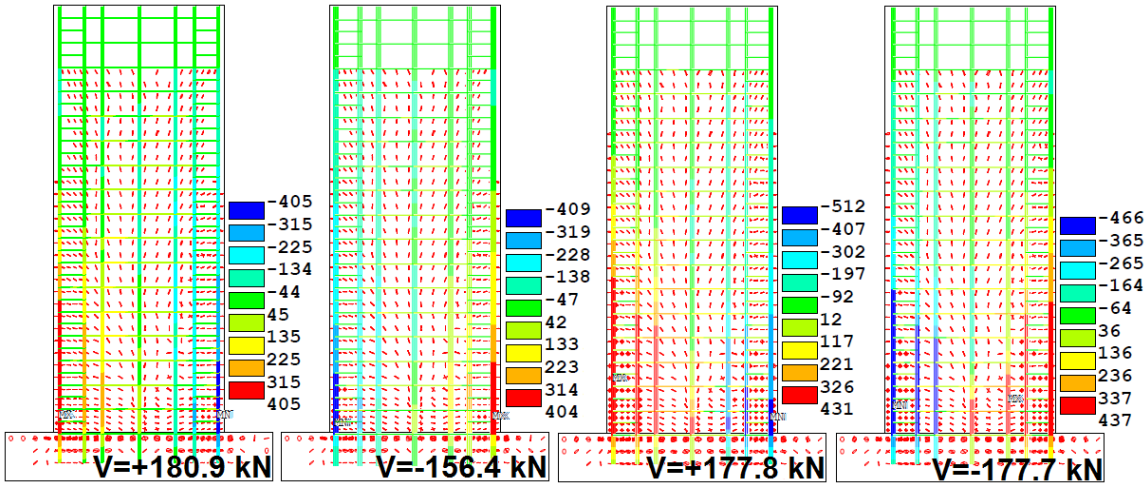

Figure 4.11. Crack pattern and rebars axial stresses at different stages of the analysis resulted from FE-ZSW7

The maximum lateral load carrying capacity of the wall during the FE analysis is 218.3 kN which is 8.5% higher than 201.2kN stated as the load capacity of the wall from the experimental and theoretical analysis. The failure mode of the wall specimen was "boundary element crushing" at 171.0kN load and 31.27 mm lateral displacement as shown in Figure 4-12(a). FE analysis resulted in 31mm ultimate displacement with 177.7

kN corresponding lateral load which is 3.9% higher than the ultimate base shear of the wall from the experimental tests (Zhang and Wang, 2000) under the same failure mode. Figure 4.12 shows a comparison between the cracked experimentally tested wall and the FE model at the failure stage.

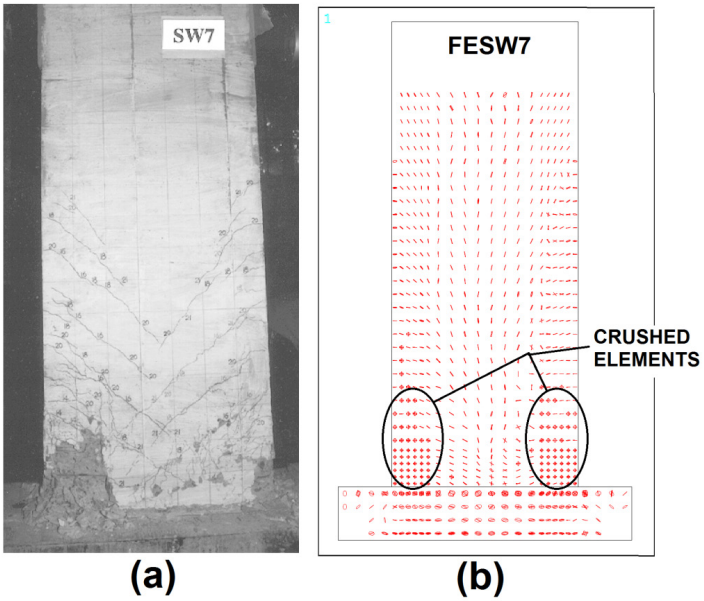

Figure 4.12 Cracks at failure for SW7 (a) experimental (Zhang and Wang, 2000) (b) FE analysis

Figure 4.13 shows a comparison between the numerically predicted load-displacement hysteretic relationship using the FE model and the experimentally measured one. The figure also shows a comparison between the backbone force-deformation curves of the FE model of the wall and test. More specific comparison between the results of FE analyses and experimental tests at key performance points, namely cracking, yielding, and ultimate levels, are presented in Table 4.4 at the end of this chapter.

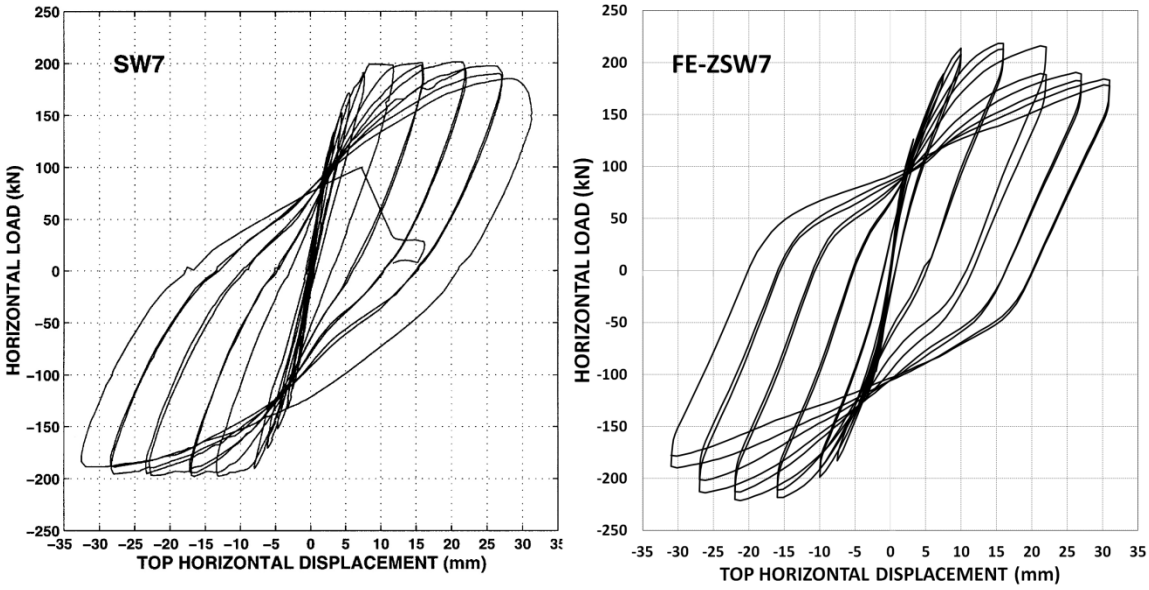

Figure 4.13. Lateral load-deformation curve of ZSW7 and FE-ZSW7

4.3 LOMBARD ET AL. (2000)

A total of three shear wall specimens were tested experimentally by Lombard et al. (2000) to study the repair and retrofitting of RC squat shear walls by externally bonded FRP. A control wall (LCW) was tested under incremental cyclic lateral load reversals without applying any axial force or moments to the top of the wall. The control wall then repaired by replacing the concrete in the heavily cracked regions and applying a layer of vertical CFRP sheet to the wall surface at each side. The repaired wall (RW) then tested under the same loading history as the control wall. Two additional retrofitted walls were also tested by Lombard et al. (2000); the first one (LSW1) had the same arrangement as the repaired wall and the second one (LSW2) had one vertical and one horizontal layer of CFRP in addition to the first retrofitted wall. Figure 4.14 shows the geometry and reinforcement arrangement of the wall specimens of Lombard et al. (2000).

Two of the four walls from the experimental work of Lombard et al. (2000) namely, the control wall (LCW) and the first retrofitted wall (LSW1) are modeled in this chapter.

The geometry of the wall specimens tested by Lombard et al. (2000) and the FE model are shown in Figure 4.14.

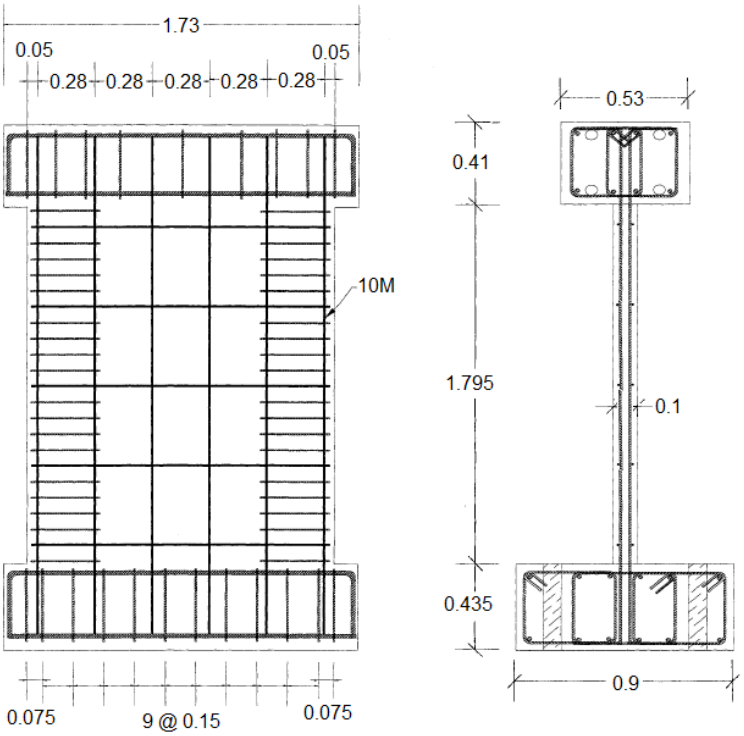

Figure 4.14. Geometry and reinforcement details of shear wall specimens (Lombard et al., 2000)

The bottom block was fixed to the rigid floor using six 75mm bolts. Each shear wall was reinforced in the vertical direction by six pairs of 10M deformed reinforcement bars spaced uniformly at 280 mm with a cover of 50 mm whereas the horizontal reinforcement was consisted of five pairs of 10M deformed bars spaced uniformly at 400 mm and the premature buckling of the vertical compressive bars was prevented by stirrups spaced at 80 mm through the height of the wall around the two edge bars at each end of the wall. The stirrups were of 6.4 mm diameter bars for the control/repaired wall and 10M deformed bars for the two retrofitted walls. The reinforcing steel used was grade 400, two coupon tests were conducted by Lombard et al. (2000) in order to obtain the monotonic stress-strain relationship of steel material. Figure 4.15(a) shows the stress-strain

relationship for steel from the coupon tests of Lombard et al. (2000) and the steel material model used in the FE modelling of this thesis. The concrete compressive strength, f'_c was measured at the age of 28 days and at the time of the test; the stress-stress curve from the experimental test was used to define the material model of concrete in the FE modeling as shown in Figure 4.15(b).

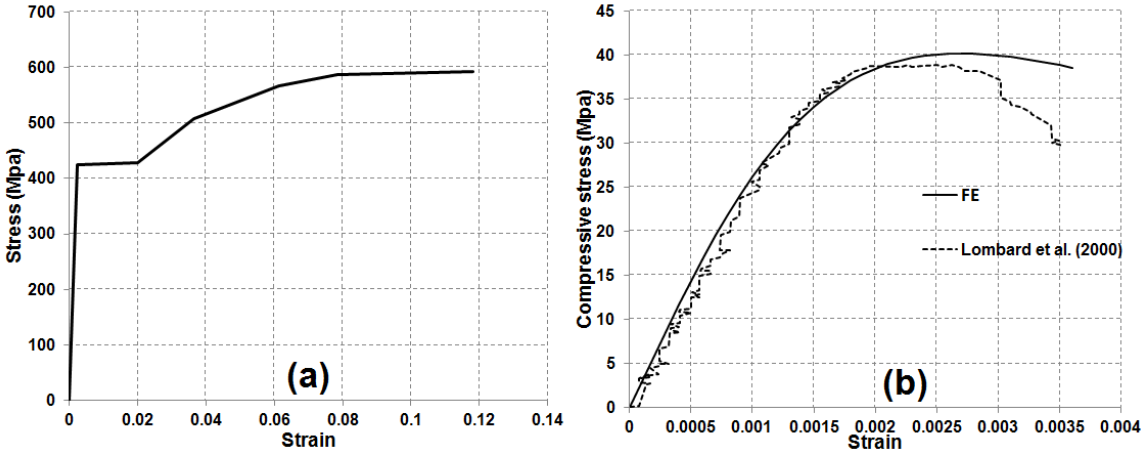

Figure 4.15. Stress-strain relationship for (a) reinforcement steel (b) concrete

The FE mesh and the elements arrangement are shown in Figure 4.16 for the models of Lombard et al. (2000) specimens.

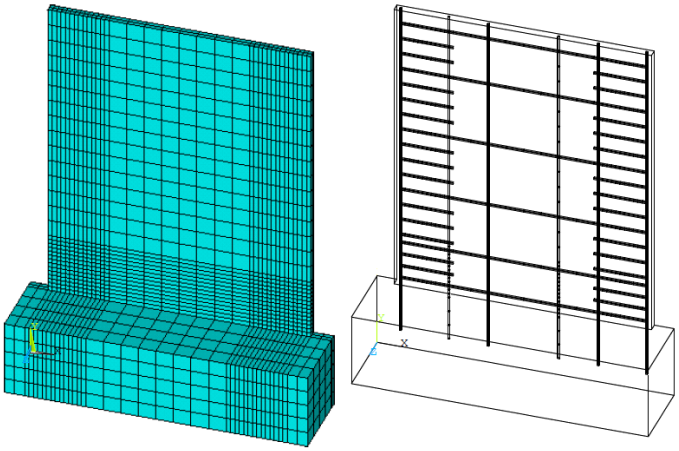

Figure 4.16 FE mesh and elements arrangement of FE models based on the specimens of Lombard et al. (2000)

Figure 4.17 shows the lateral load vs. Top displacement of the LCW specimen from the experimental work of Lombard et al (2000) and FE-LCW model.

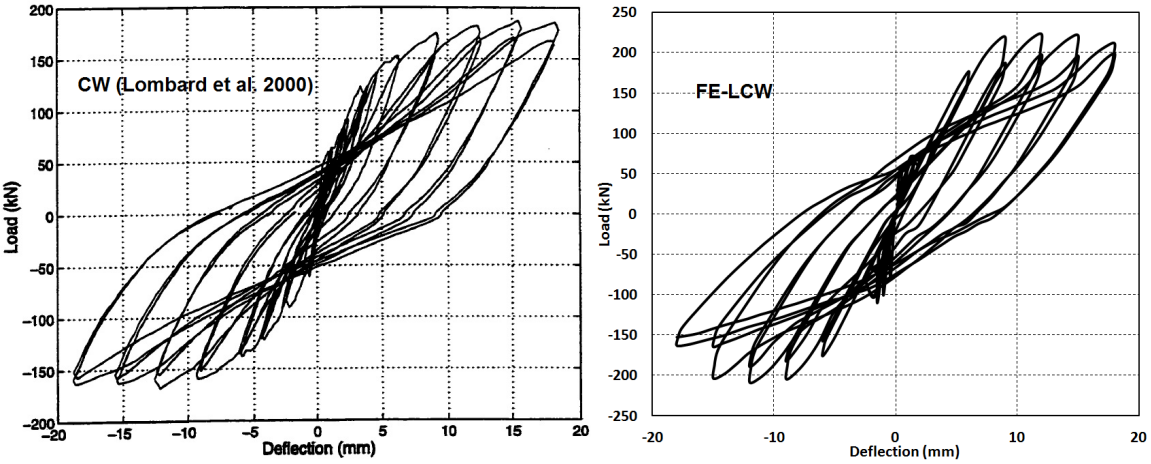

Figure 4.17. Lateral load-deformation curve of LCW (Lombard et al., 2000) and FE-LCW model

Lombard et al. (2000) reported the first flexural cracks for the control wall (CW) at load 49.6 kN (0.6 mm) in the "push" direction and -60 kN (-0.6 mm) in pull direction formed near the edge of the wall at the construction joints. First flexural cracks appeared in the FE model at 47.3 kN (0.27 mm) in push direction and -41.3 kN (-0.24 mm) in pull direction at the bottom corners of the wall. First diagonal cracks reported to occur in the third load step of the test at ±90 kN for the CW specimen. The appearance of diagonal cracks started in the FE model at 99.5 kN in push direction and -98.7 kN in pull direction. Yielding of the extreme vertical layer of reinforcement was reported to be obtained from the load-deflection curve in the experimental work (Lombard et al., 2000). It was reported that the yielding of the extreme layer of reinforcement occurred at the load levels of +122.7 kN with a top displacement of +3.4 mm and -122.1 kN with a top displacement of -4.2 mm. An average yield load and displacement of 122.4 kN and 3.8 mm was reported respectively. Yielding stress occurred in the extreme layers of

reinforcement steel at +129.1 kN load and -128.05 kN as shown in Figure 5(c) with respective displacements of +3.82mm and -4.54mm. The average yield load and displacement from the FE analysis are 128.6 kN and 4.18 mm. The ultimate load carried by the tested wall was reported to be 187.1 kN (15.44 mm) in push direction and -168.1 kN (-12.15 mm) in pull direction. The ultimate load carried by the wall in the FE analysis was 223.3 kN (15.0 mm) in push direction and -208.5 kN (-12.1 mm) in pull direction. The test was stopped at the ninth load step after reaching 18.2 mm top displacement in push direction at 185.6 kN and -18.3 mm top displacement in the pull direction at -162.0 kN regarding the degrading of wall strength due to the crushing of concrete in the toe regions. At the ninth loading cycle of the FE analysis with ±18 mm top displacement, 212.0 kN load in the push direction and -162.7 kN load in the pull direction are resulted and the analysis stopped in order to comply with the experimental work. Figure 4.18 shows the crack pattern and rebars axial stresses at different stages of analysis resulted from the FE-LCW model.

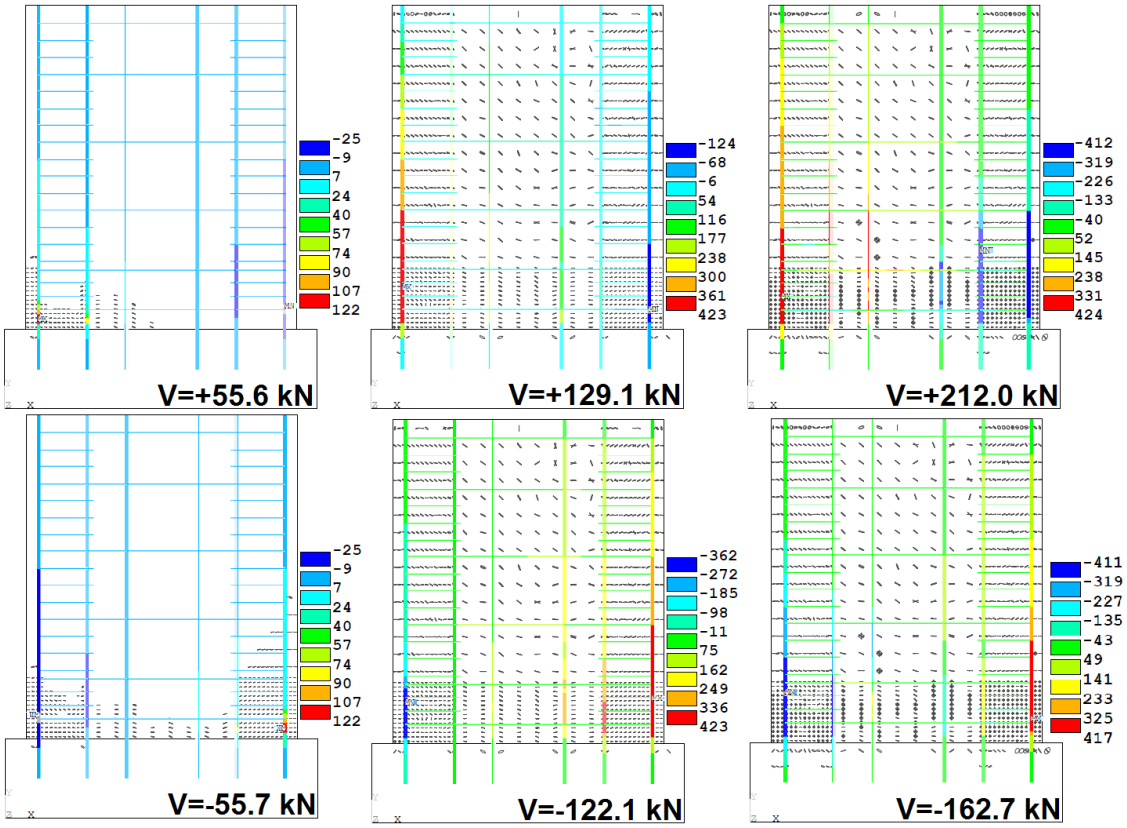

Figure 4.18. Crack pattern and rebars axial stresses at different stages of the analysis resulted from FE-LCW model

CFRP sheets used in the experimental tests of Lombard et al. (2000) were unidirectional with a vertical fiber direction. In order to best simulate the CFRP sheets applied to the surface of concrete elements based on the methodologies explained previously in chapter 3, the tributary width for each FRP element is calculated for various parts of the wall model based on the meshing specifications shown in Figure 4.19 in which b_1, b_2, and b_3 are the tributary widths in different regions of the wall considering the element mesh sizes.

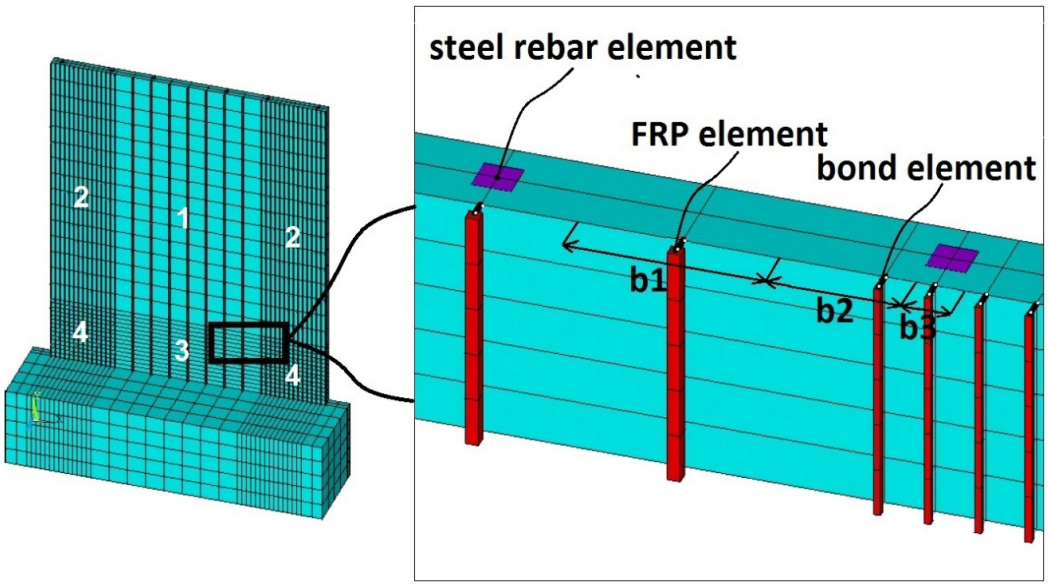

Figure 4.19. Specification of the FRP external reinforcement and the bond interface

The cross-sectional area of each LINK180 element is calculated based on its appropriate tributary width respectively in the modeling. In order to connect the FRP sheets to the wall base and provide the appropriate anchorage, Lombard et al. (2000) used an anchoring device as shown in Figure 4.20 which consisted of an angle profile bolted to the bottom block of the specimen.

A full end anchorage is assumed in the modeling for the FRP sheets by restraining the bottom nodes of FRP to the bottom block. This is based on the full anchoring provided by the anchorage system as stated in the tests by Lombard et al. (2000).

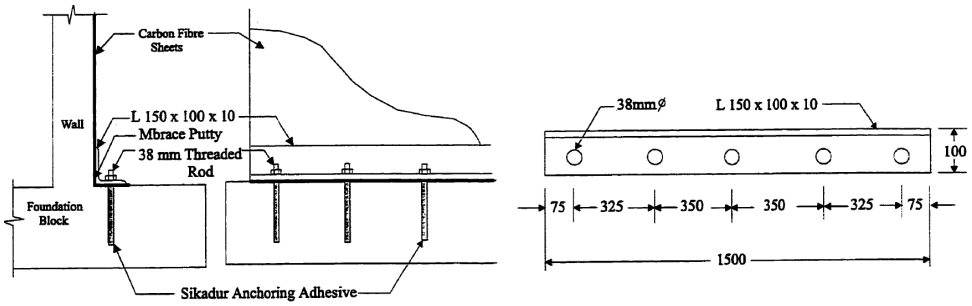

Figure 4.20. FRP anchor device (Lombard et al., 2000)

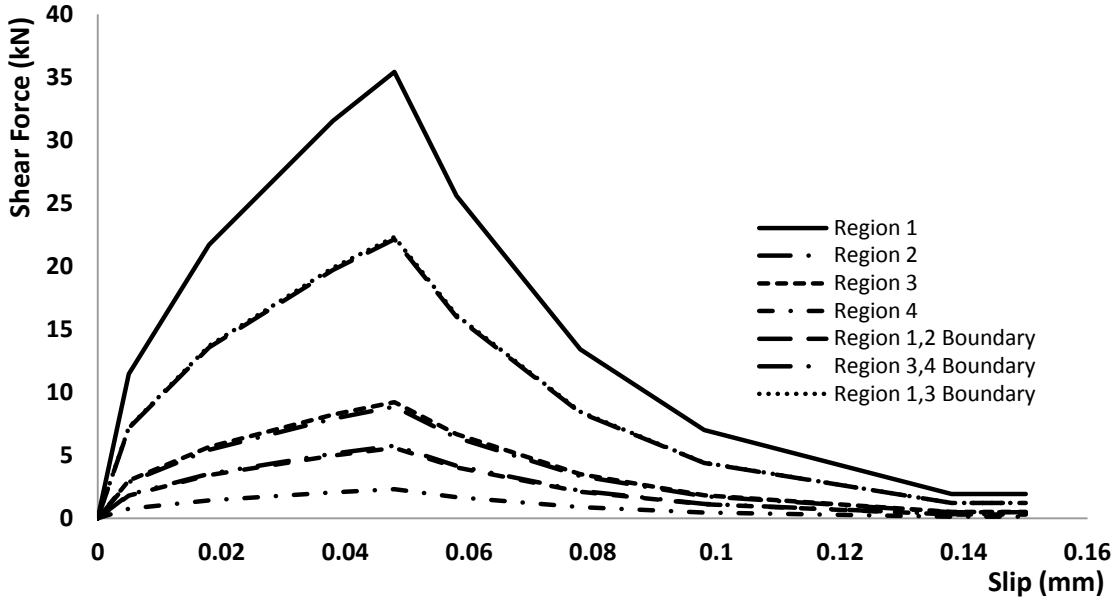

Figure 4.21. Bond-Slip relationships for various regions of the wall model FE-SW1

The bond interface between the FRP wrap and the concrete surface was modeled using tributary area of each node with the same procedure used for the FRP elements based on Lu et al. (2007) model explained earlier in chapter 3, shown in Figure 4.21 by 10-points estimations. The tributary areas and FRP cross-sectional areas at various regions of the wall are shown in Table 4.2.

Table 4.2. FRP and bond elements real constants

Region	b_i (mm)	h_i (mm)	A_i (mm^2)	A_{FRP} (mm^2)
1 (wall web)	100	96	9600	11
2 (wall edges)	25	96	2400	2.75
3 (bottom of web)	100	25	2500	11
4 (wall toes)	25	25	625	2.75
1 , 2 border	62.5	96	6000	6.78
3 , 4 border	62.5	25	1562.5	6.78
1 , 3 border	100	60.5	6050	-
2 , 4 border	25	60.5	152.5	-

The wall surface was first prepared by applying epoxy putty to flatten any possible unevenness in the concrete surface two-to-three weeks prior to the application of CFRP

sheet in the experimental works; in addition, a coating of epoxy primer was also applied to the wall surface one day before the main retrofitting application. The CFRP sheets were placed into wet saturant and were bonded to the wall using a coat of epoxy saturant, where a ribbed roller was used to remove any air bubbles trapped behind the CFRP sheets to ensure proper bonding (Lombard et al., 2000). The mechanical properties of the CFRP sheets and the bonding materials are shown in Table 4.3.

Table 4.3. Material properties of FRP and the bond interface (Lombard et al., 2000)

Material	Tensile Strength (MPa)	Tensile Modulus (GPa)	Shear Strength (MPa)	Ultimate tensile strain (%)	Thickness (mm)
Epoxy Putty	12	1.8	26	N/S*	N/S
Epoxy Primer	12	0.717	24	N/S	N/S
Epoxy Saturant	54	3.034	124	N/S	N/S
Epoxy Resin	20-40	1-10	15-35	N/S	N/S
FRP Sheet	4800	230.5	N/S	1.7	0.11

**N/S: Not Stated*

Lombard et al. (2000) stated that since the observation of cracks was not possible in the experimental tests due to the presence of the FRP layers on the surface of the wall, the crack analysis was done based on estimation by referring to the load-displacement curves. The first flexural cracks were reported to appear at +97.1 kN and a top displacement of +0.7 mm in push direction and at -105.0 kN with a top displacement of -0.6 mm in the pull direction. The cracking load and top displacement were +103.2 kN, +0.5mm, -110.0 kN, and -0.6mm respectively. The yielding of extreme layer of reinforcements was reported to occur at +139.1 kN with a top displacement of +1.5mm in push direction and -167.1kN with -1.7mm displacement at the top of the wall specimen in pull direction in the experimental tests while the yielding occurred at +169.3 kN and -169.8 kN with +1.67mm and -1.68mm top displacements respectively in the FE analysis. The ultimate load carried by the wall in the experimental tests of Lombard et al. (2000)

was reported to be 260.9 kN in push direction and -256.6 kN in pull direction. The load at failure was 202.1 kN in push direction and 246.6 kN in pull direction with final displacements of 29.1 mm and 27.2 mm respectively after degradation of the load carrying capacity during the final load step due to the fracture of the ultimate tensile rebar and crushing of concrete at the compressive toe. The maximum load calculated to be 354.3 kN in the FE model in the push direction with 29.1mm top displacement and -347.9 kN (-23.5 mm) in pull direction. The load-deformation curves of the SW1 specimen are displayed in Figure 4.22 and 4.23 as results of experimental tests of Lombard et al. (2000) and FE analysis. A comparison between the results of FE analysis and experimental tests is presented in Table 4 where a good agreement between the results is achieved.

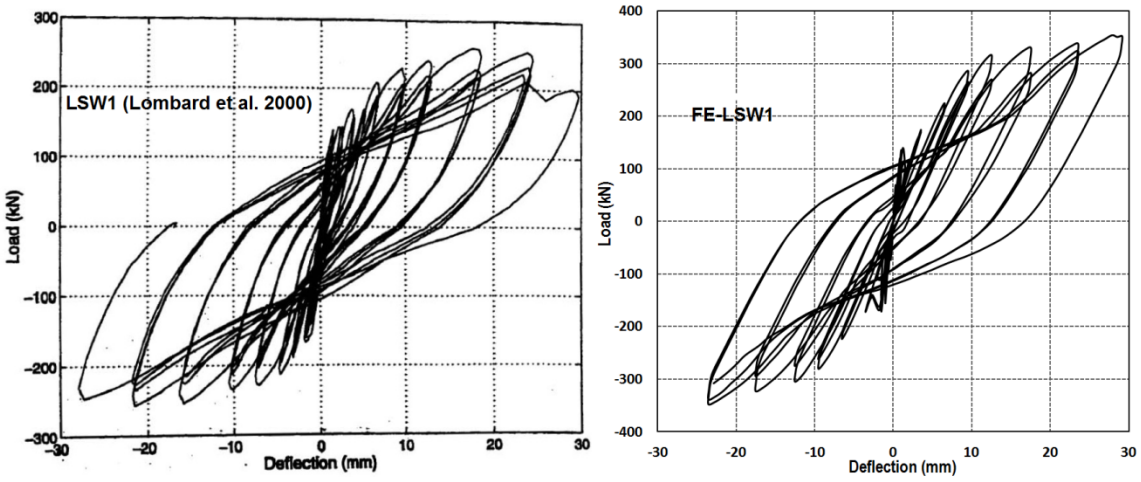

Figure 4.22. Lateral load- top displacement curve of LSW1 (Lombard et al., 2000) and FE-LSW1 model

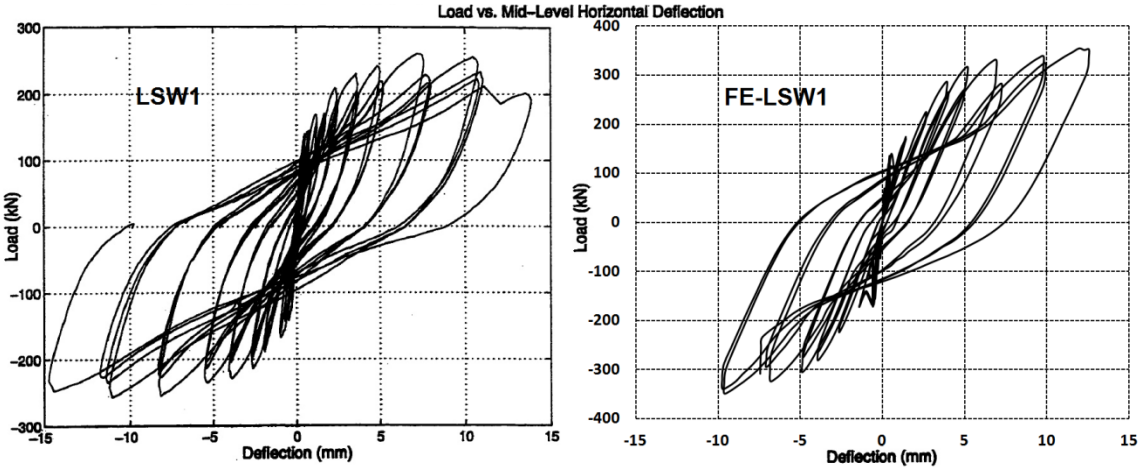

Figure 4.23. Lateral load- mid displacement curve of LSW1 (Lombard et al., 2000) and FE-LSW1 model

4.4 HIOTAKIS ET AL. (2004)

Experimental work of Hiotakis et al. (2004) was a continuation of Lombard et al. (2000) work with the same specimen geometry and arrangements for the control wall (HCW), repaired wall (RW) and the two retrofitted walls, HSW1 and HSW2. In addition, a third specimen with three vertical and one horizontal layer of CFRP external sheets on each side of the wall was tested. The main advantages of the tests of Hiotakis et al. (2004) comparing to Lombard et al. (2000) work were the lateral support provided at the top of the specimen to restrain the lateral buckling of the walls and the method of loading application wherein the loads were applied more slowly and the loading continued after reaching the failure load until the full degradation of the specimen.

Figure 4.23 shows the lateral load vs. top displacement curves of the HCW (Hiotakis et al., 2004) and the corresponding FE model (FE-HCW). The model failed in an earlier stage of loading than the experimental specimen due to the sliding shear failure. The failure mode and the behaviour of this model are explained in more details in chapter 5.

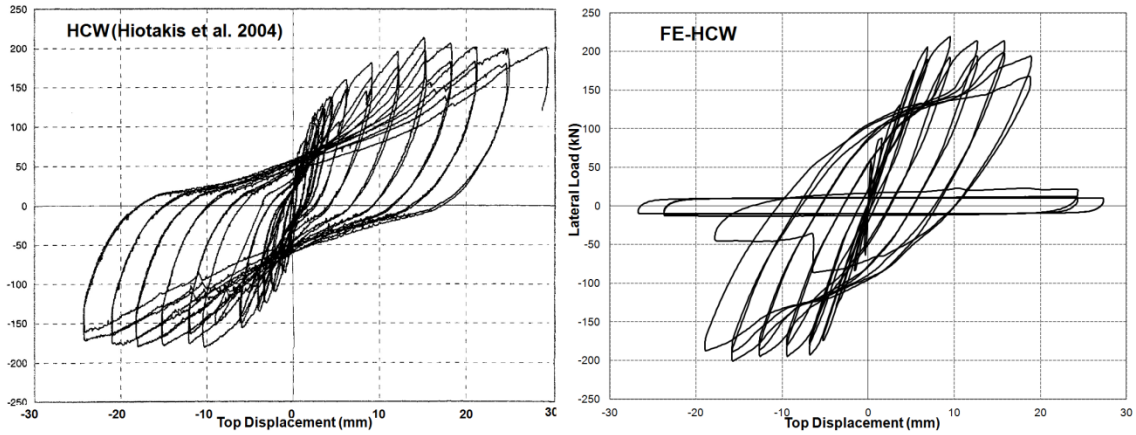

Figure 4.24. Lateral load-deformation curve of HCW (Hiotakis et al., 2004) and FE-HCW model

Hiotakis et al. (2004) reported the first flexural cracks for the control wall (HCW) at load 67.7 kN in the push direction with 0.63 mm top displacement and -59.3 kN in the pull direction formed near the edge of the wall at the construction joints with -0.43 mm top displacement. First significant cracks appeared in the FE model at 57.9 kN in push direction and -40.3 kN in pull direction at the bottom corners of the wall with corresponding top displacements of 0.35 mm and -0.21 mm respectively. The average cracking load resulted from the FE analysis is 49.1 kN comparing to the 63.5 kN load reported in the experimental testing. Yielding of the extreme vertical layer of reinforcement was reported to be obtained from the load-deflection curve in the experimental work. It was reported that the yielding of the extreme layer of reinforcement occurred during the fourth loading cycle at 121.1 kN with top displacement of 2.99 mm in push direction and -123.58 kN with top displacement of -3.09 mm in pull direction. An average yield load and displacement of 122.3kN and 3.04 mm was reported. Yielding of reinforcement steel first occurred at 145.8 kN in push direction and -144.4 kN in pull direction with corresponding top displacements of 4.2 mm and -4.1 mm respectively in the FE analysis. The ultimate load carried by the tested wall was 212.7 kN in the push

direction and -180.4 kN in pull direction comparing to the 219.5 kN ultimate load achieved from the FE model in push direction and -200.8 kN in pull direction. The average ultimate load was 196.5 kN and the average displacement at ultimate load was 12.78 mm. The average ultimate load from the FE analysis is 210.1 kN with a corresponding average displacement of 12.63 mm.

The retrofitted model of Hiotakis et al. (2004) experimental work, HSW1, had the same arrangements in terms of geometry of the specimen and FRP application as those of Lombard et al. (2000) but the loads were applied to the model in smaller steps allowing the degradation of the model to complete. Also, the anchoring of CFRP sheets to the base of the wall was achieved by using a different anchorage device (Hiotakis et al., 2004) consisted of a hollow-sectioned tube bolted to the bottom of the wall holding the CFRP sheet as shown in Figure 4.25(a). The device was stated to provide a full anchorage after being set up as shown in Figure 4.25(b) by means of the free body diagram shown in Figure 4.25(c).

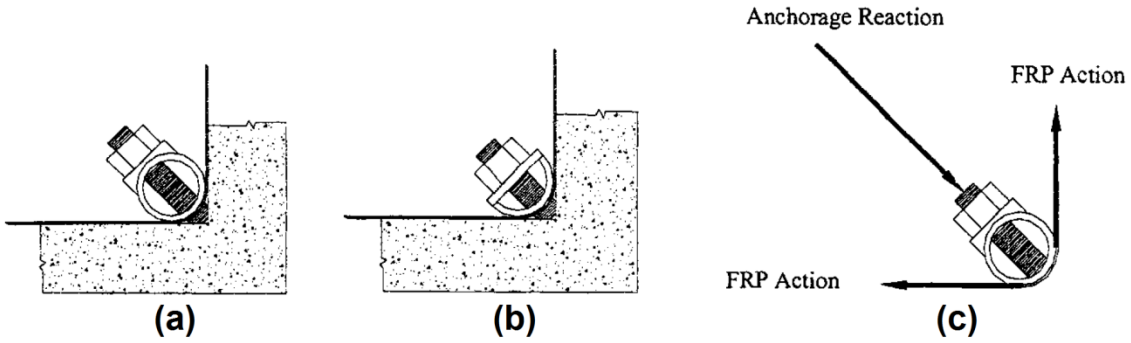

Figure 4.25 The anchorage device used for the anchoring of CFRP sheets (Hiotakis et al., 2004)

A full end anchorage is assumed in the modelling for the FRP sheets by coinciding of the bottom nodes of FRP and the bottom block. This is based on the full anchoring provided by the anchorage system as stated in the tests of Hiotakis et al. (2004).

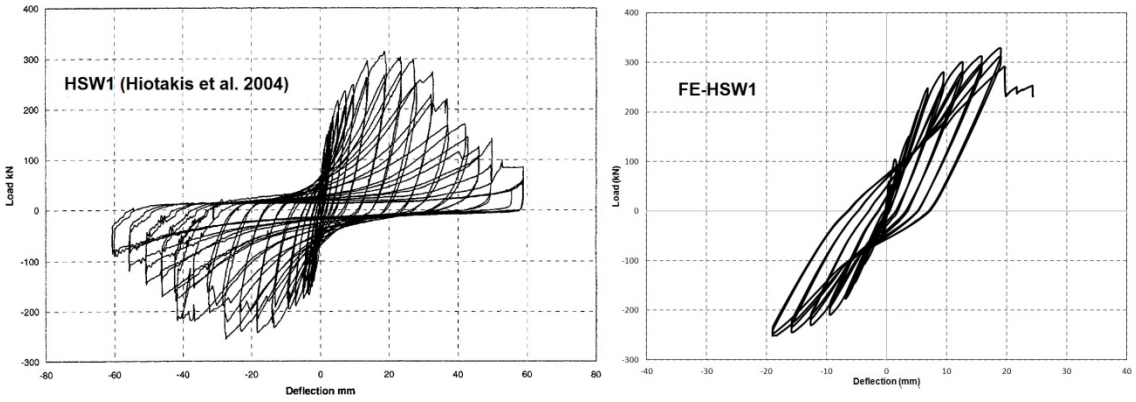

Figure 4.26. Lateral load-deformation curve of HSW1 (Hiotakis et al., 2004) and FE-HSW1 model

Figure 4.26 shows the lateral load-deformation curves resulted from the FE model and experimental test on the strengthened wall specimen HSW1 by Hiotakis et al. (2004). The analysis continued up to the ultimate loading but did not complete the degradation cycles acheived in the experimental test.

Hiotakis et al. (2004) stated that since the observation of cracks was not possible in the experimental tests due to the presence of the FRP layers on the surface of the wall, the crack analysis was done based on estimation by referring to the load-displacement curves. The first flexural cracks were reported to appear at 119.9 kN (0.26 mm) in push direction and at -120.2 kN (-0.53 mm) in pull direction. The first cracks appeared in the FE model in push and pull directions at 59.3 kN (0.35 mm) and -24.5 kN (-0.19 mm) respectively. The yielding of extreme layer of reinforcements was reported to occur at 154.9 kN with a top displacement of 3.06 mm in push direction and -148.4 kN with -2.3 mm displacement at the top of the wall specimen for the experimental tests while the yielding of the extreme layer of vertical reinforcement occurred at 190.3 kN and -123.0 kN in push and pull directions with 3.82 mm and -3.31 mm top displacements respectively in the FE analysis. The ultimate load carried by the wall in the experimental

tests of Hiotakis et al. (2004) was reported to be 313.24 kN (18.69 mm) in push direction and -255.26 kN (-27.38 mm) in pull direction. The ultimate loads achieved during the FE analysis were 328.4 kN (19.01 mm) in push direction and -252.0 kN (-19.01 mm) in pull direction.

4.5 SUMMARY

A total of seven experimentally tested specimens were modeled based on the analysis methodology discussed in chapter 3 and the results were compared to those of the experimental tests and good agreements achieved. The case of RC shear walls without any additional strengthening elements was studied in all of the available experimental studies in order to setup reference results by means of control specimens. A summary of the results of FE analyses of this chapter with the experimental data is shown in Table 4-4. The error percentage in table 4.4 is calculated using the following equation for applicable results.

$$Error\ \% = (FE\text{-}EXP)/EXP*100 \qquad (Eq.\ 3.31)$$

In which "FE" is the output from analysis and "EXP" is the output from experimental data regardless of their sign.

In Table 4.4, the cracking load and deformation are not compared between the FE and EXP because of the fundamental difference between the method of measuring these values in the experimental and FE analysis as discussed before.

The overall average of error for the analysis of RC shear walls of this chapter could be estimated as 11.69% which is an acceptable error percentage for the analysis considering the sophisticated failure criteria and other modeling assumptions explained in chapter 3. From the results presented in Table 4.4, it can be seen that the FE analysis was able to

estimate on average the yield load with 92.8% accuracy, the ultimate load with 84.6% accuracy, the yielding displacement with 83.3% accuracy and the ultimate displacement with 92.5% accuracy.

Table 4.4 Comparison of the FEA and experimental results of RC shear walls at the key performance points (cracking, yielding, and ultimate)

Specimen/Model ID		V_{crack}	Δ_{crack}	V_{yield}	Δ_{yield}	V_{ult}	Δ_{ult}	average error %
Lefas et al. (1991)	LSW14	35	0.34	170	3.9	247	10.75	
	FE-LSW14	35.6	0.32	173.5	2.94	267.1	11.9	
	Error %	N/A	N/A	2.1	-24.6	8.1	10.7	11.37
Lefas et al. (1991)	LSW26	10	0.39	68	5.51	123	20.94	
	FE-LSW26	9.4	0.22	73.8	5.32	152.2	23.8	
	Error %	N/A	N/A	8.5	-3.4	23.7	13.7	12.32
Zhang and Wang (2000)	ZSW7	95.6	1.92	172.3	5.91	201.2	31.27	
	FE-ZSW7	65.4	1.14	168.6	6.23	218.3	31.0	
	Error %	N/A	N/A	-2.1	5.4	8.5	0.9	4.22
Lombard et al. (2000)	LCW	54.8	0.6	122.4	3.8	177.6	13.79	
	FE-LCW	44.3	0.25	128.6	4.18	215.9	13.55	
	Error %	N/A	N/A	5.1	10.0	21.6	-1.7	9.60
Lombard et al. (2000)	LSW1	101.0	0.64	153.1	1.6	258.8	28.15	
	FE-LSW1	106.6	0.55	169.5	1.67	354.3	26.3	
	Error %	N/A	N/A	10.7	4.3	36.9	-6.6	14.62
Hiotakis et al. (2004)	HCW	63.5	0.63	122.3	3.04	196.5	12.78	
	FE-HCW	49.1	0.28	145.1	4.15	210.1	12.63	
	Error %	N/A	N/A	18.6	36.5	6.9	-1.2	15.80
Hiotakis et al. (2004)	HSW1	120.7	1.2	151.6	2.68	284.2	23.03	
	FE-HSW1	41.9	0.27	156.7	3.56	290.2	19.01	
	Error %	N/A	N/A	3.4	32.8	2.1	-17.4	13.92

CHAPTER 5

INFLUENCE OF DESIGN PARAMETERS ON THE SEISMIC PERFORMANCE OF RC SQUAT SHEAR WALLS

5.1 INTRODUCTION

Reinforced Concrete (RC) walls are classified according to CSA (2004) as bearing walls, non-bearing walls, and shear walls: including flexural shear walls and squat shear walls. Many design codes refer to slender shear walls (or simply, shear walls) as a vertical cantilever structural element that is loaded axially and laterally at the story levels of the buildings with a potential plastic hinge region located at the base of the wall (Paulay and Priestley, 1992). There is a conceptual difference in the behaviour of such *slender* shear walls dominated by the flexure response of the wall and other non-slender (squat) shear walls, where the response is mainly driven by the strut-and-tie model (Yanez et al., 1989). The definition of squat shear walls differs from one reference to the other. Some references use the height-to-length ratio and identify those walls with H_w/L_w less than 2 or 3 as squat walls (Paulay and Priestley, 1992) where H_w and L_w are the wall height and length, respectively. Whereas other researchers refer squat walls to the walls with a low shear span-to-length ratio namely M/VL_w less than 1.5 (Salonikios et al., 1996) as squat walls where M and V are the equivalent applied moment and shear force and the maximum moment located at the bottom of the wall, respectively (thus M/V represents the shear span of the wall). Aside from the categorizing method, an agreement on the difference between the type of behaviour of squat and slender shear walls exist in all

references which mainly is the failure of the wall to be dominated by flexure in the slender shear walls and shear in the squat ones.

In this chapter, the behaviour of squat shear walls under applied lateral loads is explained and the influence of some major parameters on its response will be discussed using the experimental data available in the literature and the results of performed FE analyses.

5.2 FAILURE MODES OF RC SQUAT WALLS

Loading a RC squat shear wall beyond its cracking limit would make the wall undergo a nonlinear behaviour with extensive cracking in concrete and the post-yield stains in the reinforcing steel until the wall reaches its failure limit (Paulay and Priestley, 1992). In this case, four possible modes of failure exist for a typical RC squat wall as follows:

Diagonal tension mode: In walls with insufficient horizontal reinforcement, if the shear forces at the top of the wall are not evenly distributed by means of a rigid top beam or a slab with sufficient in-plan rigidity, the concrete in the web region subjects to tensile stresses and a corner-to-corner tensile failure plane may develop as shown in Figure 5.1(a). Paulay and Priestly (1992) indicate that such failure may also occur along a steeper failure plane in cases where there are paths existing to transfer the shear forces through the wall (Figure 5.1(b)).

Flexural failure: When the diagonal tension mechanism is restricted by providing sufficient horizontal reinforcement, the concrete at the compressive toe may crush under the high axial loads resulted by the bending moments and the extreme layers of vertical reinforcement bars in the tensile edge may yield and undergo plastic deformations. This failure mode is the result of well design and detailing with a ductile

manner but it would only occur if the geometry of the wall permits the high bending moments to be generated during the lateral loading history.

Diagonal compression failure: In cases where the flexural mode does not occur due to the low moment-to-shear ratio and the horizontal reinforcement is sufficient, the concrete in the compressive diagonal region may crush as shown in Figure 5.1(c). This mode of failure is more likely in cases of cyclic loading reversals that result in two sets of shear cracks in the diagonals wherein the overall concrete strength reduces by the closing and reopening of the cracks (Paulay and Priestley, 1992). The crushing of concrete may spread through the length of the wall in the last reversals of a cyclic loading as shown in Figure 5.1(d). If a wall undergoes such a failure mechanism during a loading event, the loss of strength is almost irrecoverable and such failure mode must be avoided in cases where the repairing of the wall is regarded. Although this mechanism is more desirable comparing to the diagonal tension, it is to be avoided because of its brittle manner.

Sliding Shear failure:

If both diagonal tension and compression modes are restricted in a RC squat shear wall, a flexural behaviour causes the horizontal cracking of concrete under the tensile stresses at each load reversal. The sliding resistance of the wall at base region in the first load reversals where the concrete strength in the compressive toe is not yet affected significantly by the closing and reopening of the horizontal cracks occurred in the previous reversal of each cycle is mainly provided by concrete. As the concrete in the boundary of the wall and foundation cracks throughout the entire wall length, the main resistance against the sliding forces at this region is provided by the dowel action

of the vertical rebars. With compressive yielding of the rebars, extensive deformations in the base of the wall occur due to the sliding shear until the complete loss of strength as shown in Figure 5.1(e).

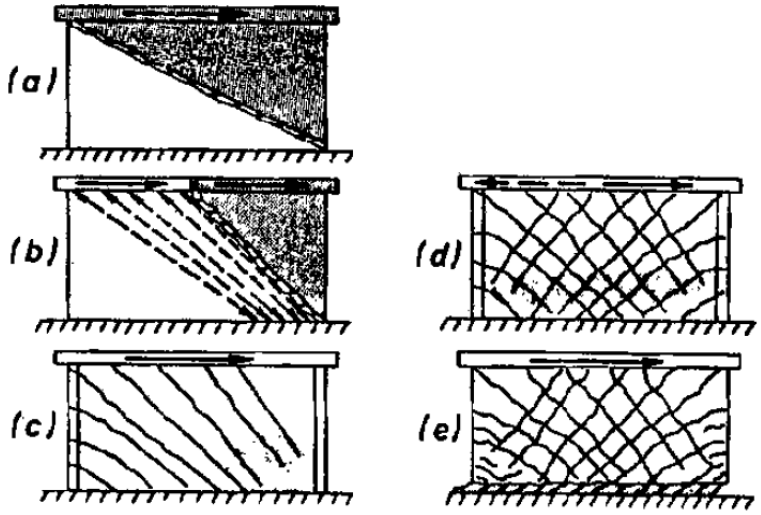

Figure 5.1 Shear failure modes in squat walls (Paulay and Priestley, 1992)

In order to design a RC squat shear wall with adequate strength and ductility, special care must be taken to restrict the undesirable failure modes. Thus, the shear and flexural capacities of the wall must be calculated using appropriate models.

5.3 SHEAR DEGRADATION MODELS

The nominal shear capacity of RC shear walls, V_R, results from the contribution of two main mechanisms, namely; shear resistance attributed to the concrete , V_c, and shear resistance provided by the steel reinforcement V_s. In cases where additional external retrofitting materials V_{ex} exist, their effects should be included in the nominal shear capacity in the following sequence;

$$V_R = V_c + V_s + V_{ex} \qquad \textit{(Eq. 5.1)}$$

Aside from the basic equations for V_c, several models have been proposed during the recent years for the contribution of the shear strength of concrete in the nominal shear capacity of RC walls and squat columns with the effects of shear degradation included. Amongst those equations available in the literature, the models proposed by (Priestley et al., 1994), (Kowalsky and Priestley, 2000) and (Moehle et al., 2001) are cited by most of the authors. In the case of squat walls, the proposed models only take into account the diagonal tension model of failure without accounting for the effects of axial forces. The first family of models with considerations of the axial forces along with the degradation of the concrete material started with the following model proposed by the CEB/FIP model code (1990) for circular columns.

$$V_c = \sqrt{f_c'}\, K(\mu_\Delta) min\left(1.5, max\left(1{,}3 - \frac{L_s}{h}\right)\right) min(1{,}0.5 + 20\rho_{tot.})\left(0.8A_g\right) + N\frac{h-C}{2L_s}$$

(CEB/FIP model code, 1990) *(Eq. 5.2)*

Where $\rho_{tot.}$ is the ratio of longitudinal steel, A_g is the gross area of the cross section, D_c is the diameter of the confined concrete core, N is the total axial force applied, c is the compression zone depth and L_s is the shear span. The effect of the shear strength degradation is imposed into the model by the $k(\mu_\Delta)$ coefficient.

$$k(\mu_\Delta) = \frac{1.07 - 0.115\mu_\Delta}{3}\ ,\ 0.05 \le k(\mu_\Delta) \le 0.28 \qquad \textit{(Eq. 5.3)}$$

Eq. 5.3 denotes the value of $k(\mu_\Delta)$ for an applicable range of μ_Δ, the displacement ductility of the column (Kowalsky and Priestley, 2000).

Although the above equations were derived for circular columns, Kowalsky and Priestley (2000) stated that the same equations could be used for the rectangular columns by

replacing the term $0.8A_g$ by $b_w.d$ where b_w is the width of web and d is the effective depth of the column.

Moehle et al. (2001) introduced a new family of models on the basis of previous models for rectangular columns wherein the effect of axial forces is included in the concrete strength term instead of acting separately in the equation.

$$V_c = 0.5k(\mu_\Delta)\sqrt{f_c'}\left(\sqrt{1+\frac{N}{0.5A_g\sqrt{f_c'}}}\right)\left(A_g\frac{d}{L_s}\right) \textit{ (Moehle et al., 2001)} \qquad \textit{(Eq. 5.4)}$$

Where $A_g=b_w.h$, and V_c is in MN. The $k(\mu_\Delta)$ coefficient is calculated from the following equation,

$$k(\mu_\Delta) = 1.15 - 0.075\mu_\Delta\,,\ 0.7 \le k(\mu_\Delta) \le 1.0 \qquad \textit{(Eq. 5.5)}$$

The most recent models provided for the calculation of the nominal shear capacity of the walls are based on an extensive work by (Biskinis et al., 2004) from the results of 53 tests on columns with circular sections, 161 tests on columns or beams with rectangular or square sections, 19 on piers with hollow or T-shaped sections, and 6 shear walls. Three models were provided to match the most cases and cover almost every possible failure modes.

$$V_c = \frac{h-c}{2L_s}min\left(N, 0.55A_gf_c'\right) + 0.16\left(1-0.095min\left(4.5,\mu_\Delta^{pl}\right)\right)max(0.5,100\rho_{tot})\left(1-0.16min\left(5,\frac{L_s}{h}\right)\right)\sqrt{f_c'}A_g \qquad \textit{(Biskinis et al. 2004)} \qquad \textit{(Eq. 5.6)}$$

Where $\mu^{pl}_\Delta=\mu_\Delta-1$ represents the plastic part of the displacement ductility factor. The value of V_c resulted from Eq. 5.6 could be used in Eq. 5.1 as the contribution of concrete in the shear resistance of the wall.

All of the above models calculate the value of V_c to be used separately in Eq. 5.1 indicating the fact that in all of them the shear degradation only affects the concrete strength and the contribution of transverse steel reinforcement is calculated as:

$$V_s = \rho_w b_w (d - c) f_{yw} cot\theta \qquad \textit{(Eq. 5.7)}$$

Where ρ_w denotes the ratio of transverse steel and θ indicates the truss inclination in the strut-and-tie model with the suggested value of 45 degrees (Moehle et al., 2001).

As a complimentary to Eq.5.6, Biskinis et al. (2004) suggested a more accurate model wherein both V_c and V_s degrade with inelastic cyclic displacements.

$$V_R = \frac{h-c}{2L_s} min\left(N, 0.55A_g f_c'\right) + \left(1 - 0.05min\left(5, \mu_\Delta^{pl}\right)\right)\left[0.16max(0.5,100\rho_{tot})\left(1 - 0.16min\left(5, \frac{L_s}{h}\right)\right)\sqrt{f_c'}A_g + V_S\right] \qquad \textit{(Biskinis et al., 2004)} \qquad \textit{(Eq. 5.8)}$$

The shear strengths resulted from equations 5.6 and 5.8 fit the experimental data for a vast range of parameters at their right hand side with the suggested range for the axial load ratio, $N/A_g f_c^{'}$, from -0.01 to 0.85; shear span ratio, L_s/h, from 0.5 to 6.0; total longitudinal reinforcement ratio, ρ_{tot}, from 0.55% to 5.5%; concrete compressive strength, $f_c^{'}$, from 13.0 to 113.0 MPa; and displacement ductility ratio, μ_Δ, from 1.0 to 9.5 (Biskinis et al., 2004).

All of the previously discussed models refer to the diagonal tension as the principal mode of failure, the only model available in the literature that empirically calculates the shear degradation model for shear walls and columns with diagonal compression failure mode is the third model offered by Biskinis et al. (2004).

$$V_R = 0.85\left(1 - 0.06min\left(5, \mu_{\Delta}^{pl}\right)\right)\left(1 + 1.8min\left(0.15, \frac{N}{A_c f_c'}\right)\right)(1 + 0.25max(1.75, 100\rho_{tot}))\left(1 - 0.2min\left(2, \frac{L_s}{h}\right)\right)\sqrt{min(f_c', 100)}b_w Z$$

(Biskinis et al. 2004) *(Eq. 5.9)*

Where $Z=0.8L_w$ for the rectangular walls and $Z=d-d'$ for the barbell sectioned walls.

The research on the externally applied retrofitting material e.g. FRP wraps or steel plates on the shear degradation model of columns and walls is still on the early stages. Up to the author's knowledge at the date of preparing this thesis, no model was found in the reported literature indicating the effect of external FRP wraps on the shear degradation model.

5.4 BEHAVIOUR OF RC SQUAT SHEAR WALLS UNDER CYCLIC AND MONOTONIC LOADING

As seen in the previous section, there are two possible methods of analysis considering the loading scheme when modeling RC squat shear walls namely, incremental monotonic and incremental reversed (cyclic analysis). In case of cyclic analysis, the main output resulted from the analysis would be the load-displacement cyclic loops giving a general idea about the type of behaviour and the quality of performance of the wall. One other significant data achievable from the cyclic analysis is the total energy dissipation which is the area occupied by the load-displacement loops. On the other hand, a monotonic analysis also gives a general view of the overall behaviour and performance of the wall but the data is only based on a one-step loading where the degradation of the strength of materials through cyclic loading may not be considered. A detailed study on the output resulted from the cyclic and monotonic analysis of FE-HCW (Hiotakis et al., 2004) is

presented in the section. Figure 5.2 presents the lateral load at different top displacements resulted from the cyclic and monotonic analysis.

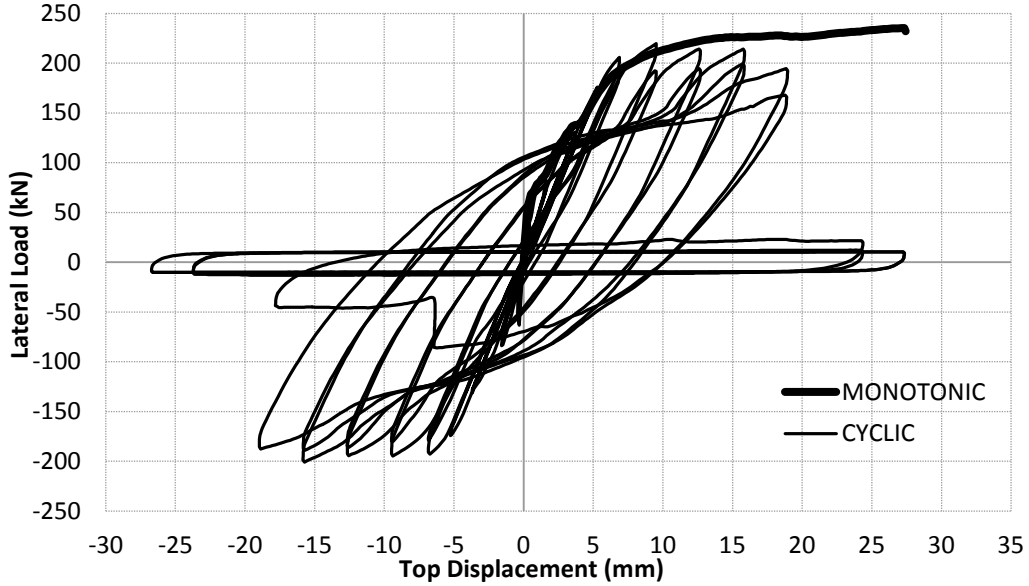

Figure 5.2 Lateral load-displacement results of the FE-HCW model under monotonic and cyclic loading

In the monotonic analysis, the top displacement is applied to the model through incrementally increasing substeps. The rate of applying the displacement is 0.2 mm at each step resulting in a total of 136 data points for the analysis with several output data available at each point. On the other hand, the cyclic analysis consists of 11 displacement increments with two reversals at each increment resulting in a total of 45 loadsteps for the analysis as shown in Figure 5.3 with the same rate as for the monotonic analysis. The last two load increments are completed after the complete degradation of the wall model strength in the cyclic analysis as shown in Figure 5.2 and the maximum top displacement achieved before failure was 18.9 mm, on the other hand, the monotonic analysis continued up to the maximum top displacement of 27.4 mm which is 45% greater than

the cyclic analysis result. The latter observation implies that the failure of the model is highly dependent on the loading protocol: i.e. monotonic versus cyclic loading.

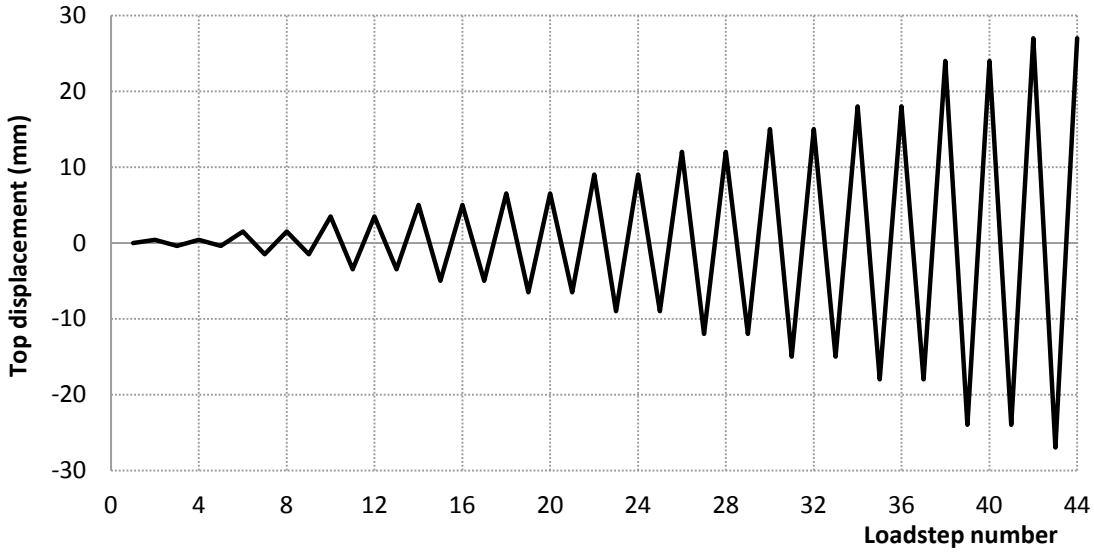

Figure 5.3. Loading scheme in the displacement-controlled cyclic analysis

The cracking of concrete in the tensile toe region occurred at the first loadstep during the cyclic analysis at the same load and displacement values as in the monotonic analysis. As the loading continues in the monotonic analysis, the cracks propagate from the tensile toe into the web of the wall and the vertical rebars in the tensile toe region start to exhibit increasing tensile forces until the extreme layer of reinforcement bars (tensile tie) yield under the tensile forces. Figure 5.4 shows the crack pattern and the rebars axial stresses at 3 different stages of loading namely, cracking, yielding and failure as obtained from the monotonic analysis. Since the forces generated in the vertical and horizontal rebars were not in a close range, the contour ranges in Figure 5.4 are only showing the vertical rebars axial stress, thus the axial stresses in the horizontal rebars at the same analysis stages are shown separately in Figure 5.5.

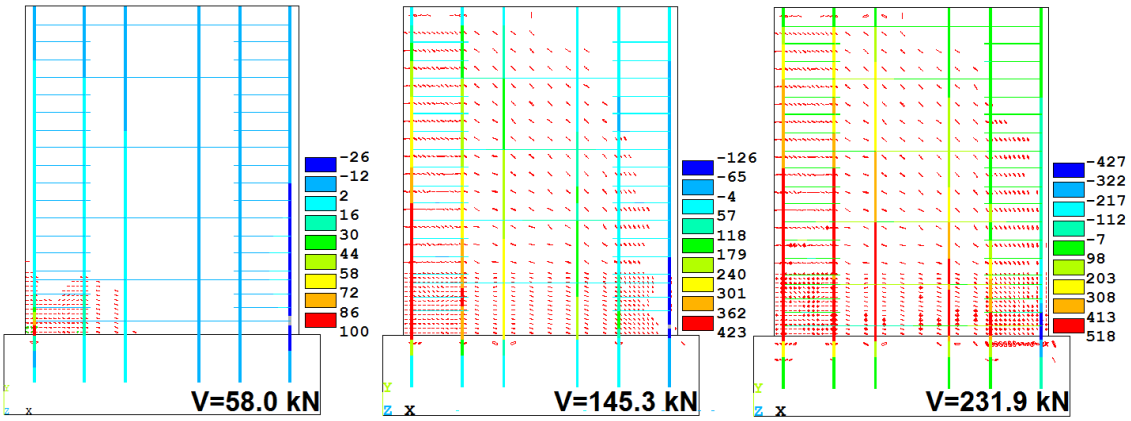

Figure 5.4. Crack pattern and vertical rebar axial stress at various stages of monotonic analysis of the FE-HCW wall model

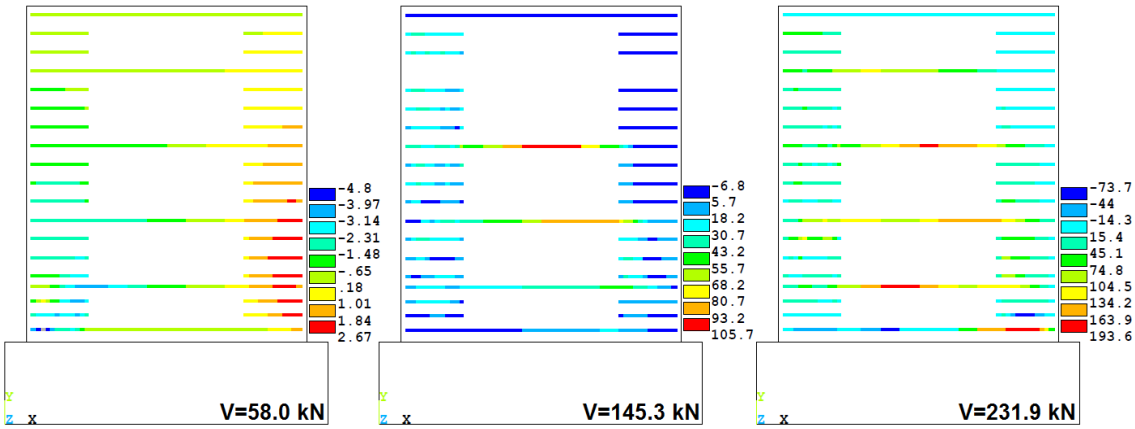

Figure 5.5. Horizontal rebar axial stress at various stages of monotonic analysis of the FE-HCW wall model

In order to better understand the behaviour of the wall under the applied loads during the monotonic analysis, the stress distribution over the wall is shown in Figure 5.6 at the same three stages of loading. The development and increase in compressive stresses in the diagonal strut of the wall is shown in Figure 5.6; also at final stages of loading, the sliding shear stress at the bottom of the wall is visible, but the failure of the wall is due to the crushing of concrete in the compressive toe under the flexural failure mode. As seen in Figures 5.4 and 5.5, the behaviour of the wall in the early stages of analysis is more flexural dominated considering the tensile and compressive stresses in the rebars at the tensile and compressive toes.

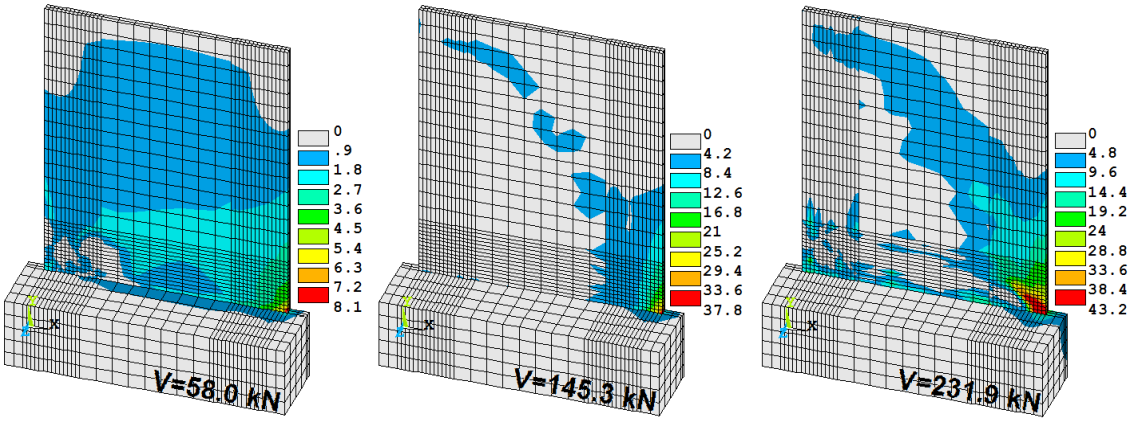

Figure 5.6. Stress distribution in the model at various stages of monotonic analysis of the FE-HCW wall model

After cracking, as the cracks distribute through the wall web, the contribution of vertical rebars (i.e. the tie) in the lateral load resistance increases and more layers of reinforcement exhibit tensile forces, this phenomenon is shown in Figure 5.7 in terms of the axial strains in the six layers of vertical reinforcement. The behaviour of the wall model is also studied here in terms of the axial stresses generated in the horizontal rebars. Figure 5.8 shows the axial stresses generated in the horizontal rebars in the 5 layers from bottom to the top of the wall. From Figure 5.8, it is understandable that the three upper layers namely layers 3, 4 and 5 start to contribute in the shear strength of the wall only after the cracking and their tensile stress grows slowly as the analysis continues. The contribution of horizontal reinforcement bars in the wall performance varies for different layers at different stages of loading as shown in Figure 5.8. The stress in the first layer of horizontal reinforcement start to increase significantly after yielding of the fifth layer of vertical reinforcement but it did not reach the yield limit during the analysis.

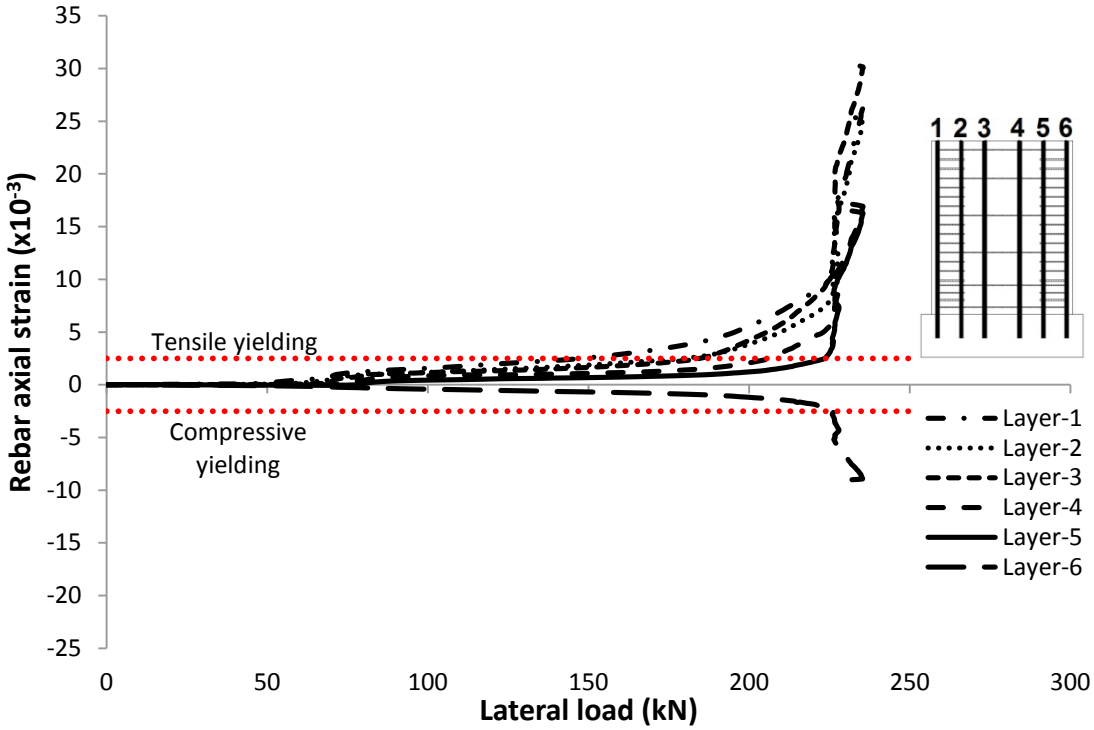

Figure 5.7. Stress in various layers of vertical reinforcement during the monotonic analysis of FE-HCW

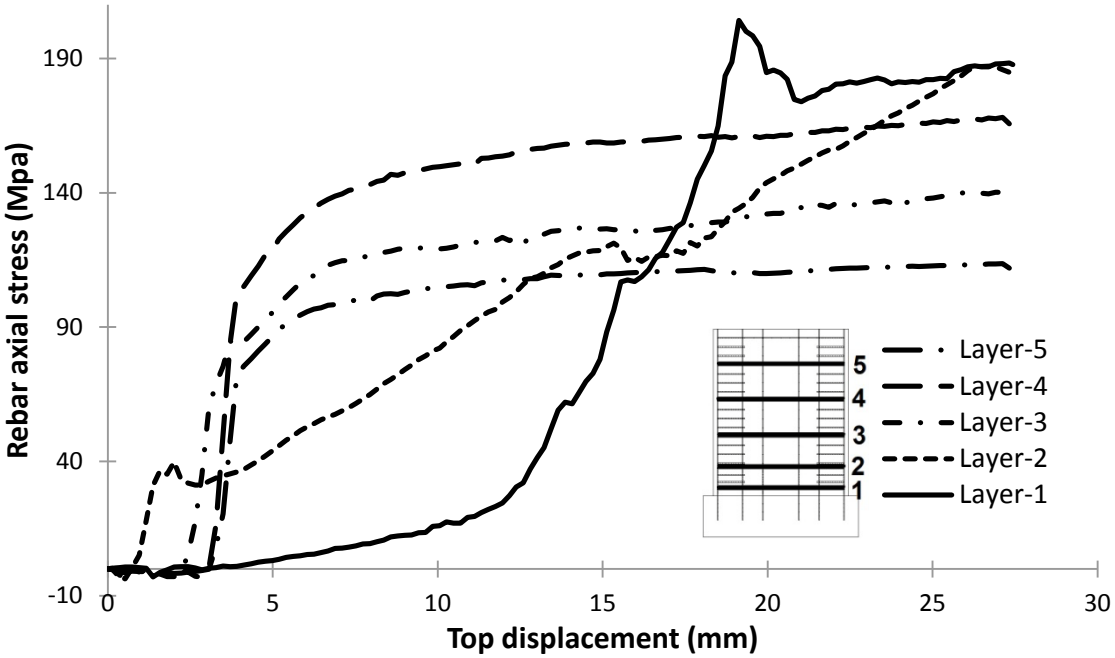

Figure 5.8. Maximum axial stress in various layers of horizontal reinforcement during the monotonic analysis of FE-HCW

The axial stress in the second layer of reinforcement generated immediately after the cracking and continued to increase almost linearly through the analysis but did not reach the yield limit. The three upper layers of horizontal reinforcement start to contribute in the strength of the wall after cracking in concrete developed into the middle regions and the stress remains almost constantly in these three layers during the analysis as shown in Figure 5.8.

In order to better assess the behaviour of the wall, the plane sections hypothesis (usually used for slender walls) is also investigated by comparing the vertical displacement of the wall at 2 different sections through the height of the wall namely H/2 and H/8 where H is the height of the wall in 4 stages of analysis namely, pre-cracking, post-cracking, yielding and failure as shown in Figures 5.9 and 5.10.

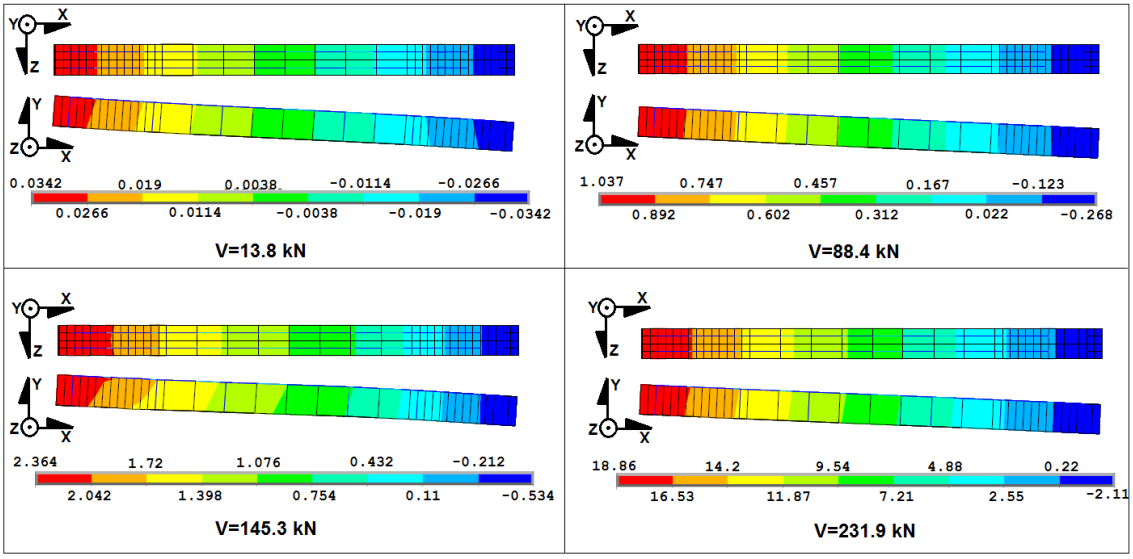

Figure 5.9. In-plane deformations in mid-height of the wall at 4 loading stages during the monotonic analysis of FE-HCW

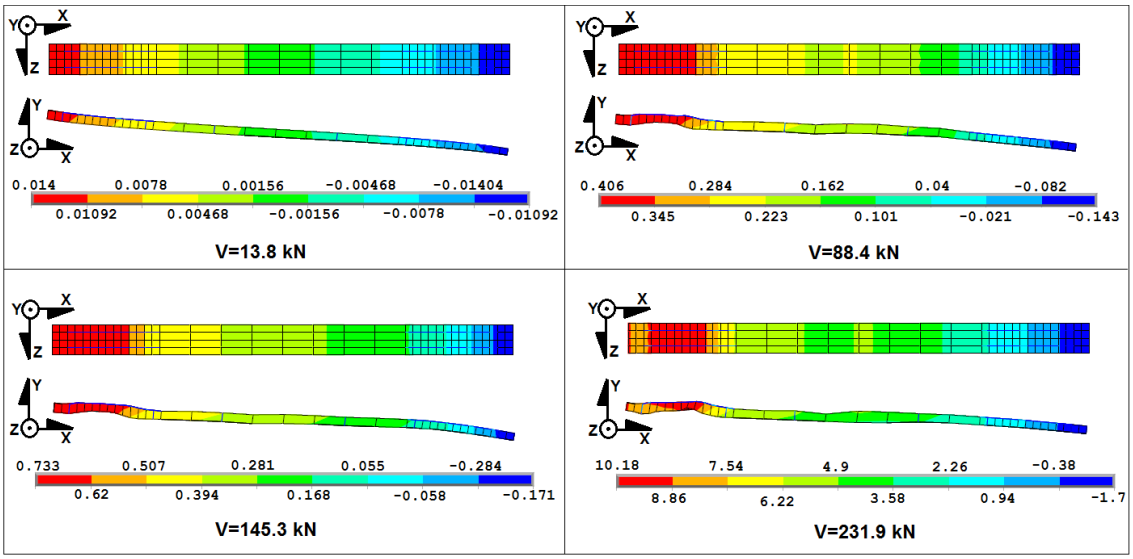

Figure 5.10. In-plane deformations in 1/8-height of the wall at 4 loading stages during the monotonic analysis of FE-HCW

As shown in Figures 5.9 and 5.10, the plane sections at 1/2-height of the wall retain their shape in different stages of the analysis but the shape is highly distorted at 1/8-height of the wall. Figure 5.11 shows the vertical displacement of 5 selected points along the wall length namely, the tensile edge, the second vertical rebar layer, mid-length, the fifth vertical rebar layer and the compressive edge of the wall at different elevations namely, section-A (1/36-H), section-B (1/8-H), section-C (1/4-H) and section-D (1/2-H). At the bottom of the wall, the load-vertical displacement curves for the three interior points namely 2, 3 and 4 are almost equal indicating a flat surface in the web of the wall but the tensile and compressive edges of the wall exhibit more vertical deformations. This indicates that the plane section at the bottom of the wall deforms significantly during the analysis. As we move through the wall height, the difference between the vertical displacements of the points along the wall length increases indicating the invalidity of the plane sections hypothesis, and that the wall is on the verge of following a strut-and-tie model as its H/L=1.193.

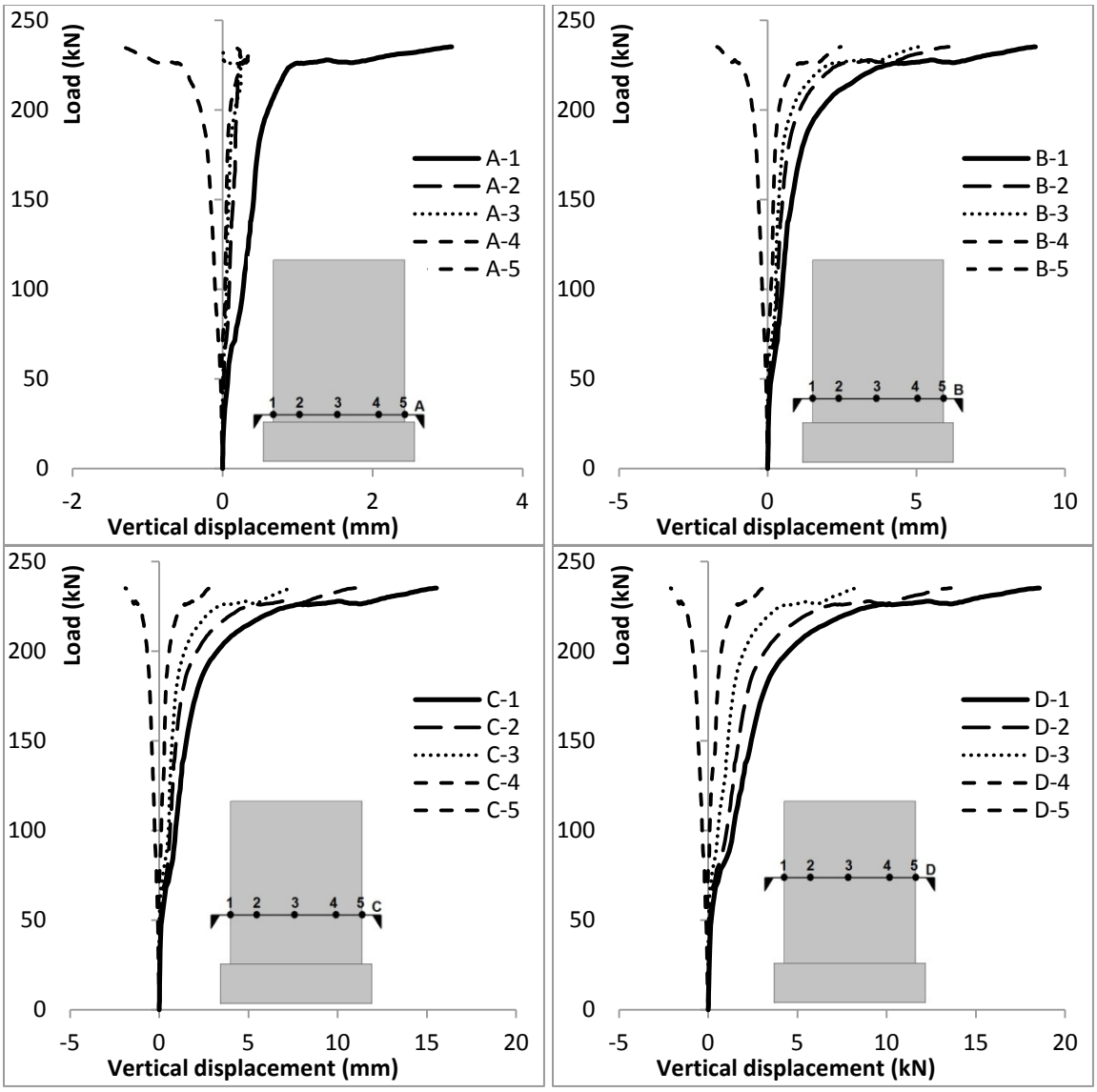

Figure 5.11. Vertical displacement of 5 selective points in different heights during the monotonic analysis of FE-HCW

As shown previously in Figure 5.2, the load-displacement curve of the wall under monotonic loading matches the peak points on the positive side of the cyclic load-displacement curve in the first cycles. As the cyclic loading continues after yielding of the first and second layers of vertical reinforcement, a softening in the performance of the wall starts and continues until the failure displacement which is 45% lower than that of the monotonic analysis. The wall fails during the second loop of the 17th cycle after

completion of one and half cycles with top displacement of 18.9 mm. The load and displacement at failure were -86.2 kN and -6.5 mm respectively. Figure 5.12 shows the cracks pattern and the vertical reinforcement bars axial stresses at three loading stages namely, cracking, yielding and failure.

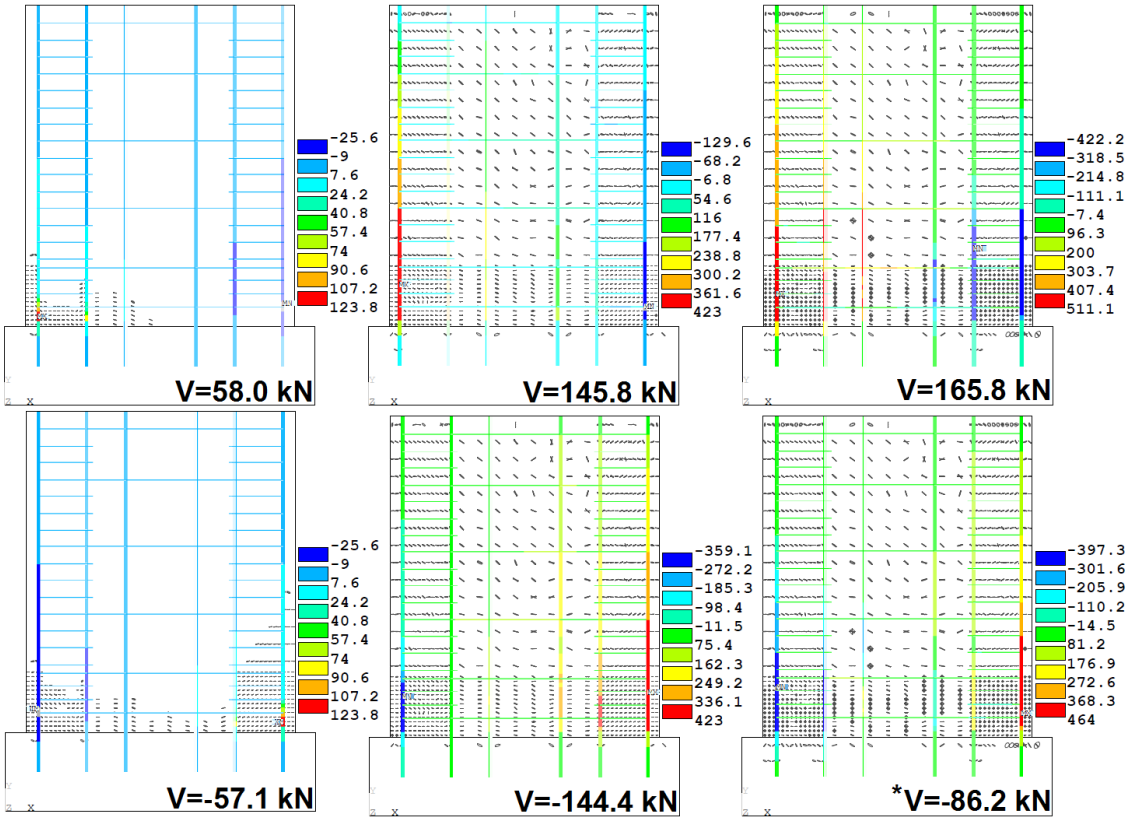

Figure 5.12. Crack pattern and vertical rebar axial stress at various stages of cyclic analysis of the FE-HCW wall model

The average (from push and pull directions) cracking load resulted from the cyclic analysis is 57.55 kN which is almost equal to the cracking load in monotonic analysis. The yielding of the first layer of vertical reinforcement occurred at 145.8 kN and -144.4 kN in the first loop of the 7th cycle in the positive and negative half-cycles, respectively. The average yielding load resulted from the cyclic analysis is 145.1 kN which is slightly less than that of the monotonic analysis. The horizontal reinforcement bars did not reach the yielding stress during the analysis as shown in Figure 5.13.

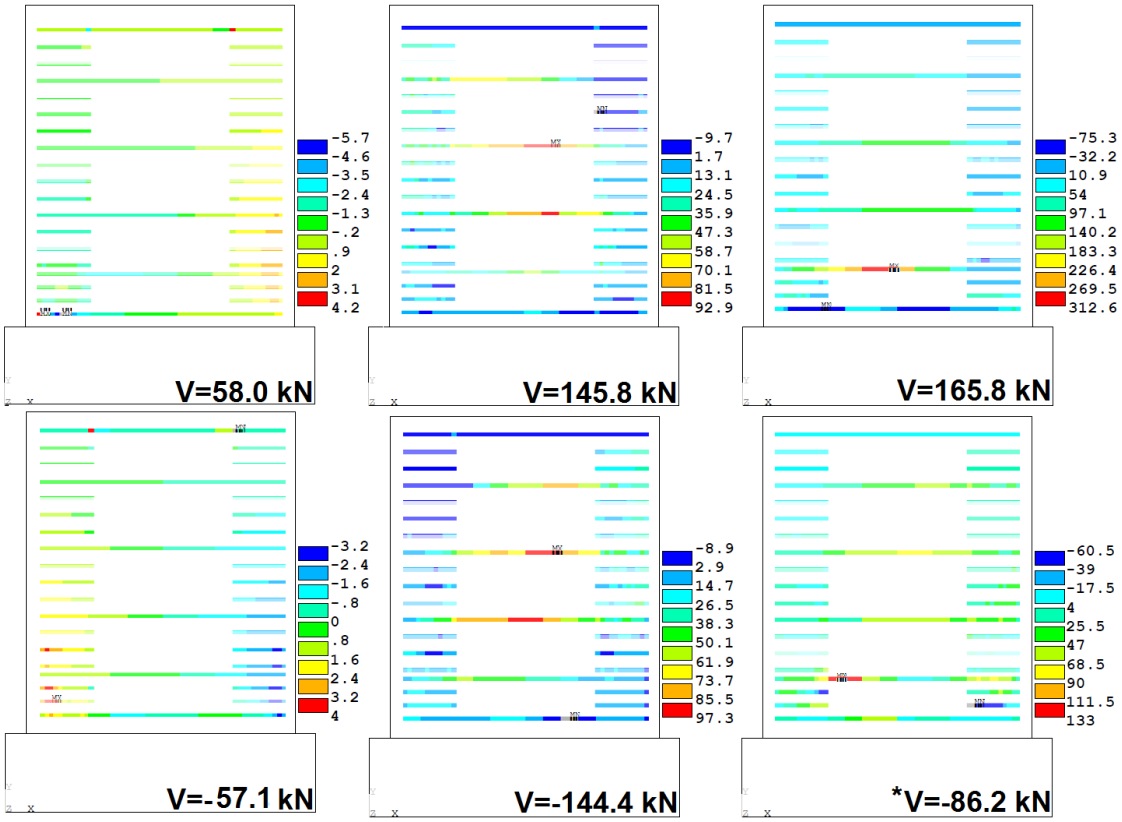

Figure 5.13. Horizontal rebar axial stress at various stages of cyclic analysis of the FE-HCW wall model

Same like the response of the RC wall model subjected to a monotonic load, the axial stresses in the horizontal reinforcement bars of the cyclically loaded model increase significantly after the cracking load. The stress distribution along the layers of horizontal reinforcement changes during the loading cycles. The maximum stress occurs in the 3rd and 4th layers of horizontal reinforcement at the yielding load but as the analysis continues the stresses in the first and second layers of horizontal reinforcement increase significantly while the three top layers exhibit almost constant stresses. This phenomenon is related to the stress distribution through the wall as shown in Figure 5.14 at various stages of cyclic loading.

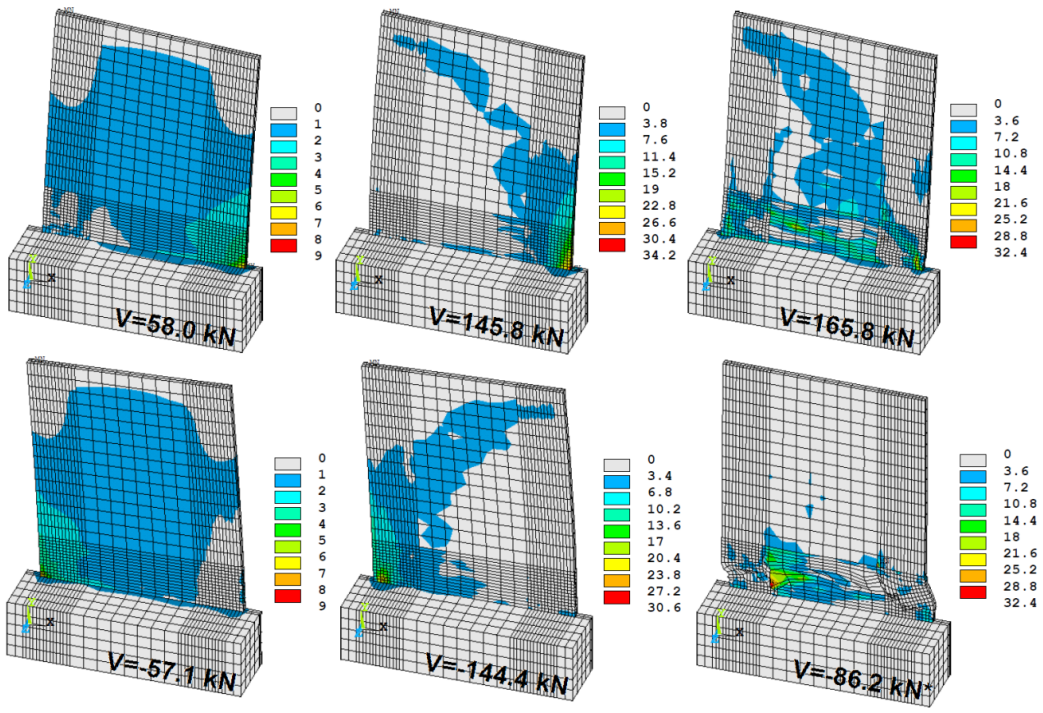

Figure 5.14. Stress distribution in the model at various stages of cyclic analysis of the FE-HCW wall model

After the cracking stage, the uniform distribution of stresses through the wall changes and forms a diagonal compression shape when the contribution of horizontal reinforcement in the wall strength grows. At the end of the positive half-cycle of the 9th loading cycle before failure, the stresses distribute along the bottom of the wall web as shown in Figure 5.14 resulting in the high tensile stress in the second layer of the horizontal rebars in the form of sliding shear failure. The wall finally fails due to the high stresses at the bottom of the web as shown in Figure 5.14 before completion of the second half-cycle of the 9th loading cycle at the load and displacement of -86.2 kN and -6.24 mm respectively. The strain in vertical and horizontal reinforcement layers are shown in Figures 5-15 and 5-16 from the cyclic analysis.

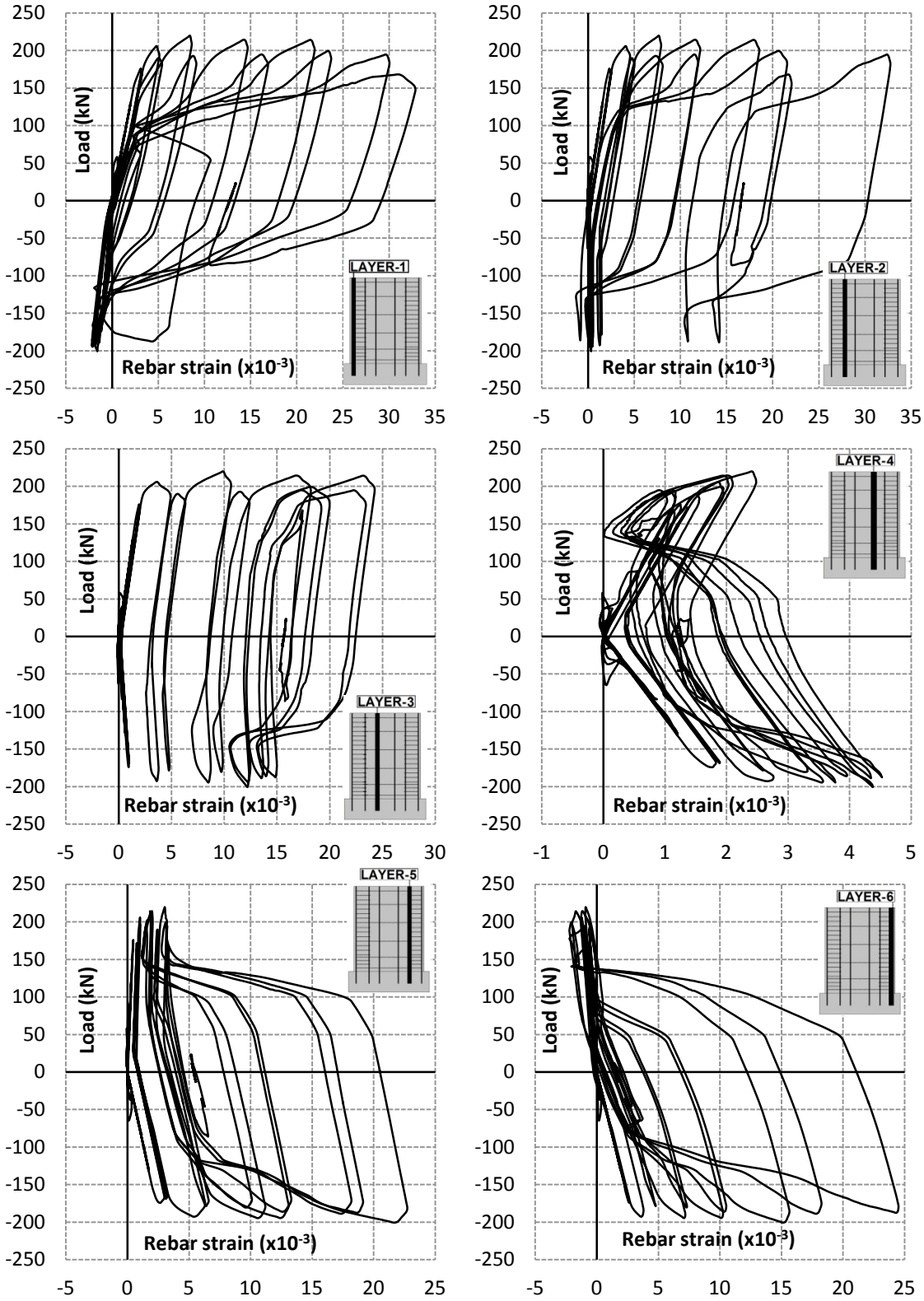

Figure 5.15. Lateral load vs. maximum rebar axial strain for the six vertical rebar layers of FE-HCW model

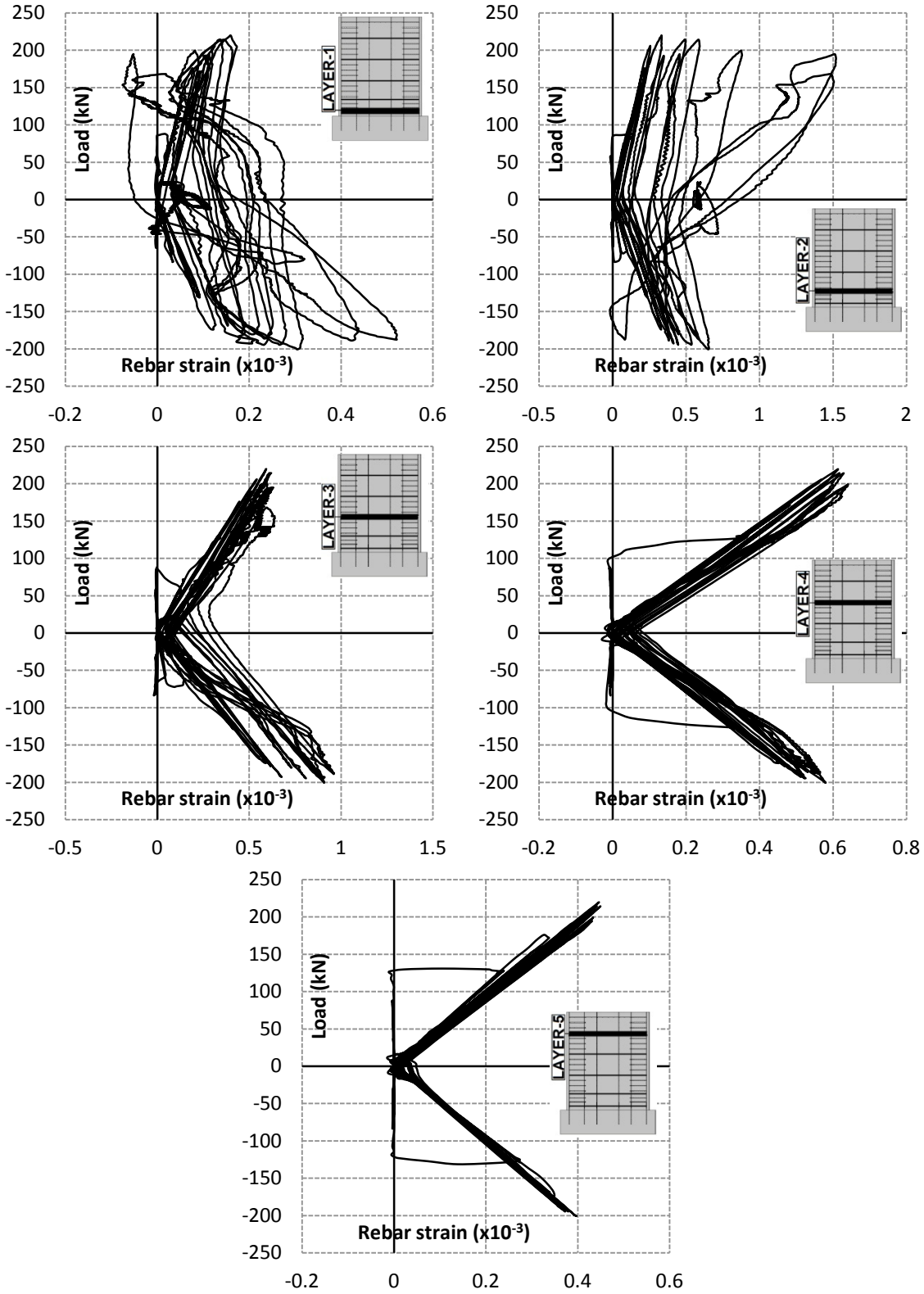

Figure 5.16. Lateral load vs. maximum rebar axial strain for the five horizontal rebar layers of FE-HCW model

5.5 INFLUENCE OF CONCRETE STRENGTH ON THE SEISMIC PERFORMANCE OF RC SQUAT SHEAR WALLS

Changing the value of f'_c influences the material properties of concrete defined in the FE model in ANSYS in three different criteria as described previously in Chapter 3 namely, the initial modulus, the stress-strain relation and the smeared cracking model. In order to study the influence of f'_c on the seismic performance of squat shear walls, the FE model studied earlier in this chapter is analysed with six different f'_c values. The compressive stress-strain curve for different values of concrete compressive strength is shown in Figure 5.17. The compressive strength also influences the tensile strength of concrete which is used to define the cracking stress in the smeared cracking model. Figure 5.18 shows the tensile strength varying by changing the value of f'_c.

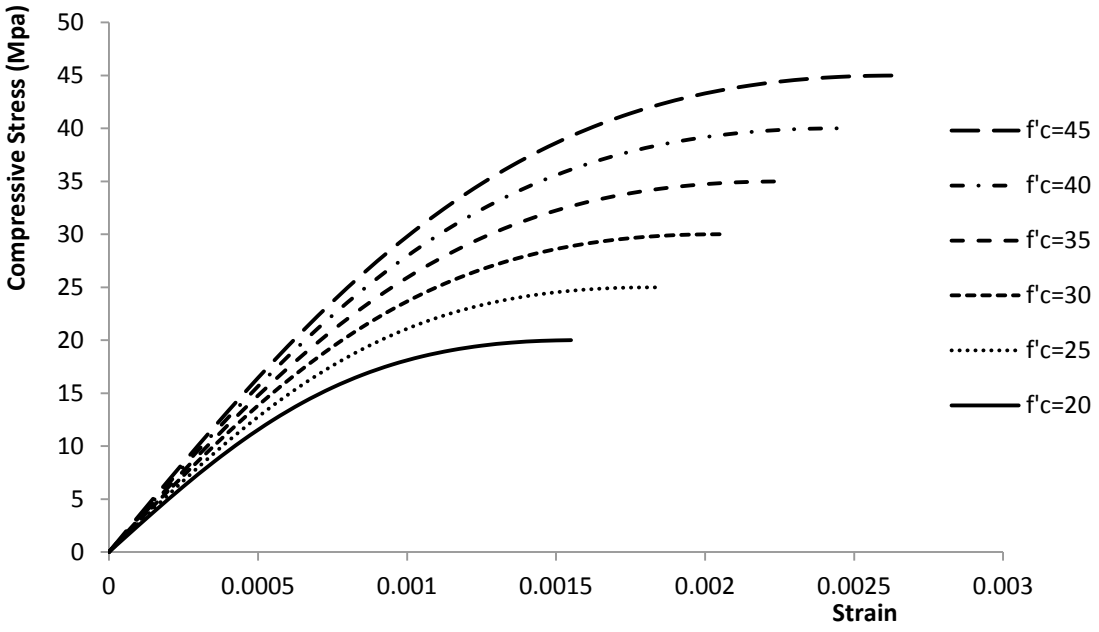

Figure 5.17 Compressive stress-strain relationship of concrete for different values of f'_c

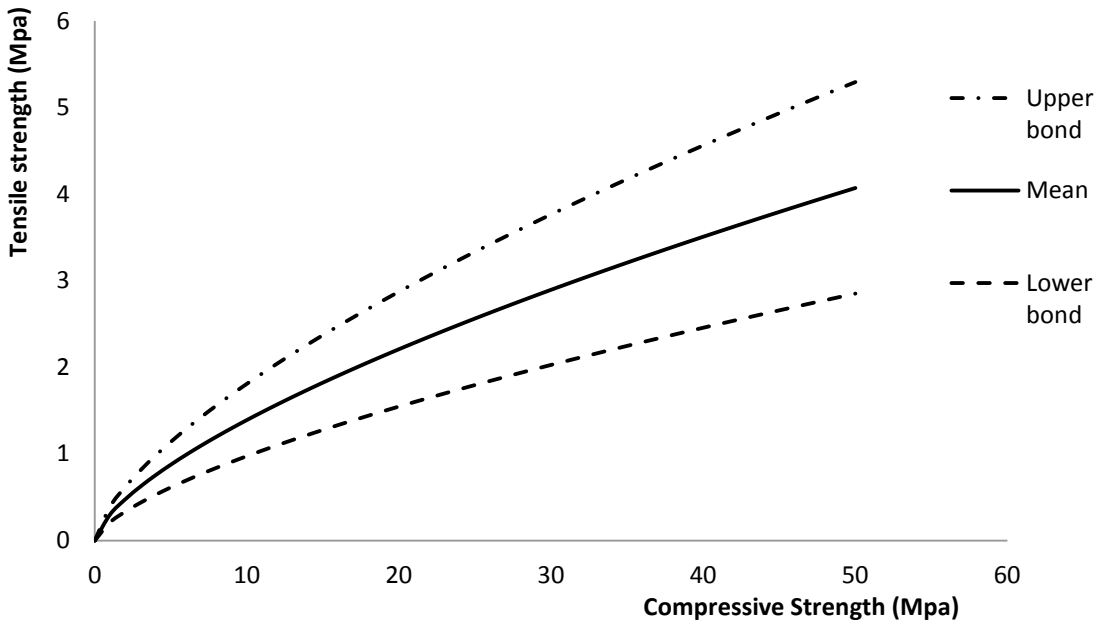

Figure 5.18 Tensile strength of concrete for range of f'_c<50

In order to study the influence of f'_c on the performance of the walls a total of six walls with various concrete compressive strengths are modeled and analyzed under monotonic and cyclic loadings. The nominal shear capacity of each wall is calculated using equations 5-6, 5-8 and 5-9 for different displacement ductility values then the cyclic and monotonic curves are matched with the load-displacement ductility using the yield displacement from each analysis separately. The displacement ductility (μ_Δ) is calculated by dividing the displacement by the yield displacement at each level of the analysis. The value of yield displacement is achieved from the analysis as the displacement where the first vertical rebar reaches the yield strain limit i.e. 0.002. The load-displacement ductility curves as well as the nominal shear capacities are shown for each wall model in Figure 5-19.

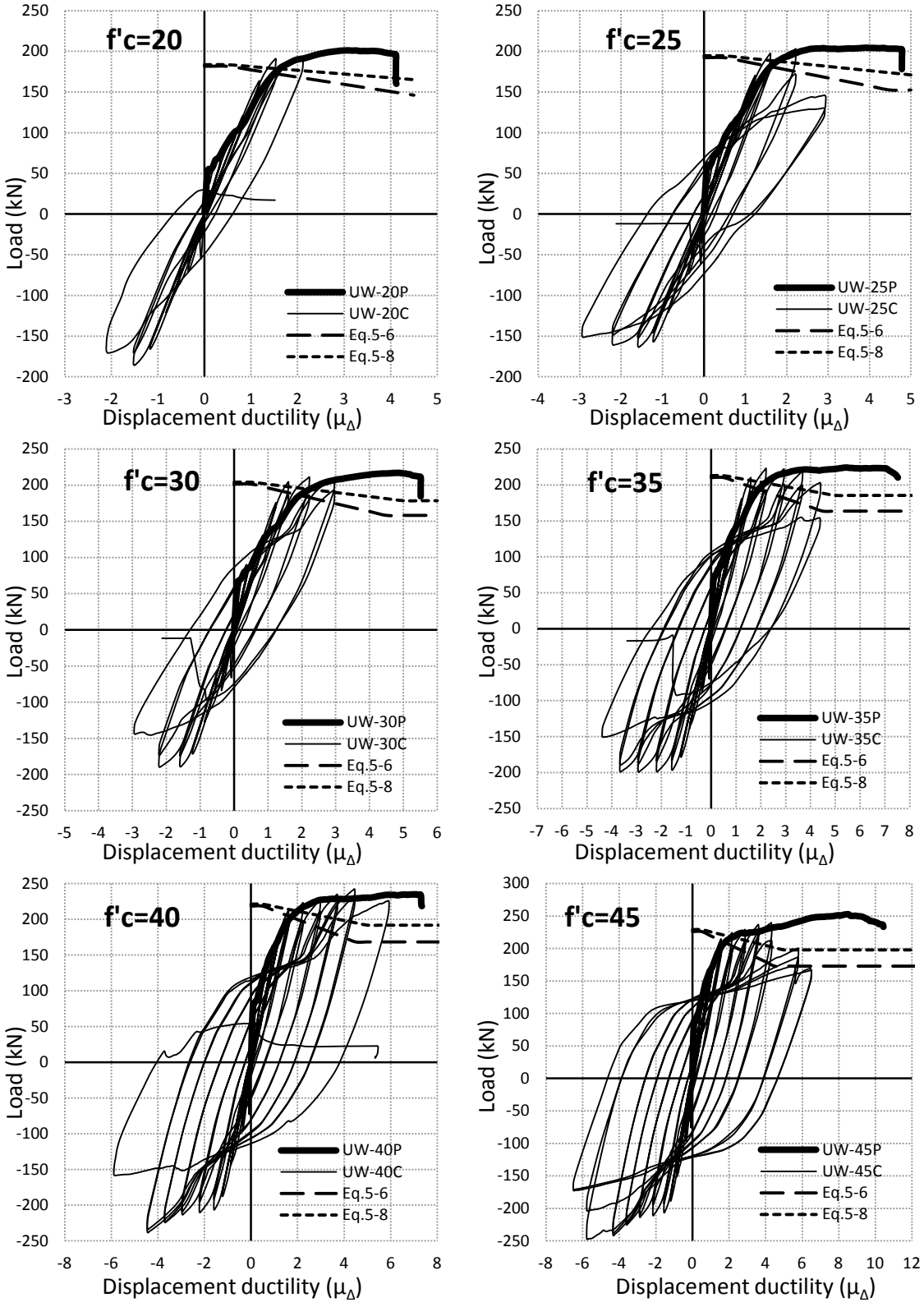

Figure 5.19. Load-Displacement ductility and nominal shear capacities of walls with various f'$_c$ values

The main observation made from the above figures is that all of the FE wall models showed higher strength levels than those of the diagonal tension failure mode as provided in Biskinis et al. (2004) in Eq. 5.6 and 5.8. Those would imply that the results of the current FE models anticipate that the diagonal tension is not the case of failure mode. On the other hand, however, the FE results showed that none of the wall models reached the diagonal compression failure mode limits, affirming Biskinis et al.'s Eq. 5.9 predictions. The failure of the FE models of the walls was due to the crushing of concrete in the compressive toe under monotonic loading and due to sliding shear under cyclic loading. The latter observation for walls subjected to cyclic loading indicates that in order to have the failure mode as diagonal compression this requires significantly higher flexural strengths combined with prevention of the sliding shear. It is worth mentioning that the modelled walls were not subjected to axial load that could have increased the possibility of eliminating the sliding shear failure mode.

As previously shown in Figure 5.18, the tensile strength of concrete increases with f'_c which influences the wall cracking load, the wall cracking force resulted from the cyclic and monotonic analysis is shown in Figure 5-20 for different values of f'_c.

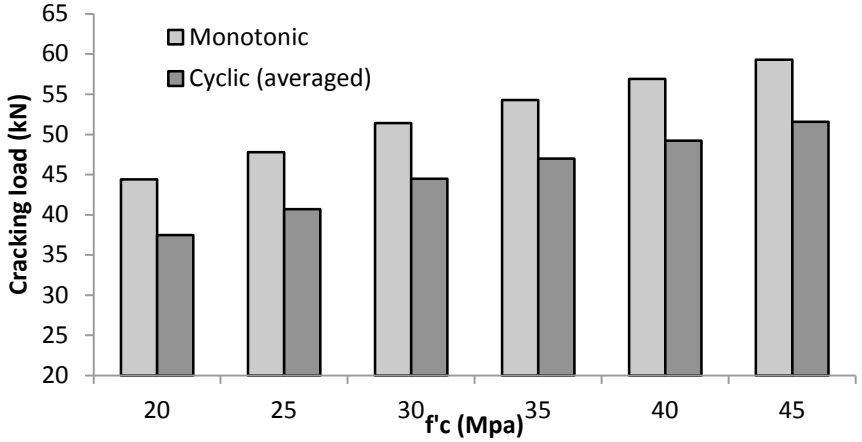

Figure 5.20. Wall cracking load for different values of f'_c resulted from cyclic and monotonic analysis

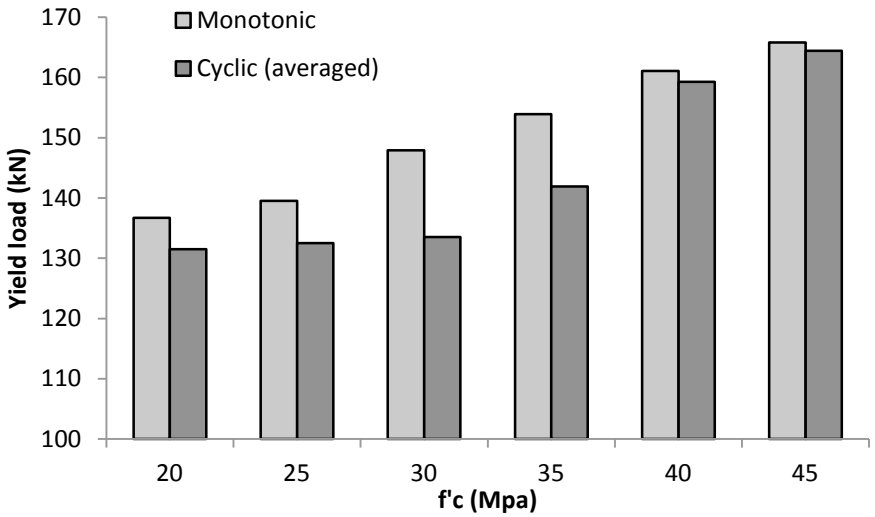

Figure 5.21. Load corresponding to the yielding of the first vertical rebar for different values of f'$_c$ resulted from cyclic and monotonic analysis

The analysis shows an incremental linear increase in the wall's cracking load upon increasing the f'$_c$. The cracking load resulted from the cyclic analysis is on average 14% less than the load from the monotonic analysis because of the reduction in the stiffness of the wall after cracking in the push direction. The load corresponding to first yield of vertical reinforcement also increases with the increase in f'$_c$ as shown in Figure 5.21.

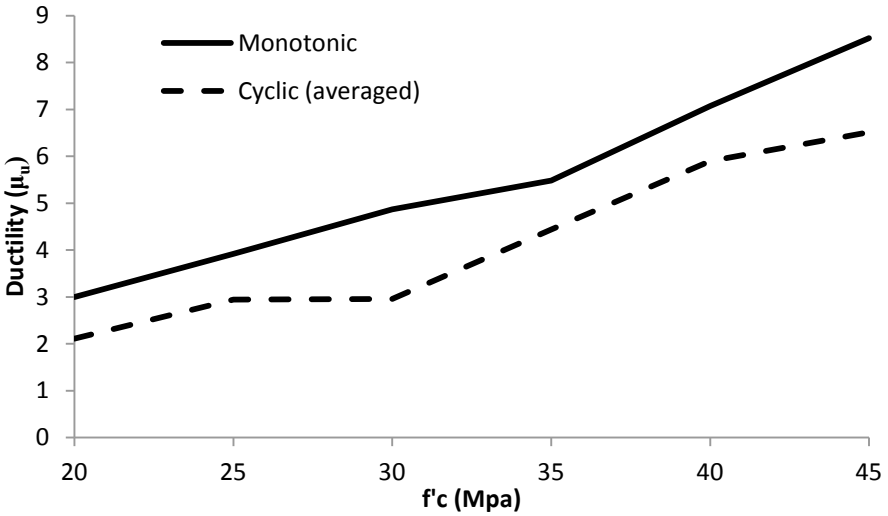

Figure 5.22. Effect of the fc' on the displacement ductility capacity of the studied walls when subjected to cyclic and monotonic lateral loads

Figure 5.22 shows the displacement ductility capacity for the modelled walls at different f'_c values when subjected to either cyclic or monotonic lateral load. From the figure, it could be seen that the ductility of the wall increases with the increase in the concrete compressive strength. The figure also shows that the displacement ductility capacities of cyclically-loaded RC shear wall models are typically less than their counterpart wall models that are monotonically loaded.

Figure 5.23 shows the energy dissipation by the ductile behaviour of the wall calculated from the area enclosed by the cyclic load-displacement curve for each wall. The energy dissipation significantly increases by the concrete strength due to the capability of the walls to complete new load cycles at larger displacement levels.

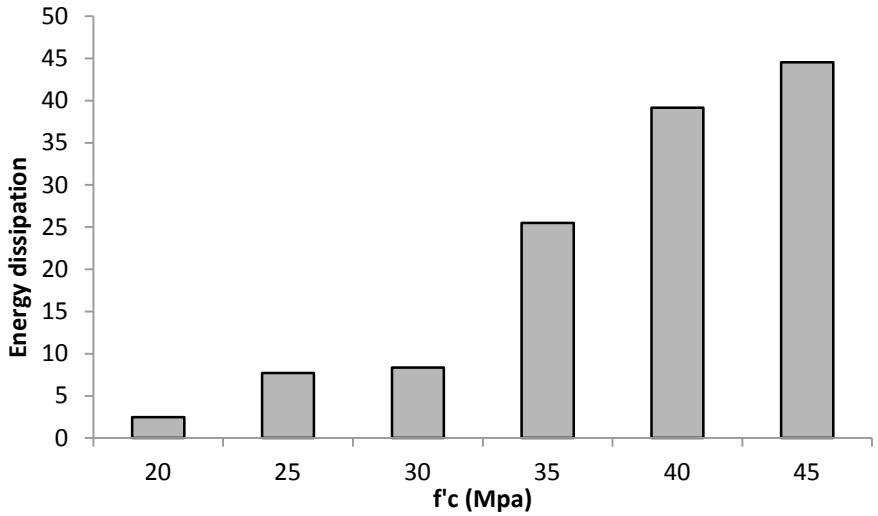

Figure 5.23. Effect of f'_c on the wall's energy dissipation capacity for cyclically loaded walls

The wall models are evaluated with respect to the four main performance levels defined by FEMA (1997) namely: Fully Operational (F.O.), Operational (O.), Life Safety (L.S.) and Near Collapse (N.C.). Figure 5.26 shows the monotonic shear force-deflection curves for the wall models with various concrete compressive strength values. The low strength walls i.e. UW-20C, UW-25C and UW-30C only passed the F.O. and O. Performance

levels and failed before reaching the L.S. level while the UW-35C model could barely reach the L.S. performance level. Both high strength walls UW-40C and UW-45C passed the L.S. performance level but only UW-45C wall completed the performance by reaching the N.C. level.

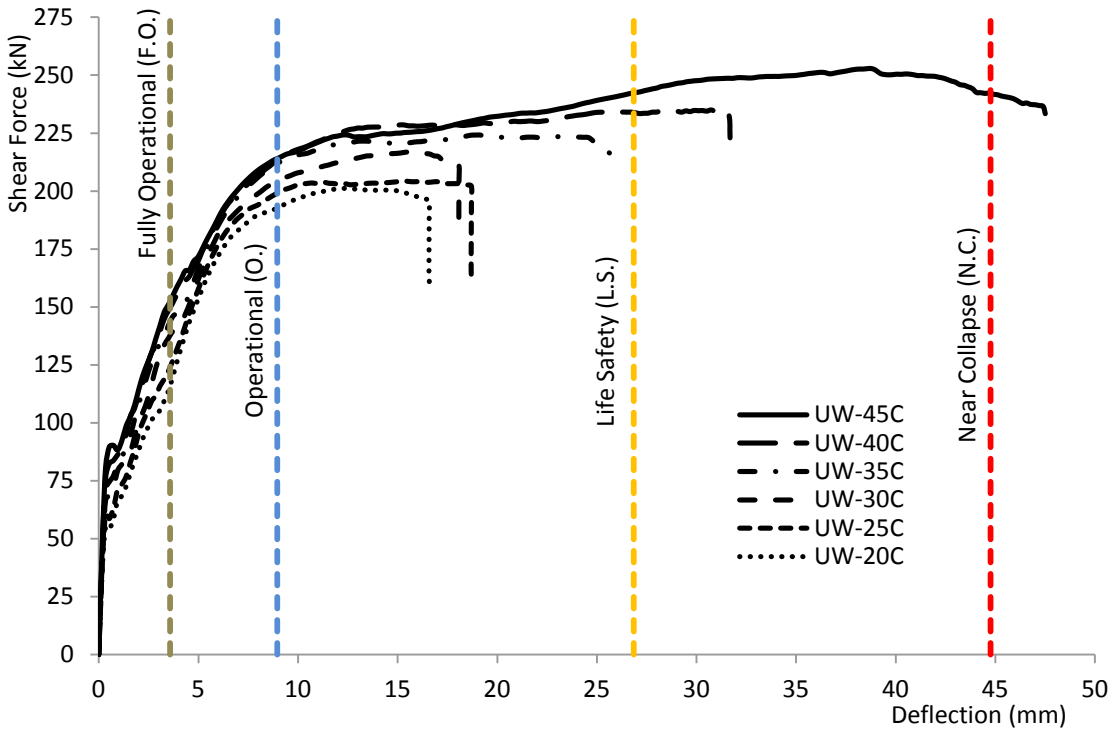

Figure 5.24. Lateral force-deflection relationships of the studied walls with various f'_c values along with the seismic performance levels

5.6 BEHAVIOUR OF FRP-RETROFITTED RC SQUAT SHEAR WALLS UNDER CYCLIC LOADING

Applying one vertical layer of CFRP on the surface of the shear wall on both sides have been experimentally tested by Lombard et al. (2000) and Hiotakis et al. (2004) as seen in the previous chapter. The main influence of retrofit on the shear wall behaviour in this method is the increase in the flexural capacity by strengthening the "tie" in the strut-and-

tie model. The FE-HSW1 model from chapter 4 is discussed in more details in order to study the influence of the FRP external reinforcement on the behaviour of the wall.

Figure 5.25 shows the crack pattern and the rebar axial stresses in the three main stages of analysis, namely cracking stage, yielding stage, and ultimate stage.

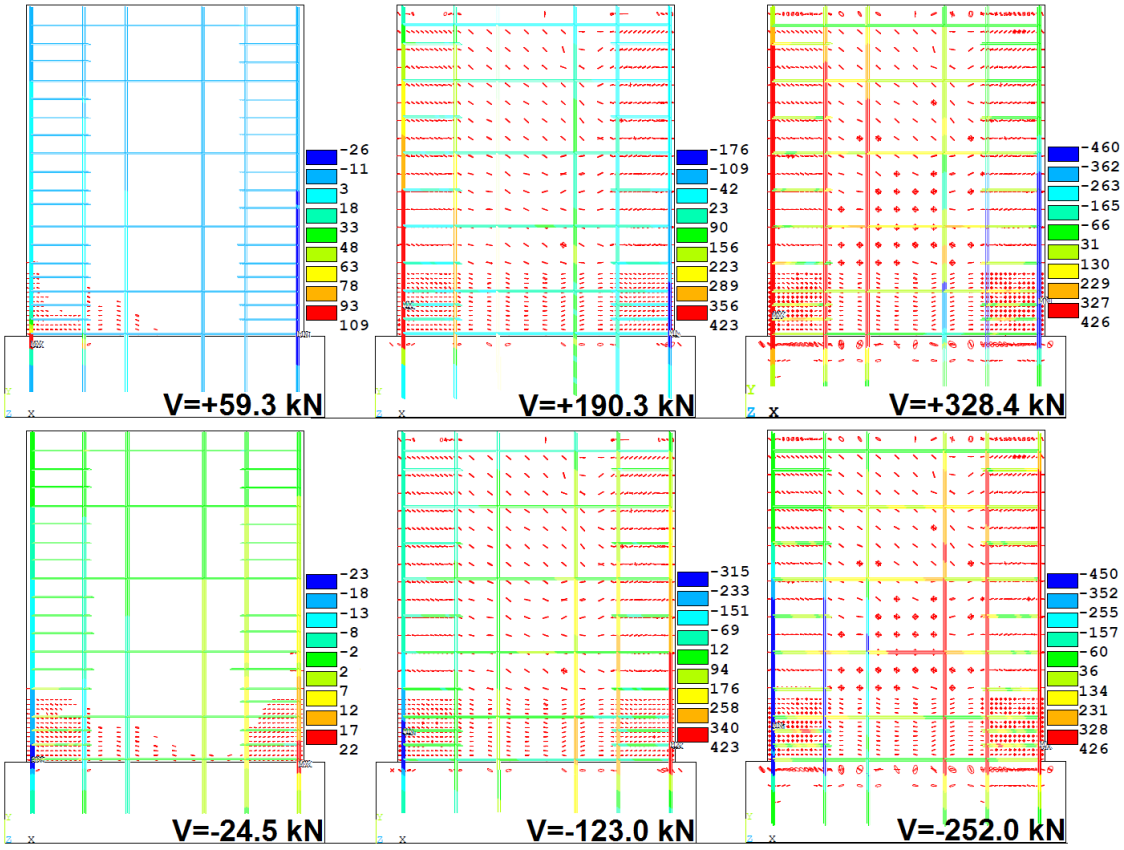

Figure 5.25. Crack pattern and rebar axial stress at various stages of cyclic analysis of the FE-HSW1 wall model

Comparing the current results with the results from the analysis of the HCW model (Figures 5.12 and 5.13), it is seen that the cracking pattern and stress distribution in the rebars are not significantly different at the load corresponding to the yielding of the extreme layer of vertical rebar in each cycle. At the ultimate loading stage, the stress throughout the whole length of the two extreme layers of vertical reinforcement reaches the yielding limit; also, the horizontal reinforcement in the mid-height exhibit yielding at

the ultimate load in pull direction. Crushed concrete elements are visible in both toe regions of the wall as well as the web region due to the extensive shear stresses induce into the wall regarding the extra flexural capacity provided by the external FRP reinforcement. The axial stresses in the FRP elements are shown in Figure 5.26.

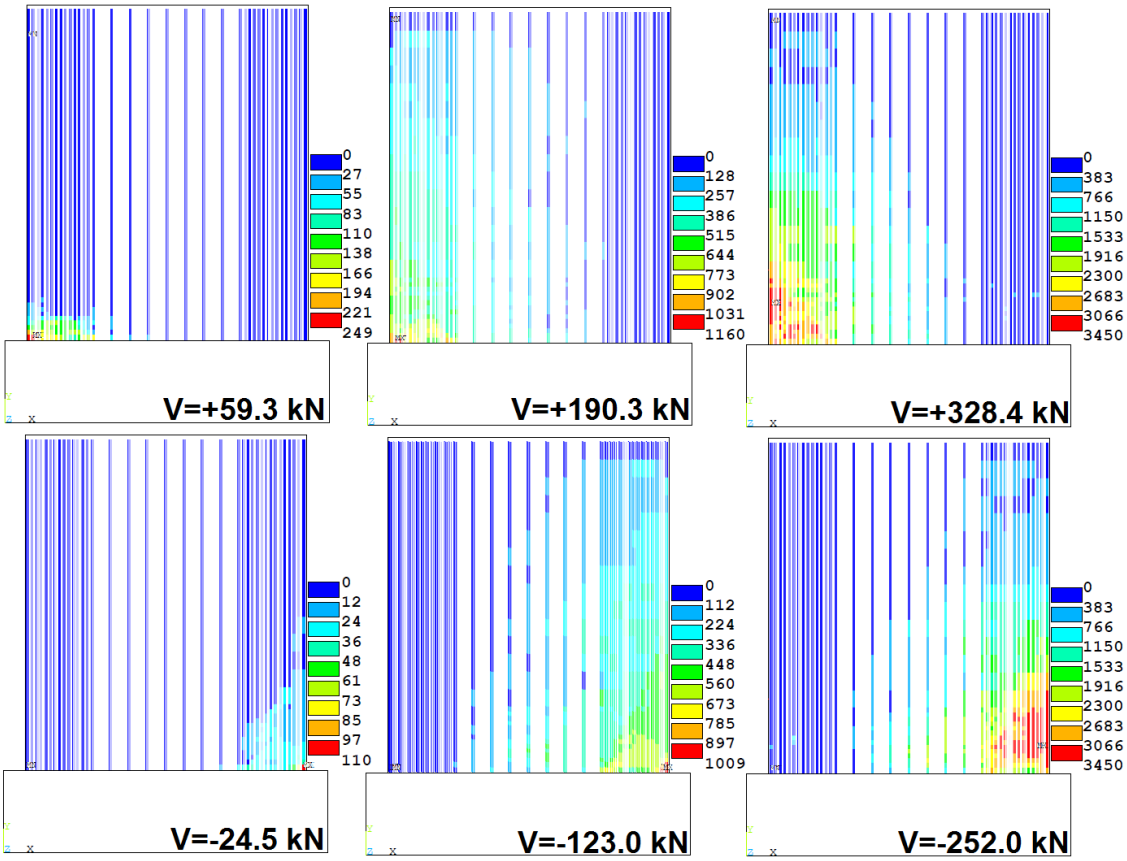

Figure 5.26. FRP axial stress at various stages of cyclic analysis of the FE-HSW1 wall model

The tensile stress in the FRP layer reached the fracture limit in the tensile toe region of the wall at the ultimate load. There is no compressive stress generated in the FRP layer during the analysis because of the tensile-only element used in the modeling as explained previously in chapter 3. Figure 5.26 shows that the axial stresses generated in the FRP layer in the web region is negligible compared to the two edges of the wall. This indicates

that applying FRP only to the edges of the wall would have the same influence on the behaviour of the wall regarding the distribution of the internal forces through the wall. Figure 5.27 shows the stress distribution over different regions of the wall in the FE-HSW1 model at three stages of the analysis.

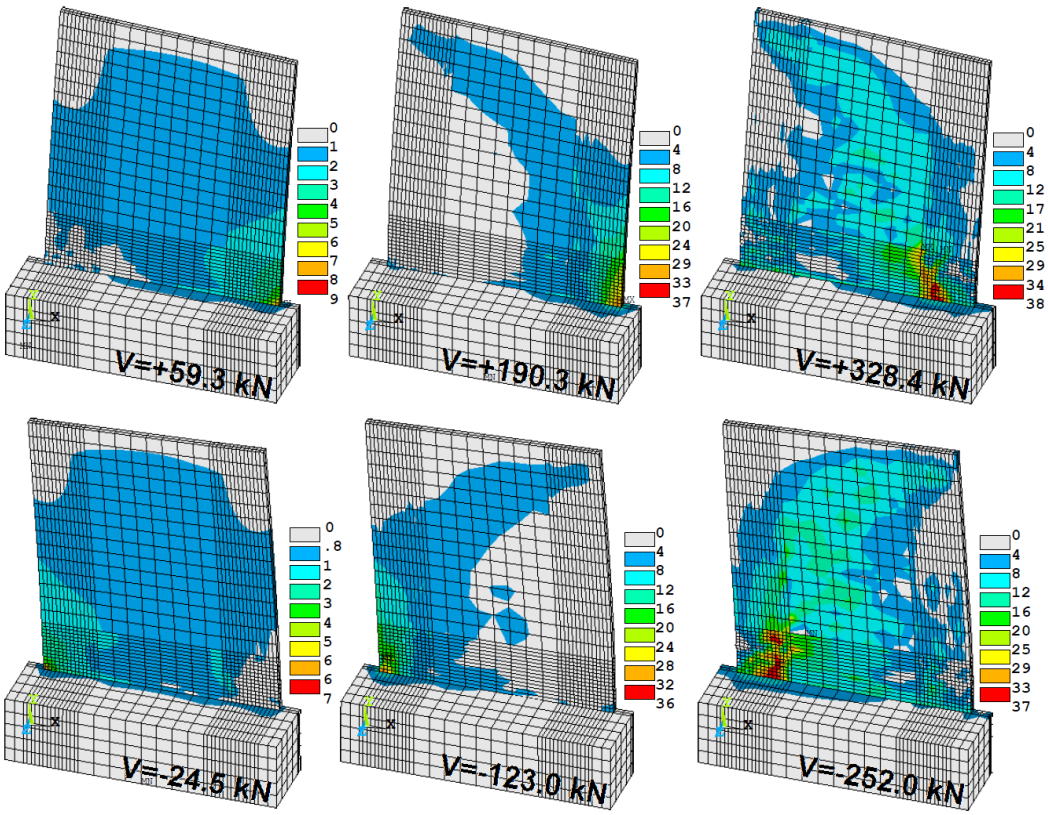

Figure 5.27. Stress distribution in the model at various stages of cyclic analysis of the FE-HSW1 wall model

The distribution of stress over the wall shows that due to the significant increase in the strength of tie (due to the addition of vertical FRP, and their effectiveness at the wall ends), the strut exhibits high stresses and the diagonal tension would be the case for the failure mode because of the low amount of horizontal reinforcement. The stress distribution complies with the high tensile stresses generated in the horizontal reinforcements as shown earlier in Figure 5.25. Figures 5.28 and 5.29 show the strain in vertical and horizontal reinforcement bars during the cyclic analysis.

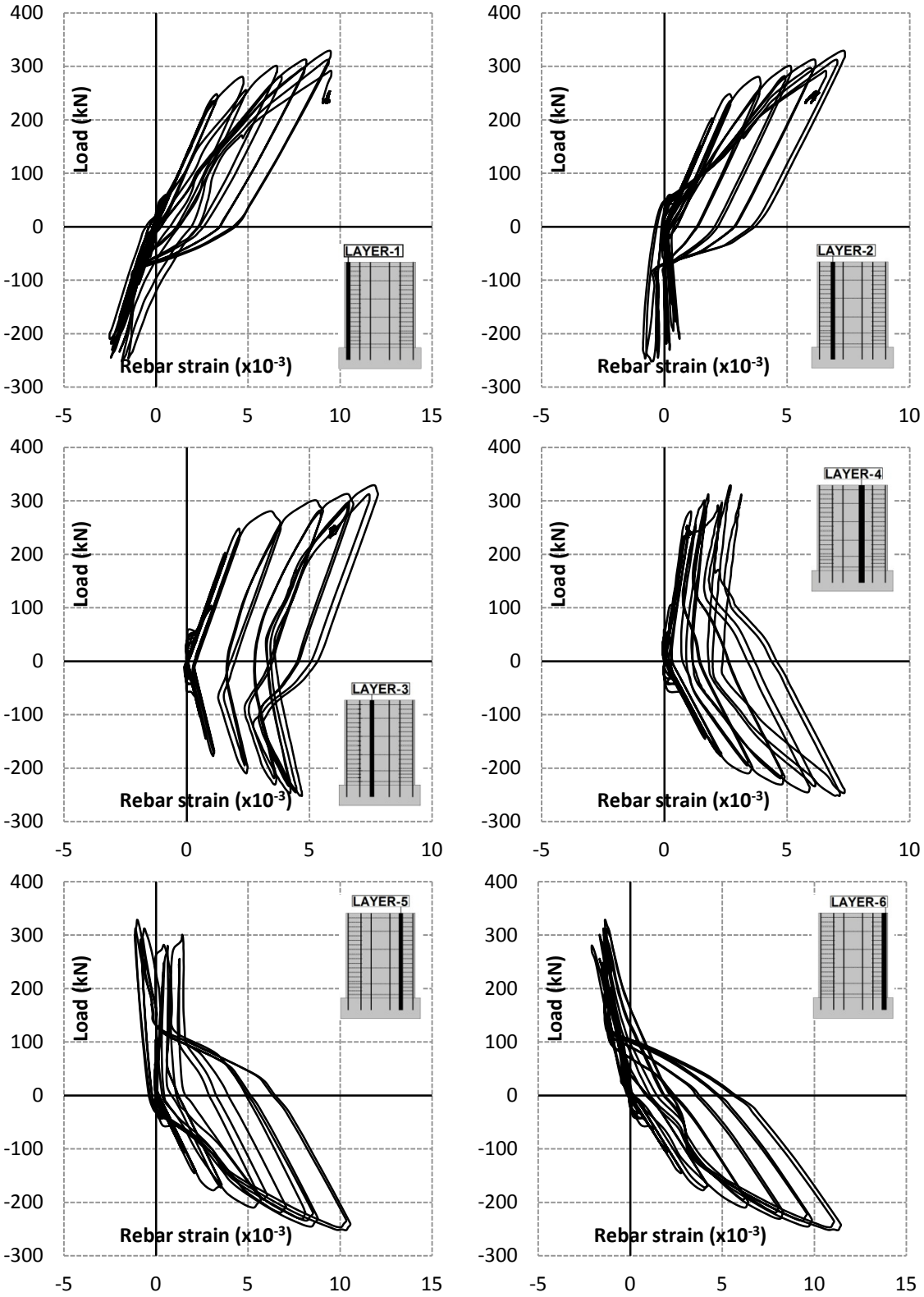

Figure 5.28. Lateral load vs. maximum rebar axial strain for the six vertical rebar layers of FE-HSW1 model

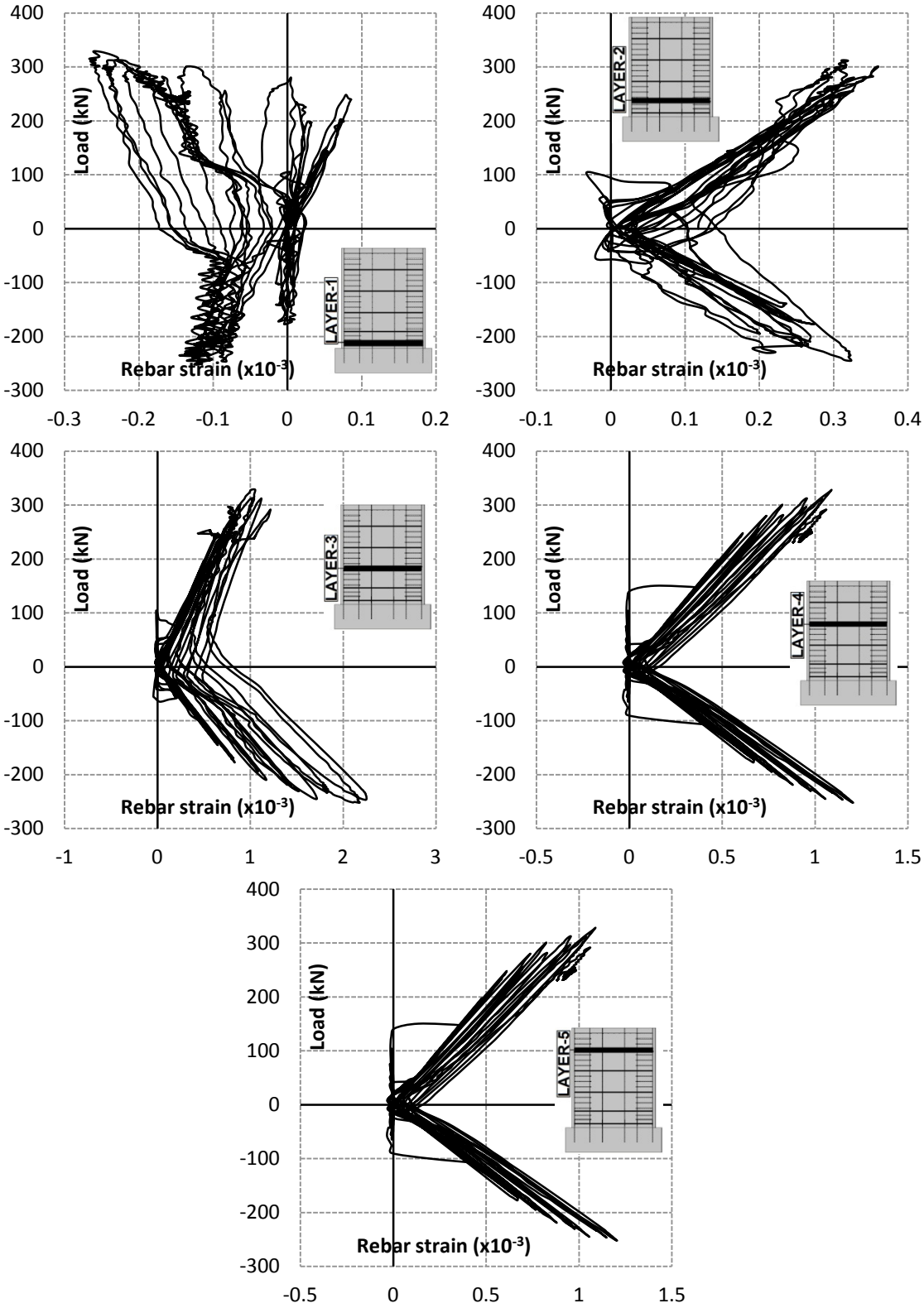

Figure 5.29. Lateral load vs. maximum rebar axial strain for the five horizontal rebar layers of FE-HSW1 model

Although the vertical reinforcement bars exhibit yielding but the strains did not go well beyond the yielding strain compared to the strains resulted from the unretrofitted wall (HCW) due to the low flexibility of the FRP layers which also resulted in limited top displacement. Unlike the vertical rebars, the strains in the horizontal reinforcement layers increases compared to the HCW model. The third layer of horizontal reinforcement yielded during the analysis but the strains in the other four layers remain within the elastic limits.

5.7 INFLUENCE OF CONCRETE STRENGTH ON THE SEISMIC PERFORMANCE OF FRP-RETROFITTED SQUAT SHEAR WALLS

The influence of f'_c on the performance of retrofitted walls is discussed in the section. In order to compare the results of FRP-retrofitted RC shear wall models with those of the unretrofitted walls, the same loading history is used. The retrofit method used complies with the HSW1 specimen from the experimental works of Hiotakis et al. (2004). Since the bonding interface model (Lu et al., 2005-a) depends on the tensile strength of concrete, the bond interface elements are updated in each model based on the f'_c of the model accordingly.

Figure 5.30 shows the lateral load-displacement ductility curves of the FRP-retrofitted walls with various values of f'_c between 20 MPa and 45 MPa. The concrete compressive strength influences the performance of the FRP-retrofitted walls in two ways by affecting the overall strength and ductility of the wall as shown previously for the unretrofitted walls and also influencing the strength of the bond interface between FRP and concrete surface.

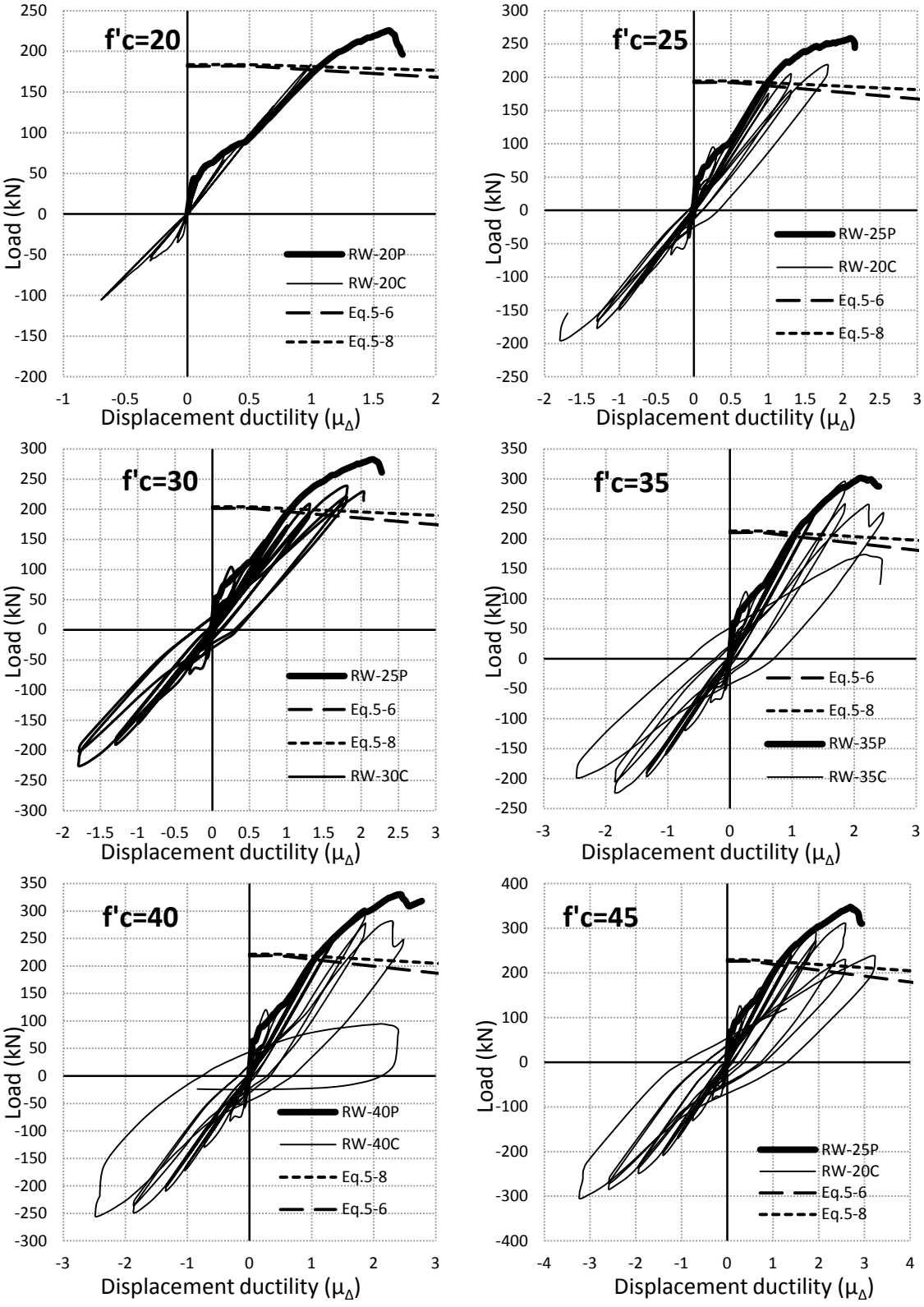

Figure 5.30. Load-Displacement ductility and nominal shear capacities of FRP-retrofitted walls with various f'$_c$ values

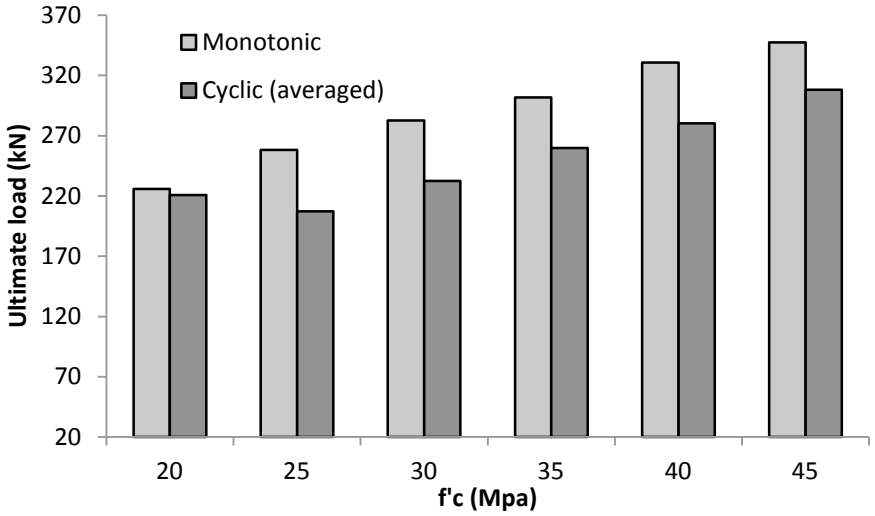

Figure 5.31. Effect of f'$_c$ on the FRP-retrofitted wall's ultimate load carrying capacity

Figure 5.31 shows the influence of f'$_c$ on the ultimate load carrying capacity of FRP-retrofitted walls. The concrete compressive strength significantly affects the ultimate load. On average, the ultimate load carrying capacity is about 46% higher for the wall with f'$_c$=45MPa as compared to that of the wall with f'$_c$=20 MPa.

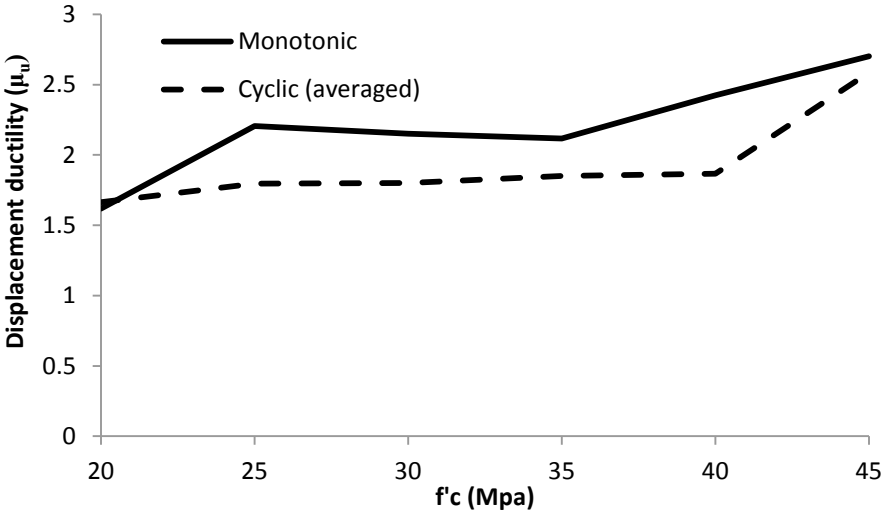

Figure 5.32. Effect of the f'$_c$ on the displacement ductility capacity of the FRP-retrofitted walls when subjected to cyclic and monotonic lateral loads

The ultimate displacement of the FRP-retrofitted walls is significantly lower than the unretrofitted walls, thus the displacement ductility of these walls is generally less than

that of the unretrofitted walls. The change in the displacement ductility of the FRP retrofitted walls with the variation of f'_c is shown in Figure 5.32. From the figure it can be seen that the displacement ductility of the FRP-retrofitted walls is not particularly influenced by the concrete compressive strength.

CHAPTER 6

CONCLUSIONS AND RECOMMENDATIONS

6.1 SUMMARY

Establishing effective retrofit methods for upgrading the seismic performance of existing reinforced concrete (RC) shear walls requires a reliable means for estimating the behaviour of RC shear walls with various geometry and internal reinforcement configurations when subjected to different combinations of axial and lateral loads. Generally, experimental testing of retrofitted RC shear walls is considered as the most reliable method of performance evaluation, yet this requires great efforts in terms of the testing equipment and time in addition to the high cost. On the other hand, a numerical model that would consider the main parameters that influence the complex performance of original and retrofitted RC shear walls is seen to be an effective and promising tool. Such analytical approach would be particularly useful for parametric studies and development of code provisions for the design or evaluation purposes. Despite the wealth in research information in the area of retrofitting RC bridges using fibre-reinforced polymer (FRP) composite materials, yet the experimental and analytical research in the area of assessing the seismic performance of FRP-retrofitted RC shear walls is still in its early stages. A number of experimental tests are available in the literature which could be used for the primary verification of possible numerical analyses. Similarly, a number of numerical and analytical approaches are available with a great potential for improvements in order to converge into a precise and usable analytical approach. Finite

Element (FE) modeling of reinforced concrete structural elements deals with the composite behaviour of concrete material with the embedded steel reinforcement and possible additional externally bonded/anchored retrofit reinforcement, such as FRP. Appropriate use of elements and meshing techniques that closely represents the composite nature of the steel-reinforced concrete with or without FRP is a key factor in numerical simulations for the predicted behaviour of RC shear walls.

In this thesis, the FE modeling of RC shear walls using general purpose FE package ANSYS were explored. A total of seven experimentally tested wall models from four experimental programs were selected and analysed under monotonic and reversed cyclic loading and the numerical predictions were in good correlation with the experimental data. One of the experimentally tested models was selected for further detailed investigation on the effect of various design parameters on the behaviour of the squat walls and their modes of failure, namely the influence of the concrete compressive strength and the addition of one layer of externally-bonded vertical CFRP sheet.

6.2 CONCLUSIONS

Based on the results of the FE analysis on the modeled shear walls and the extended parametric study investigation, the following conclusions were drawn:

General conclusions on FE modeling of RC shear walls

1. The SOLID65 element provided in the elements library of ANSYS is capable of simulating the behaviour of shear walls under the applied monotonic and cyclic loading with a good precision.

2. The LINK180 element provided in the elements library of ANSYS is capable of simulating the behaviour of embedded rebars and external reinforcement with good precision and convenient output data capabilities, but it does not simulate the rebar dowel action along the element's normal plane which results in a premature failure in some cases under cyclic loading.
3. The COMBIN39 element provided in the elements library of ANSYS is capable of simulating the bond-interface between external reinforcement and the surface of concrete with good precision.

For the studied unretrofitted squat shear wall FE model

1. The performance of unretrofitted shear wall model is sensitive to the loading protocol on the wall. The monotonically loaded wall model exhibits higher ultimate displacement and higher displacement ductility compared to the cyclically loaded model.
2. If the diagonal tension mode of failure is prevented by sufficient providing horizontal reinforcement, the failure mode of the squat wall will become flexural in the absence of axial compressive force.
3. The concrete compressive strength significantly influences the displacement ductility of the wall model.
4. The concrete compressive strength significantly influences the seismic energy dissipation capacity of the model.
5. The concrete compressive strength significantly influences the loads correspond to the first cracking of concrete and first yielding of the reinforcement bars.

6. The sliding shear was the dominating failure mode for the wall models subjected to cyclic loading in the absence of axial compressive forces due to the incapability of the used reinforcement elements in providing the extra shear resistance by means of the rebars dowel action.

For the studied FRP-retrofitted RC squat shear wall FE model

1. Addition of an external layer of vertical FRP to the wall model significantly influences the failure mode of the wall by providing a great additional flexural strength to the wall. The model mode of failure migrates from the sliding shear failure mode to diagonal tension after strengthening by vertical FRP reinforcement.
2. The concrete compressive strength does not significantly influence the performance of the FRP-retrofitted wall models. However, the ultimate load carrying capacity of the wall significantly increases by the concrete compressive strength.

6.3 RECOMMENDATIONS FOR THE FUTURE WORK

The author strongly recommends further numerical modeling of a bigger group of experimental work in order to achieve the following objectives:

1. In the case of squat shear walls, the axial forces significantly influence the behaviour of the wall; this phenomenon should be investigated through a series of models subjected to different axial load levels.

2. The effect of horizontal reinforcement ratio on the failure mode of unretrofitted and retrofitted walls should be investigated through a series of models with different horizontal reinforcement ratios.
3. The use of beam elements with rotational degrees of freedom for the vertical reinforcement bars could resemble the rebar dowel action and solve the premature failure of the model under cyclic loading but it may affect the other results of the analysis and impose additional sophistications into the analysis; this could be studied through a comparative modeling.
4. Other methods of application of FRP sheets to the surface of the walls should be modeled and the most efficient methods would be introduced by comparing the different aspects of the influence of each method on the performance of the wall.
5. The case of wall panels with top moments, axial and lateral forces would be a major achievement in the modeling.
6. The use of steel plates as the externally bonded reinforcement as a retrofit method through a series of numerical modeling and experimental testing.

REFERENCES

ACI Committee, 4. (2002). Guide for the design and construction of externally bonded FRP systems for strengthening concrete structures. USA: American Concrete Institute.

ANSYS, Inc. (2010-a). ANSYS Element Reference. Canonsburg, PA: SAS IP, Inc.

ANSYS, Inc. (2010-b). Theory Reference for the Mechanical APDL and Mechanical Applications. Canonsburg, PA: SAS IP, Inc.

Antoniades, K., Thomas, K., Salonikios, N. and Kappos, A. J. (2003). Cyclic Tests on Seismically Damaged Reinforced Concrete Walls Strengthened Using Fiber-Reinforced Polymer Reinforcement. ACI Structural Journal, 100(4), 510-518.

Biskinis, D. E., Roupakias, G. K., and Fardi, M. N. (2004). Degradation of Shear Strength of Reinforced Concrete Members with Inelastic Cyclic Displacements. ACI Structural Journal-Technical Paper, 101(6), 773-783.

British Standards Institution. (1996). Eurocode 8: Design provisions for earthquake resistance of structures. London: British Standards Institution.

CNR DT/200. (2004). Guide for the design and construction of externally bonded FRP systems for strengthening existing structures. Rome, Italy: National Research Council, Italy.

CAN/CSA-A23.3 Concrete Design Handbook (3rd ed. 2008). Canadian Standard Association.

Cortés-Puentes, L. W., and Palermo. D. (2012). Modeling of RC Shear Walls Retrofitted with Steel Plates or FRP Sheets. JOURNAL OF STRUCTURAL ENGINEERING, ASCE 138(5) 602-612.

Cruz-Noguez, C. A., Lau, D. T. and Sherwood, E. T. (2012). Analythical modeling of shear walls flexurally-reinforced with carbon fibre sheets. 6th International Conference on Advanced Composite Materials in Bridges and Structures. Kingston, ON, Queen's University.

Dai, J., Ueda, T., and Sato, Y. (2005). Development of the Nonlinear Bond Stress–Slip Model of Fiber Reinforced Plastics Sheet–Concrete Interfaces with a Simple Method. Journal of Composites for Construction, ASCE, 9(1), 52-62.

Elnady, M. M. (2008). Seismic Rehabilitation of RC Structural Walls. Hamilton, ON, Canada: PhD Thesis, McMaster University.

Elnashai, A. S., and Pinho, R. (1998). Repair and Retrofitting of RC Walls using Selective Techniques. Journal of Earthquake Engineering, 2(4), 525-568.

El-Sokkary, H., Galal, K., Ghorbanirenani, I., Léger, P. and Tremblay, R., (2012). Shake Table Tests on FRP-Rehabilitated RC Shear Walls. *Journal of Composites for Construction*, 17(1), 79–90.

El-Sokkary, H. and Galal, K. (2013). Seismic Behavior of FRP-Strengthened RC Shear Walls. Journal of Composites for Construction, 10.1061/(ASCE) CC.1943-5614.0000364

fib Model Code 2010 first complete draft (2010), Volume1. Lausanne, Switzerland: DCC Document Competence Center Siegmar Kästl e.K., Germany.

Fiorato, A.E., Oesterle, R.G. and Corley, W.G. (1983). Behavior of Earthquake Resistant Structural Walls Before and After Repair. ACI Advancing concrete knowledge, 80(5), 403-413.

Galal, K., and El-Sokkary, H. (2008). RECENT ADVANCEMENTS IN RETROFIT OF RC SHEAR WALLS. The 14th World Conference on Earthquake Engineering . Beijing, China.

Ghobara, A., and Khalil, A. A. (2004). Seismic Rehabilitation of Reinforced Concrete Walls using Fibre Composites. 13th World Conference on Earthquake Engineering. Vancouver, B.C, Canada: WCEE, 3316 1-14.

Hiotakis, S., Lau, D. T., and Londono, N. (2004). Research on Seismic Retrofit and Rehabilitation of Reinforced Concrete Shear Walls using FRP Materials. Ottawa, ON, Canada: Carlton University.

Hognestad, E. (1951). A Study of Combined Bending and Axial Load in Reinforced Concrete Members. Bulletin 399, University of Illinois Engineering Experiment Stations, Urbana Ill., 128 pp.

Hwang, S. J., Chiou, T. C. and Tu, Y. S. (2004). Reinforced Concrete Squat Walls Retrofitted With Carbon Fiber Reinforced Polymer. Proceedings of 2nd International Conference on Frp Composites in Civil Engineering - CICE. Adelaide, Australia, 47-56.

Kobayashi, K. (2005). Innovative application of FRPs for seismic strengthening of RC shear wall. Fiber-Reinforced Polymer (FRP) Reinforcement for Concrete Structures. Framington Hills, Mi, USA, ACI, 1269-1288.

Kong, K. H., Tan, K. H. and Balendra, T. (2003). Retrofitting of Shear Walls Designed to BS 8110 for Seismic Loads using FRP. Proceedings of Sixth International Symposium on FRP Reinforcement for Concrete Structures (FRPRCS-6). Singapore, 2003. 1127-1136.

Kowalsky, M. J., and Priestley, M. J. (2000). Improved Analythical Model for Shear Strength of Circular Reinforced Concrete Columns in Seismic Regions. ACI Structural Journal, 97(3), 388-396.

Lefas, I. D. and Kotsovos, M. D. (1990). Strength and Deformation Characteristics of Reinforced Concrete Walls under Load Reversals. ACI Structural Journal, 87(1), 716-726.

Lefas, I. D., Kotsovos, M. D. and Ambraseys, N. N.(1990). Behavior of Reinforced Concrete Structural Walls: Strength, Deformation Characteristics, and Failure Mechanism. ACI Structural Journal 87(1), 23-31.

Li, B., and Lim, C. L. (2010). Tests on Seismically Damaged Reinforced Concrete Structural Walls Repaired Using Fiber-Reinforced Polymers. ASCE Journal of Composites for Construction, 10.1061 ASCE CC.1943-5614.0000110, 597-608.

Li, Z. J., Balendra, T. Tan, K. H. and Kong. K. H. (2005). Finite element modelling of cyclic behaviour of shear wall structure retrofitted using GFRP. Proceedings of 7th International Symposium on Fiber-Reinforced Polymer (FRP) Reinforcement for Concrete Structures. Farmington Hills, MI, ACI Symposium Publication, 1305-1324.

Lombard, J., Lau, D. T., Humar, J. L., Foo, S. and Cheung, M. S. (2000). Seismic Strengthening and Repair of Reinforced Concrete Shear Walls. Proceedings of

12th World Conference on Earthquake Engineering. Aukland, Silverstream, N.Z., New Zealand Society for Earthquake Engineering, 2032 1-8.

Lu, X. Z., Teng, J. G., Ye, L. P., and Jiang, J. (2007). Intermediate Crack Debonding in FRP-Strengthened RC Beams: FE Analysis and Strength Model. Journal Of Composites For Construction, ASCE, 11(2), 161-175.

Lu, X. Z., Teng, J. G., Ye, L. P., and Jiang, J. J. (2005-a). Bond-slip models for FRP sheets/plates bonded to concrete. Journal of Engineering Structures, 27(6), 920-937.

Lu, X. Z., Teng, J. G., Ye, L. P., and Jiang, J. J. (2005-b). Meso-scale finite-element model for FRP sheets/plates externally boned to concrete. Journal of Engineering Structures, 27(4), 564-575.

Moehle, J. P. (2000). State of Research on Seismic Retrofit of Concrete Building Structures in the US. US-Japan Symposium and Workshop on Seismic Retrofit of Concrete Structures-State of Research and Practice.

Moehle, J., Lynn, A., Elwood, K., and Sezen, H. (2001). Gravity Load Collapse of Building Frames During Earthquakes. Richmond, California: Pacific Earthquake Engineering Research Center.

Ombres, L. (2010). Prediction of Intermediate Crack Debonding Failure in FRP-Strengthened Reinforced Concrete Beams. Journal of Composite Structures, 92, 322-329.

Palermo, D. and Vecchio, F. J. (2007). Simulation of cyclically loaded concrete structures based on the finite-element method. Journal of Structural Engineering, 133(5), 728-738.

Paulay, T., and Priestley, M. (1992). Seismic Design of Reinforced Concrete and Masonry Buildings. Wiley.

Peterson, J. and Mitchell, D. (2003). Seismic Retrofit of Shear Walls with Headed Bars and Carbon Fiber Wrap. ASCE Journal of Structural Engineering, 129(5), 606-614.

Priestley, M. J., Verma, R., and Xiao, Y. (1994). Seismic Shear Strength of Reinforced Concrete Columns. Journal of the Structural Devision, ASCE, 120(8).

Rosenboom, O., and Rizkalla, S. (2008). Experimental Study of Intermediate Crack Debonding in Fiber-Reinforced Polymer Strengthened Beams. ACI Structural Journal, 105(1), 41-50.

Salonikios, T., Tegos, I., Kappos, A., and Penelis, G. (1996). Squat R/C Walls Under Inelastic Shear Reversals. Paper No. 749.: Elsevier Science Ltd.

Sato, Y., and Vecchio, F. J. (2003). Tension Stiffening and Crack Formation in Reinforced Concrete Members with Fiber-Reinforced Polymer Sheets. Journal of Structural Engineering, ASCE, 129(6), 717-724.

Sittipunt, C. and Wood, S. L. (1993). Finite Element Analysis of Reinforced Concrete Shear Walls. Department of Civil Engineering, University of Illinois at Urbana - Champaign, Urbana, Illinois.

Teng, J. G., Smith, S. T., Yao, J., and Chen, J. F. (2003). Intermediate crack-induced debonding in RC beams and slabs. Journal of Construction and Building Materials, 17, 447-462.

Ueda, T., Dai, J. G. and Sato, Y. (2005). Development of non-linear bond stress slip model of fiber reinfored plastics sheet-concrete interfaces with a simple method. Journal of Composite Construction, 9(1), 52-62.

Vasiliev, V. V., and Morozov, E. V. (2007). Advanced Mechanics of Composite Materials (2nd ed.). Oxford: Elsevier Ltd. .

Vecchio, F. J. (1989). Nonlinear finite element analysis of reinforced concrete membranes. ACI Structural Journal, 26-35.

Vecchio, F. J., and Collins, M. P. (1986). The modified compression field theory for reinforced concrete elelments subjected to shear. Journal of American Concrete Institute, 219-231.

Wight, J. K. and MacGregor, J. G. (2011). Reinforced Concrete Mechanics and Design 6th Edition. Pearson Education Inc., Upper Saddle River, NJ.

Willam, K. J., and Warnke, E. D. (1975). Constitutive Model for the Triaxial Behavior of Concrete. International Association for Bridge and Structural Engineering. Bergamo, Italy.

Wong, P. S., and Vecchio, F. J. (2002). VecTor2 and FormWorks user's manual. Toronto: University of Toronto.

Yanez, F. A., Park, R., and Paulay, T. (1989). Strut and Tie Models for Reinforced Concrete Design and Analysis. New Zealand Concrete Society Silver Jubilee Conference, (pp. 43-45). Wairakei, New Zealand.

Yao, J., Teng, J. G., and Lam, L. (2005). Experimental Study on Intermediate Crack Debonding in FRP-Strengthened RC Flexural Members. Journal of Advanced in Structural Engineering, ASE, 8(4), 365-396.

Yuzugullu, O. (1972). Finite Element Approach for the Prediction of Inelastic Behavior of Shear Wall-Frame System. Department of Civil Engineering, University of Illinois at Urbana-Champaign, Urbana, Illinois.

Zhang, Y., and Wang, Z. (2000). Seismic Behavior of Reinforced Concrete Shear Walls Subjected to High Axial Loading. ACI Structural Journal 97(5), 739-750.